To the Graduate Council:

I am submitting herewith a thesis written by Andrew W. Moore entitled "The Effects of Changes in Water Content on Uranium(VI) Leaching in Sediment Mixtures Containing Gravel." I have examined the final electronic copy of this thesis for form and content and recommend that it be accepted in partial fulfillment of the requirements for the degree of Master of Science, with a major in Geology.

Edmund Perfect, Major Professor

We have read this thesis
and recommend its acceptance:

Melanie A. Mayes

Larry D. McKay

Accepted for the Council:

Carolyn R. Hodges
Vice Provost and Dean of the Graduate School

(Original signatures are on file with official student records.)

The Effects of Changes in Water Content on Uranium(VI) Leaching in Sediment Mixtures Containing Gravel

A Thesis Presented for the
Master of Science Degree
The University of Tennessee, Knoxville

Andrew Weber Moore
August 2010

Dedication

This thesis is dedicated to Carole for her enthusiasm and unwavering support over the last four and a half years.

Acknowledgements

I would like to thank my entire committee from whom I have learned so much over the last two years. I would like to thank Ed Perfect, my advisor at the University of Tennessee, for his support and contributions. He always had an open door and for that I am grateful. I would like to thank Melanie Mayes, my advisor at Oak Ridge National Laboratory, for giving me the opportunity to perform this work. I would like to thank Larry McKay for his contributions to the proposal.

I owe a great deal of gratitude to many of the people in the Environmental Sciences Division of Oak Ridge National Laboratory. Guoping Tang provided help with numerical and analytical modeling. Tonia Mehlhorn and Xiangping Yin provided assistance with a variety of analytical instruments. Jana Phillips and Jonathan Reagan helped me navigate through many of the hoops associated with this research. Scott Brooks provided many insightful suggestions to this work.

Finally, I would like to thank the Department of Energy's Environmental Remediation Science Program for funding this work.

Abstract

This study is aimed at understanding the physical and chemical effects that changes in water content have on uranium leaching in sediment containing gravel. It was hypothesized that leaching will be more efficient under unsaturated conditions because flow will be restricted to the smallest pores and will have the most contact with the uranium contaminated sediment. Under saturated conditions, a large portion of the flow will bypass the < 2 mm material, and in turn not come into contact with uranium contaminated material. Batch adsorption and desorption experiments were performed on < 2 mm ERDF sediment to determine the linearity and reversibility of sorption processes and to aid in the interpretation of the leaching experiments. Results of the desorption experiments on aged, contaminated sediments show that the mass percent of sorbed U(VI) released to solution decreased as the sorbed concentration of U(VI) decreased. The opposite trend was observed on freshly contaminated sediments. This indicated that aging increased U(VI) affinity for the solid phase and was attributed to either the crystallization of calcite, which incorporated a portion of the sorbed U(VI) as it crystallized, or the presence of voids in basaltic lithic fragments accessed by diffusion. Column leaching experiments were performed at two water contents on artificially contaminated sediment collected from the Department of Energy's (DOE) Hanford Site, Washington state. The sediment contained 81.3% gravel (> 2 mm) by mass. Non-reactive tracers were well fit with the convection-dispersion equation (CDE) at both high and low water contents indicating physical equilibrium. The column experimental data were fitted to an analytical solution to the CDE; the results of the modeling show an increase in the distribution coefficient ($Kd_{effective}$) with decreasing water content. Several potential explanations for this trend were proposed; one is

based on a physical effect in which solute exposure to reactive surfaces changes as a function of water content and the others are based on results of the batch desorption experiments. This work has important implications for the Hanford Site where there is ongoing research regarding the persistence of U(VI) in the vadose zone and underlying aquifer.

Table of Contents

Section		Page
1.	Introduction	1
	1.1 Overview	2
	1.2 Hanford Area Geology	3
	1.3 Uranium Chemistry	4
	1.4 Uranium(VI) Sorption	5
	1.5 Unsaturated Transport	9
	1.6 Effect of Gravel on Physical Hydrologic Properties of Soil	16
	1.7 Effect of Gravel on Solute Transport	19
	1.8 Effect of Gravel on Solute Partitioning in Batch Experiments	19
	1.9 Effect of Particle Scale Heterogeneity on Solute Transport	21
	1.10 Goals	22
	1.11 Objectives	23
2.	Materials and Methods	25
	2.1 Characterization of Sediment	26
	2.2 Sediment Contamination	26
	2.3 Batch Adsorption Experiments	29
	2.4 Desorption Experiments	31
	2.5 Column Leaching Experiments	32
	2.6 Column Hydrologic Properties	36
	2.7 Estimation and Solute Transport Parameters	39
3.	Results and Discussion	47
	3.1 Distribution Coefficient Values Determined from Sediment Contamination	48
	3.2 Batch Adsorption Experiments	49
	3.3 Desorption Experiments	50
	3.4 Column Physical and Hydrologic Properties	56
	3.5 Non-Reactive Tracer Modeling	57
	3.6 Distribution Coefficient Values Determined from Leaching Experiments	60
4.	Conclusions and Suggestions for Future Research	70
	References	75
	Appendix	90
	Vita	123

List of Tables

Page

Table 1. Mineralogy of 200W Area Hanford flood deposits (from Pace et al., 2003)……. 91

Table 2. Grain size distribution of repacked columns……... 91

Table 3. Chemical composition of synthetic groundwater (SGW)……92

Table 4. Measured distribution coefficients from contamination event…… 92

Table 5. Results of ANOVA examining the difference in distribution coefficients between sediment contaminated with two different U(VI) solution concentrations…... 93

Table 6. Results of ANOVA examining the difference in the pH of the supernatant of the two groups of sediment contaminated with different U(VI) solution concentrations…..93

Table 7. Linear sorption and Freundlich isotherm fits to the batch adsorption experiments…….94

Table 8. Distribution coefficients determined on sediment from the batch desorption experiments……..... 94

Table 9. Mass percent of U(VI) desorbed from sediment samples Y1 and Y2 after each of three desorption equilibrations……..95

Table 10. Mass percent of U(VI) desorbed from sediment samples contaminated with 15.1 and 31.5 ug/l U(VI) after each of three desorption equilibrations…….96

Table 11. Mass percent of U(VI) desorbed from sediment samples contaminated with 71.8 and 80.1 ug/l U(VI) after each of three desorption equilibrations…….97

Table 12. Columns A and B physical properties……... 98

Table 13. Transport parameters determined from non-reactive tracer breakthrough…… 98

Table 14. Relative saturation at high and low water contents and distribution coefficients determined for each experiment using the leached mass ratio approach……...99

Table 15. Cation concentrations for select effluent samples from columns A and B……99

List of Figures

Page

Figure 1. General representation of stratigraphic units within the Central Pasco Basin (from Bjornstad, 2002)……..101

Figure 2. U(VI) speciation as a function of pH and carbonate concentration (from Peterson, 2008)……... 102

Figure 3. U(VI) speciation as a function of calcium, calcium and magnesium, and calcium and phosphate concentrations in the top, middle, and lower panels, respectively (from Peterson, 2008)…..……... 103

Figure 4. Average grain size distribution curve of two grab samples from Core 2-26, 300 Area, Hanford, WA……104

Figure 5. Modified constant head setup for measuring saturated hydraulic conductivity on repacked sediment cores……... 104

Figure 6. A schematic illustration of the traditional approach to modeling contaminant transport in column experiments subject to a plug input concentration……105

Figure 7. A schematic illustration of the leached mass ratio approach to modeling U(VI) breakthrough……. 105

Figure 8. Results of batch adsorption experiment at 48 hours…….106

Figure 9. Results of batch adsorption experiment at 96 hours…….106

Figure 10. Results of batch adsorption experiment at 168 hours…….....107

Figure 11. Results of batch desorption experiment following the first desorption equilibration……... 107

Figure 12. Results of batch desorption experiment following the second desorption equilibration……... 108

Figure 13. Results of batch desorption experiment following the third desorption equilibration……... 108

Figure 14. Sediment sample Y1 sediment/solution equilibrated state following adsorption and three desorption washes …….. …… 109

Figure 15. Sediment sample Y2 sediment/solution equilibrated state following adsorption and three desorption washes…… 110

Figure 16. The mean sediment/solution equilibrated state of three sediment samples contaminated with 15.1 ug/l U(VI) following adsorption and three desorption washes…….. 111

Figure 17. The mean sediment/solution equilibrated state of three sediment samples contaminated with 31.0 ug/l U(VI) following adsorption and three desorption washes…….. 111

Figure 18. The mean sediment/solution equilibrated state of three sediment samples contaminated with 71.8 ug/l U(VI) following adsorption and three desorption washes…….. 112

Figure 19. The mean sediment/solution equilibrated state of three sediment samples contaminated with 80.1 ug/l U(VI) following adsorption and three desorption washes…….. 112

Figure 20. Average $\theta(h_c)$ relationship for column B and model fitted relationship using TrueCell software……..…..113

Figure 21. U(VI) concentrations of solution collected from column A (top) and B (bottom) while measuring the average $\theta(h_c)$ relationship of each column…….114

Figure 22. Column A bromide curve and model fit using the CDE…… 115

Figure 23. Column B bromide curve and model fit using the CDE…… 116

Figure 24. Column B PFBA curve and model fit using the CDE……117

Figure 25. Column A leaching curve and estimated water content……. 118

Figure 26. Column B leaching curve and estimated water content……. 119

Figure 27. Column A experimental leached mass ratio and model fit at high water content….. 120

Figure 28. Column A experimental leached mass ratio and model fit at low water content….. 120

Figure 29. Column B experimental leached mass ratio and model fit at high water content….. 121

Figure 30. Column B experimental leached mass ratio and model fit at low water content….. 121

Figure 31. Depiction of solute pore regime under high water content (a) and low water content (b)…… 122

Figure 32. Smaller scale conceptual depiction of the effect of water content on solute transport…… 122

List of Abbreviations

Kd_{Cont}	Point estimate distribution coefficient determined on single sediment samples from the contamination event.
Kd_{batch}	Distribution coefficient determined on sediment in the batch experiment. Batch experiments were performed on 15 samples; 3 repetitions at each of 5 concentrations. The distribution coefficient was taken as the slope of the linear sorption isotherm.
$Kd_{des\ Cont}$	Point estimate desorption distribution coefficient determined on sediment from the contamination event following equilibration with clean synthetic groundwater.
$Kd_{des\ batch}$	Desorption distribution coefficients determined on all 15 samples from the batch experiment determined by equilibrating the batch sediments with clean synthetic groundwater. The distribution coefficient was taken as the slope of the linear sorption isotherm.
$Kd_{mass\ avg}$	Distribution coefficient determined by taking the average Kd_{Cont} of the < 2 mm sediment packed into each column and multiplying by the mass percentage of sediment < 2 mm in the column.
$Kd_{effective}$	Distribution coefficient determined from fitting column leaching experimental data to analytical solution to the convection-dispersion equation.
DOE	Department of Energy
ERDF	Environmental Restoration Disposal Facility
PNNL	Pacific Northwest National Laboratory
CDE	Convection Dispersion Equation
MIM	Mobile-Immobile Model
LMR	Leached Mass Ratio
ANOVA	Analysis of Variance
SSQ	Sum of Squares of the Residuals

1. Introduction

1.1 Overview

Uranium contamination is a common occurrence among Department of Energy (DOE) facilities (Riley and Zachara, 1992). One such site is located in the 300 Area of the DOE's Hanford Reservation near Richland, Washington. The area was formerly the site of a nuclear fuels processing facility. Uranium waste infiltrated the soil surface from 1941-1973, resulting in contamination of the vadose zone and a contaminant plume in the groundwater. The water table below the 300 Area is hydraulically connected to the Columbia River and the water table fluctuates with stage changes in the river. The episodic saturation of the contaminated vadose zone sediments results in complex effects on uranium mobility which are not easily predicted. The contamination in the vadose zone and underlying aquifer has proven to be a continual source of uranium in the groundwater with relatively little change in concentration over time. Therefore, knowledge of the geochemical and hydrologic controls of uranium migration in the subsurface is necessary to accurately predict contaminant migration.

Numerous researchers have attempted to quantify and describe uranium sorption and transport phenomena in laboratory studies in order to better predict contaminant migration at the field scale. One of the most commonly used parameters in contaminant transport studies is the partition coefficient, also known as the distribution coefficient (Kd). This parameter is used to quantify the partitioning of a chemical between the solid and liquid phases. There have been several studies aimed at determining the effect imparted by changes in water content on the distribution coefficient of uranium (Lindenmeier et al., 1995; Kaplan et al., 1996) and the transport of uranium (Gamerdinger et al., 2001a, 2001b; Wellman et al., 2008a, 2008b). These experiments were performed on the < 2 mm fraction of material, which may not represent the

material found at many uranium contaminated sites. Recently, Liu et al. (2008), in comparing uranium desorption from saturated field-textured sediment in flowing columns to its < 2 mm portion, found that the kinetics of release varied between the two groups of sediment and that predictions of release in the field textured sediment required knowledge of the physical transport properties of the uranium-containing mass fraction and the field textured sediment. To accurately predict contaminant migration at the field scale, it is necessary to understand the effects that larger particle sizes (> 2 mm) have on uranium sorption processes under variably-saturated conditions. This study will attempt to describe the chemical and physical effects that the presence of coarse material has on uranium transport under variably-saturated conditions by performing leaching experiments on uranium contaminated repacked sediment cores. In accordance with the USDA soil classification system, references to coarse material, gravel, or stones will refer to material > 2 mm in diameter and references to fine material will be considered sediment < 2 mm in diameter.

1.2 Hanford Area Geology

The Hanford Site is located on the Columbia Plateau in southeastern Washington State, north of Richland, Washington. It lies within the central Pasco Basin in the Columbia Basin physiographic province. Bedrock within the basin is composed of the Columbia River Basalt Group. Several significant sedimentary units overlie the Columbia River Basalts and make up the stratigraphy below DOE's Hanford Reservation. The lowest unit, the Ringold Formation, is composed of unconsolidated fluvial-lacustrine deposits of the Miocene-Pliocene. The Pleistocene age Cold Creek Unit, also referred to as the Plio-Pleistocene unit, roughly 70-100 m depth, overlies the Ringold Formation and generally forms the boundary between the saturated

and unsaturated zones. The Cold Creek Unit is composed of sands, silts, and clays cemented with pedogenic $CaCO_3$. The upper portion of the vadose zone is referred to as the Hanford flood deposits. The Hanford flood deposits are limited in spatial extent, and as such, are not considered a formal geologic formation, though they are distinguishable from the underlying Cold Creek Unit. The Hanford flood deposits are late Pleistocene in age and composed of fluvial, colluvial, and eolian deposits resulting from the periodic breaching of ice dams of Lake Missoula and other glacial lakes. The Hanford flood deposits consist of unconsolidated boulder to pebble sized gravel, silty sand, and silt. Most often the Hanford flood deposits are composed of a clast supported structure with the matrix being composed of coarse to fine sand. Holocene age deposits of sand, silt, and gravel up to 5 m thick overlie the Hanford flood deposits (Bjornstad, 2002). A general representation of the stratigraphy of the material underlying the Hanford Site can be found in Figure 1 located in the Appendix.

1.3 Uranium Chemistry

Uranium geochemistry is dominated by two valence states: hexavalent(VI) and tetravalent(IV). Under oxidizing conditions uranium exists in the hexavalent form as the uranyl ion UO_2^{2+}. The uranyl ion converts to the uranous ion (U^{+4}) under reducing conditions and is insoluble. The uranyl ion is soluble and is the form of uranium of most interest as a contaminant in hydrologic systems (McKinley et al., 2007). The uranyl ion reacts with ions in solution to form various aqueous species. The formation of these species is quite complex and is dependent on the ions present in solution, pH, and solubility of the various aqueous species. The aqueous species that form vary in charge, size, and chemical bonding behavior. The majority of U(VI) aqueous species are composed of carbonate, hydroxide, or phosphate complexes (Peterson, 2008). The

mobility of U(VI) is controlled by multiple complexation, adsorption/desorption, and precipitation/ dissolution reactions of the various species. In general, the cationic form UO_2^{2+} is immobilized by negatively charged mineral surfaces such as metal oxides, aluminosilicates, and carbonates through adsorption or precipitation (McKinley et al., 2007).

Thermodynamic data describing U(VI) aqueous speciation under variable chemical conditions can be performed using a variety of geochemical speciation modeling programs. Peterson et al. (2008) performed these computations using stoichiometries and stability constants assembled and reviewed by Grenthe et al. (1992, 1995) and Guillaumont et al. (2003). The results of their computations can be found in Figures 2 and 3. Peterson et al. (2008) note several of the most significant aspects of the aqueous speciation calculations: (1) the neutral to negative charge of the various species, (2) the minimum presence of the free uranyl ion, (3) the prevalence of carbonate as a complexing ion, and (4) the pH control on speciation.

1.4 Uranium(VI) Sorption

Understanding the fate and transport of contaminants in the subsurface is essential for protecting water resources. Numerical modelers who attempt to predict the movement of contaminants use various parameters in their models to quantify key physical and chemical characteristics of the subsurface media. The distribution coefficient, which describes chemical partitioning in sediment/solution mixtures, can be determined by dividing the chemical sorbed concentration (mass of contaminant/mass of soil) by the chemical concentration in solution (mass of contaminant/volume of solution). Contaminants that have a strong affinity for the solid phase will have a high Kd, and contaminants that do not have a strong affinity for the solid phase will have a low Kd. The traditional method of measuring a distribution coefficient for a

chemical/sediment mixture is through the use of a batch adsorption experiment. Batch experiments have been performed on U(VI)/Hanford sediment mixtures in order to determine distribution coefficients for comparison to those derived from column studies (Barnett et al., 2000; Gamerdinger et al., 2001a, 2001b; Wellman et al., 2008b), and to examine the effects of various sediment (Waite et al., 1994; Moyes et al., 2000; Um et al., 2008) and solution (Kaplan and Serne, 1995; Kaplan et al., 1997; Zheng et al., 2003; Um et al., 2005, 2007; Stewart et al., 2010) properties on U(VI) adsorption. The results of these experiments vary greatly (0 - > 1000 ml/g) due to differences in the chemistry of the solution and the mineralogy of the sediment used. The most important factors related to solution chemistry affecting distribution coefficient values on U(VI)/Hanford sediment mixtures include solution pH, calcium and carbonate concentration, solution contact time, and U(VI) concentration in solution.

Calcium, carbonate concentration, and pH play significant roles in U(VI) geochemistry. Due to the positive charge of the uranyl ion (UO_2^{2+}) and the ubiquitous presence of dissolved CO_2 in soil and ground waters, a number of stable anionic and neutral calcium carbonate complexes form at pH values above 6 (Um et al., 2005; Kaplan et al., 1996; Zheng et al., 2003; Dong and Brooks, 2006). The presence of these anionic to neutral complexes and the solution pH greatly decrease the degree of U(VI) sorption compared to the UO_2^{2+} cation. This is because the surface charge of most minerals becomes negative as pH increases. Due to the above factors, sorption increases from pH 3.5-7, but drops to almost zero by pH 8-9 (Barnett et al., 2000).

Solution contact time refers to the amount of time soil is exposed to a solution. There is a minimum amount of time required for an adsorbate to come into equilibrium with an adsorbent. This time will vary with soil type and solute. If this time is not achieved, then the maximum

mass of adsorbate that a soil can sorb will not be known. Estimates of the amount of time required to reach equilibrium are important in modeling solute transport. In some cases, a large initial mass of solute will sorb followed by small increments over much longer time periods (Barnett et al., 2000). Reports of the time required to reach steady-state vary widely. Guo and Wu (2009) report that one hour is sufficient to reach U(VI) sorption steady-state. Giammar and Hering (2009) found that adsorption and desorption of U(VI) on synthetic goethite reached equilibrium within minutes to hours. On the other hand, Kaplan et al. (1996) showed that Kd values determined from a batch experiment consistently increased over the 13 month duration of the experiments. Several explanations were given: (1) new sorption sites were created as calcite recrystallized and buried sorbed U(VI), (2) U(VI) diffusion increased contact with reactive sites, (3) the shaking process broke particles resulting in additional sorption sites, (4) or microbial populations increased throughout the study period resulting in more sorption sites. The differences in solution contact time on U(VI) sorption may be attributed to differences in the sorbent and in experimental procedures (Guo and Wu, 2009).

In a flowing column experiment, contact time is a function of the velocity of the advecting solution. Residence time in a flowing column experiment refers to the amount of time the solution spends in contact with the soil. An assumption in using the distribution coefficient in modeling solute transport is that sorption is instantaneous with respect to groundwater velocity. This essentially means that the soil is exposed to the solution for an amount of time adequate to reach equilibrium between the two phases. Lindenmeier et al. (1995) report variations in U(VI) retardation factors measured in a column experiment when residence time increased from 0.6 hours to 5.9 hours. In situations in which the solute velocity is so high that equilibrium cannot

be attained between the solute and the soil, a kinetic model may be more appropriate in describing solute sorption.

The U(VI) concentration in solution may affect Kd values. The linear sorption model holds that as solution concentration increases, the sorbed phase increases. This assumes that there are unlimited sorption sites in a given sample or mass of soil. In fact, there must be an upper limit to the amount of contaminant a soil can hold. The important question when modeling U(VI) transport using a Kd value is whether these upper limits of solution concentration are reached. Kaplan et al. (1996) found that the linear sorption isotherm model was appropriate for Hanford Formation sediments from the 200 Area at least up to100 ug/l. Um et al. (2005) observed linear sorption on Hanford Site 200-UP-1 < 2 mm sediments up to 1190 ug/l. These results are supported by Serne et al. (2002) who report linear sorption up to 3000 ug/l. Other researchers have found similar results within these ranges (Gamerdinger et al., 2001a, 2001b).

Sediment mineralogy will affect distribution coefficient values of U(VI). It is generally accepted that iron oxides are the most reactive sorbents of U(VI) in the subsurface at Hanford. Barnett et al. (2000) investigated U(VI) adsorption to three sediments from various geographical locations. The three soils displayed similar pH-dependent adsorption trends. The trends were attributed to similar iron oxide contents and indicated that the iron oxides were controlling U(VI) adsorption to the sediments. This is supported by the work of Um et al. (2008) who report increases in U(VI) sorption as iron oxide content increased in Hanford Formation sediments. When iron oxides were not present, sorption of U(VI) was more associated with phyllosilicate minerals (Um et al., 2008). Therefore, the presence of iron oxides, and to a lesser extent phyllosilicates, will control the removal of U(VI) from contaminated solutions.

In general, batch studies have been performed examining the uptake of U(VI) from contaminated solutions and a distribution coefficient determined based on the adsorption of U(VI). The results of these batch studies are then compared to both adsorption and desorption of uranium in pulse type column studies. It is generally assumed that sorption is not only linear but reversible. This assumption may not be valid as desorption hysteresis has been noted for several contaminants. Fuhrmann et al. (1997) examined the release of U(VI) from experimentally contaminated sediment. Approximately 35% of the sorbed U(VI) was released after mixing with clean seawater and decanting three times. Guo and Wu (2009) performed desorption experiments by exchanging part of the supernatant with background electrolyte solution and measuring the new steady-state value. Their desorption isotherms show a hysteretic effect in that equilibrium was reached at a higher sorbed concentration and lower concentration in solution than during adsorption. Zheng and Wan (2005) examined the effect that ionic strength and the volume:mass ratio have on the release of U(VI) from contaminated sediments. Increasing either ionic strength or the volume:mass ratio increased the release of U(VI) to solution, with increases in the volume:mass ratio being more effective.

1.5 Unsaturated Transport

The effect of water content on U(VI) Kd values is an important physical phenomenon to consider in contaminant transport studies. Most of the contamination in Hanford is located in the unsaturated zone. Therefore, to reach the water table, where the contaminant has a greater potential for migration, it must move through this variably-saturated region. An important factor controlling the ability of contaminants to move or migrate through the soil is the hydraulic conductivity (K). Hydraulic conductivity is a property of porous media and the fluid moving

through it which describes the media's ability to transmit the fluid. It is controlled in complex ways by the size and orientation of pores, which are in turn, controlled by the size and degree of sorting of the soil particles. Degree of sorting refers to the distribution of grain sizes within a given volume of soil. A soil with a uniform grain size is said to be well-sorted and a soil with a large variety of particle sizes is considered poorly-sorted. The volume of water per unit time (Q) moving through a given cross-sectional area (A) under steady-state saturated conditions is termed the flux (q) and is defined by Darcy's Law as

$$\frac{Q}{A} = q = -K\frac{\partial h}{\partial L} \tag{1}$$

where L is length and h is hydraulic head. The term $\frac{\partial h}{\partial L}$ is the head gradient and describes the change in head over some length (L). Head values are a function of both pressure head (p) and elevation head (z), where elevation head is the height above a given datum. Pressure head is positive under saturated conditions and is equal to the height of the overlying water column. As a soil desaturates, part of the pores fill with air and some are filled with water. The air becomes a barrier to flow and therefore affects the soil's ability to transmit water. As a result, under unsaturated conditions, hydraulic conductivity decreases as a function of water content. The presence of air under unsaturated conditions causes tension at the soil-water interface. This tension is termed the matric potential (ψ). The matric potential is always negative and decreases (becomes more negative) with decreasing water content. When osmotic potential and electrochemical potential are assumed to be uniform through the soil, the sum of the matric potential and the elevation head determines the total soil water potential (φ). Whereas the steady-state advective flux in the saturated zone is the product of the saturated hydraulic

conductivity and the head gradient, the advective flux in the unsaturated zone is the product of the unsaturated hydraulic conductivity as a function of water content ($K(\theta)$) and the soil water potential gradient ($\frac{\partial \varphi}{\partial L}$).

As a soil desaturates, the largest pores are the first to drain. As the soil continues to desaturate, progressively smaller pores will drain. Under saturated conditions, the largest pores are the most conductive. Therefore, as the largest pores drain they lower the advective flux dramatically, not only because they are not conducting water but because water must travel a greater distance around empty pores. The degree to which the flux decreases as a function of water content is related to of the pore size distribution. In a well-sorted coarse grain soil, there is a near uniform pore size distribution of larger sized pores. As this soil desaturates it will initially undergo a large drop in advective flux. Rather than traveling through the pores, the remaining solution may travel as film flow along the grains, thereby greatly decreasing the flux. In a well-sorted fine-grained soil, many of the pores will be smaller in size. Therefore, as this soil desaturates many of the pores will still conduct water and the flux will not decrease as rapidly. Therefore, the flow regime under increasingly unsaturated conditions is a function of pore size and will differ greatly between coarse and fine-grained material. In poorly-sorted soils, the effect of desaturation on flux can be quite complex and is highly dependent on the distribution of grain sizes.

Another property of soil relevant to contaminant transport is the soil water retention curve (SWRC). The SWRC relates the volumetric water content (θ) of the soil to the matric potential (ψ) or to the capillary pressure head (h_c), where h_c is always positive and is equal to $-\psi$. If a soil is initially saturated, all of the pores are filled with water. As capillary pressure is raised, the soil will begin to drain until it reaches a new volumetric water content at equilibrium with capillary

pressure. At some point an increase in capillary pressure will not result in any further loss of water. This occurs because the water is so strongly held by the soil that no capillary pressure can remove it and is referred to as the residual water content. As with hydraulic conductivity, the volumetric water content at a given capillary pressure is a function of the pore size distribution of the soil. For a well-sorted soil, the pore size distribution is nearly uniform, and the range in capillary pressure over which water content will change is quite small (i.e. a small change in capillary pressure will result in a large change in water content and the corresponding SWRC will be quite steep). In a poorly-sorted soil, there are a wide range of pore sizes and small changes in capillary pressure will generally result in small changes in water content (i.e. the curve will not be steep). Several empirical models exist which relate the volumetric water content to the capillary pressure (Brooks and Corey, 1966; van Genuchten, 1980). The $\theta(h_c)$ relationship can be established by imposing several capillary pressures on a soil sample and measuring the resulting volumetric water content. A curve can then be fit to the data using one of the previously mentioned models. If the soil is initially saturated, the curve is termed a drying curve. If the water is added to an initially dry soil, the curve is termed a wetting curve. The drying and wetting curve will generally be different for the same soil. This is called hysteresis. If the sample is not initially completely wet for a drying curve or completely dry for a wetting curve, the resultant curves will fall between the main drying and wetting curves and are called scanning curves.

The preceding methods provide an average relationship between water content and capillary pressure head for the entire column and may not represent the relationship at a specific point within the column due to vertical variations in water contents (Dane et al., 1992). This is due to

the fact that the water content associated with the capillary pressure imposed at a physical point within the column is not the same as the average water content for the column at that capillary pressure. Liu and Dane (1995) developed a relationship between the average $\theta(h_c)$ relationship obtained using a pressure cell and the $\theta(h_c)$ relationship at a physical point in the cell where the pressure is measured. This relationship can be used to obtain Brooks-Corey parameters where the pressure is measured in the cell if the $\theta(h_c)$ relationship of the entire cell is known. Jalbert et al. (1999) developed the software package TrueCell which allows the user to determine $\theta(h_c)$ relations at a given point by entering average pressure cell data and employing the relationships described in Liu and Dane (1995).

Some researchers have proposed the presence of a physical nonequilibrium in the flow regime under both saturated and unsaturated conditions (Wierenga and van Genuchten, 1989; Gamerdinger and Kaplan, 2000). In modeling the physical nonequilibrium system, also termed the two-region model, or the mobile-immobile model (MIM), the geologic medium is conceptualized as being composed of two separate, but interacting domains; the mobile region and the immobile region (van Genuchten and Wierenga, 1976). However, in actuality there is likely a continuum between the solution that is mobile and solution that is completely immobile. In the mobile-immobile model, a portion of the soil water becomes disconnected from the flow regime and is termed the immobile water (θ_{im}). This immobile water is generally found in micropores, the rock matrix, or within aggregates. The remaining portion, composed of the macropores and inter-aggregate regions, through which flow occurs, is termed the mobile water (θ_m). Solute exchange within the immobile domain is conceptualized as being strictly through diffusion in models. Under these conditions, the immobile region becomes a sink for

contaminants and the mobile region may allow accelerated transport. As the concentration of contaminants decreases in the mobile region, the immobile region may become a source for contaminants into the mobile region. In this case, long after the original source of contamination has disappeared, the contaminants stored in the immobile region provide a source of contamination to the mobile region. The presence of immobile water results in both faster arrival times and longer contaminant residence times. Understanding the presence of immobile water and the effect imparted by variations in the pore size distribution are important for modeling contaminant transport under unsaturated conditions.

The degree of saturation at the Hanford site is controlled not only by precipitation events, but also by the seasonal and dam controlled fluctuations in the Columbia River. During high stage, the water table rises, saturating sediments which remain unsaturated during the rest of the year. As the river stage lowers, so does the water table, desaturating the potentially contaminated sediments. The effect of desaturation on Kd values in fine-grained soil (< 2 mm) has been studied with inconclusive results. Lindenmeier et al. (1995) performed unsaturated column and unsaturated flow apparatus (centrifuge) tests on uncontaminated Trench 8 sediments from the 200 West Area of the Hanford Site using spiked synthetic groundwater. Results of these tests indicate that Kd values decreased with increasingly unsaturated conditions. Kaplan et al. (1996) repeated the experiments with similar results. A second set of experiments were performed using more fine-grained material. In these experiments, as degree of saturation decreased U(VI) Kd values increased. The results of these experiments were attributed to the mineral distribution and the extent to which the fine material formed hydraulically connected pores. Therefore, as

with hydraulic conductivity, variations in distribution coefficients seem to be affected in complex ways by the soil's pore size distribution.

Recently, several researchers have reported on the effect that flow regime has on transport of U(VI) under unsaturated conditions. Gamerdinger et al. (2001a, 2001b) investigated the effect of water content and two-region flow on U(VI) sorption. Experiments were performed on a silt loam and mixtures of fine and coarse sand. They found that, as water content decreased in the silt loam, areas of immobile water formed. This effectively increased the velocity in the mobile region, resulting in a decrease in sorption. Results for the silt loam indicate that availability of sorption sites was not affected by changes in water content. However, in the coarse sand, a larger percentage of immobile water was present at 12% saturation than at 28% saturation and the Kd was less at 12% saturation, indicating that some of the sorption sites were disconnected from the flow regime. The overall effect of immobile water was to increase velocity in the mobile region and in some cases decrease access to the reactive sites, thereby lowering sorption.

Similar results were reported by Wellman et al. (2008a) who compared results of uranium batch experiments on mixtures of silt loam and sand to those of unsaturated transport experiments containing the same sediment mixtures. In transport experiments where silt loam composed 10% of sediment, there was an exclusion of tracers, presumably due to immobile water, and a decrease in U(VI) sorption. In this case Kd was less than predicted from batch experiments. Where silt loam composed 30% or 70% by mass, there was no exclusion of tracers, and the Kd was greater than predicted by the batch experiments. These results indicated that when the soil is dominated by sand (i.e. 10% silt), the silt fraction is excluded from the mobile domain as the soil desaturates, and sorption is less than expected. When the soil is dominated by silt, under

unsaturated conditions, flow occurs as matrix flow through the fine material, and sorption is greater than expected. Wellman et al. (2008b) performed desorption experiments on contaminated Hanford Formation sediment under unsaturated conditions. They found that decreasing water content resulted in a reduction in access to reactive sites, as well as variations in average pore water velocity.

1.6 Effect of Gravel on Physical Hydrologic Properties of Soil

The large percentage of gravels that make up the Hanford sediment are likely to have considerable impact on both hydrologic and geochemical processes related to U(VI) migration. As was mentioned previously, contaminant transport is affected in complex ways by the distribution of pores within a soil, which is a function of the degree of sorting. The Hanford Formation is composed of heterogeneous flood deposits. These deposits are composed of various mixtures of clay, silt, sand, and gravel. The effect of gravel on soil hydrologic and geochemical properties will depend on a number of factors: (1) the volumetric percentage of gravel, (2) the orientation and location of the gravel, (3) the size of the gravel, (4) the porosity of the gravel, (5), and the mineralogy (Cousin, 2003).

Intuitively, the volume of gravel in a given soil will affect the hydrologic properties of the soil. As will be seen in the discussion below, how changes in gravel volume content affects soil water transmitting properties is quite complex. Peck and Watson (1979) presented an equation which relates the hydraulic conductivity of gravel-containing soil to that of the soil alone by taking into account the volume of the gravel. Bouwer and Rice (1984) and Dunn and Mehuys (1984) obtained reasonable results using this equation. However, they achieved better results when taking into account the void ratio of the gravel-containing soil and that of the soil alone.

Therefore, the volume of the voids created by the presence of coarse material may be more important than the volume of the gravel itself.

The orientation and location of gravel within the soil can have a strong effect on the hydrologic properties of the soil. Studies generally distinguish between gravel found at the soil surface and those found below the surface. In describing gravel below the soil surface, Mehuys et al. (1975) contend that gravel would reduce the soil's porosity and restrict overall water movement by reducing the cross-sectional area for flow and by increasing the tortuosity of the system. In studying saturated hydraulic conductivity of soil containing various amounts of coarse fragments by mass, Ravina and Magier (1984) found that increasing rock fragment content decreased hydraulic conductivity. This is most likely due to decreasing the cross sectional area available for flow. The soils used in the study were then compacted and hydraulic conductivity measurements repeated. The result was an increase in hydraulic conductivity with increasing rock content. This was attributed to the fact that as rock fragment percent increased, the volume of large pores preserved increased following compaction. This hypothesis is supported by Verbist et al. (2009) who found that stones had a positive influence on infiltration, which was attributed to an increase in porosity due to the stone fragment content. These observations are also supported by the work of Poesen and Lavee (1994) who found that larger particles prevent smaller ones from compacting, thereby preserving higher porosities. However, Verbist et al. (2009) found that at the highest rock fragment contents, the rocks could limit infiltration. This is supported by Russo (1983) who found that as the stone content increased with depth in a desert soil, the saturated hydraulic conductivity decreased. Therefore, gravel may act to reduce

hydraulic conductivity by reducing the area available for flow, or increase hydraulic conductivity by acting to create and preserve higher porosities.

In addition to the effect gravel content has on hydraulic conductivity, gravel size is also likely to affect the water holding capacity of soil. Small rock fragments are generally more weathered than large fragments, and in turn more porous. The water-holding capacity of rocks is directly related to the porosity. It must then be inferred that the size and degree of weathering of the rocks will affect the hydrologic properties of soil containing rocks. The water-holding capacity is also dependent on the mineralogy. For instance, the gravimetric moisture content of flintstone at saturation is only 0.2% whereas chalk is 91.7% (Poesen and Lavee, 1994). Cousin et al. (2003) attribute differences in water holding capacity of two soils containing limestone rocks to variations in weatherability and porosity of the limestone.

In studying the soil water retention properties of soils containing stones, Russo (1983) found that under a given capillary pressure the volume of water retained by the soil decreased with increasing stone content. Brakensiek and Rawls (1994) report a study in which at lower capillary pressure heads the volumetric water content was inversely proportional to the mass of coarse fragments. However, at much higher capillary pressure heads the water content was not related to the amount of coarse material in the soil. Ravina and Magier (1984) determined water retention curves of gravelly mixtures. They found that the coarse material preserved macropores in the soil, which are the first to drain under low capillary pressure. Therefore, the coarse material affects the permeability and soil water capacity at low capillary pressure and high water contents, but becomes less important as water content is lowered and capillary pressure increases. This is supported by the work of Mehuys (1975) who found that stones had no effect

on hydraulic conductivity at more negative capillary pressures when comparing unsaturated soil columns of stony soil and soil in which the stones had been removed.

1.7 Effect of Gravel on Solute Transport

Studies of the effect of gravel on solute transport are more limited in scope. In general it seems that the presence of gravels increases the tortuosity of flowpaths thereby increasing dispersion. Bouwer and Rice (1984) saw an 18 fold increase in dispersivity in a boulder-sand column when compared to the sand alone. The presence of immobile water was indicated by the results of Butcher et al. (1995), who found that a Cl^- pulse through an unsaturated stony column only traveled through part of the cross sectional area of the column used in their experiment, with diffusion of Cl^- possibly occurring into adjacent areas.

Liu et al. (2008) compared U(VI) desorption from field textured sediment (containing gravel) to its fine fraction (< 2 mm) by performing leaching experiments on saturated repacked cores. Desorption of U(VI) from the field-textured sediment was slower than from the fine fraction. Results of numerical modeling of the experimental data indicate that the difference in release rates was due to dilution of sorbed U(VI) and sorption sites by the gravel, multiple sorption sites with varying kinetic release rates, and two-region flow. This work indicates that gravel may play both a physical and geochemical role in the transport of U(VI) in the surbsurface.

1.8 Effect of Gravel on Solute Partitioning in Batch Experiments

Laboratory studies of solute transport and soil/solution chemical partitioning are generally performed on the < 2 mm fraction of material. There are several reasons for not including larger particles when measuring the chemical partitioning between soil and solution. Reactive capacity

of soil is related to the specific surface area and the < 2 mm material has considerably more surface area per unit mass than the > 2 mm fraction (Hillel, 1980). In many soil classification schemes 2 mm is the divide between soil and gravel. In addition, there is a difficulty in accommodating the > 2 mm fraction in batch and solute transport studies. The results of such studies, when applied to modeling contaminant transport at the field scale in a geologic medium containing material > 2 mm, could lead to erroneous results.

Kaplan et al. (2000) attempted to quantify the effect the gravel portion had on Sr distribution coefficient values measured in a batch experiment using soil from the 200 East Area of the Hanford Site. Three correction values were proposed which would allow the quantification of the Kd for soil containing gravel (Kd_{Total}) to be derived from batch experiments performed on the material < 2 mm ($Kd_{< 2mm}$). These corrections were based on the assumptions that: (1) the gravel had no sorptive capacity and Kd_{Total} was the product of the mass percentage of < 2 mm sediment fraction and the $Kd_{< 2mm}$, (2) the Kd_{Total} was a composite of the $Kd_{< 2mm}$ and $Kd_{> 2mm}$ based on the mass percentage of each fraction, (3) and a correction based on surface area. Corrections (1) and (3) underestimated Kd_{Total} by 10-39%. Correction (2) provided the best estimate, overestimating Kd_{Total} by 3-5%. Their results indicate that the > 2 mm fraction has some sorptive capacity.

Um et al. (2009) built on this work by performing similar experiments on 200 East Area sediments using three radionuclides: ^{99}Tc, ^{238}U, and ^{237}Np. Kd values were determined using batch experiments on the bulk sediment (containing gravel) and < 2 mm material. Gravel correction factors (1) and (2) above were tested. In addition, a modified version of correction (1) was used in which the mass percentage of < 2 mm was multiplied by 0.77 (Cantrell et al., 2007).

Kd values on < 2 mm were generally higher than the bulk sediment. Kd values of the bulk and < 2 mm sediment for the least reactive radionuclide, Tc, were similar. Bulk Kd values were all highest in the soil with the lowest gravel fraction, while the lowest Kd values were found in the soil with the highest gravel content. In one sample the U Kd was lower in the < 2 mm than the bulk sediment possibly due to highly reactive sites on the gravel surface or the presence of microfractures with highly reactive surfaces. In comparing the bulk Kd to the predicted Kd using the < 2 mm Kd and the corrections above, the modified version of correction (1) provided the values closest to the bulk Kd. In addition, the difference between the measured and calculated Kd values increased with increasing gravel content. These results show that in some cases gravels from the Hanford Site are not inert and may play a part in sorption reactions. This may be due to micropores, microfractures, or Fe oxide coatings on the gravel surface.

1.9 Effect of Particle Scale Heterogeneity on Solute Transport

Particle scale heterogeneity includes both physical and chemical heterogeneity. Physical heterogeneity is a result of differences in the size distribution of particles. Chemical heterogeneity refers to variations in surface reactivity. It is well-documented that physical heterogeneity leads to velocity variations which cause dispersion of chemicals during reactive transport. It follows that pore scale variation in reactivity could potentially play a role in reactive solute transport. Analytical solutions which incorporate physical and chemical heterogeneity in reactive solute transport have been developed (Bellin et al., 1993) which show good agreement with numerical models containing physical and chemical heterogeneous media (Bosma et al., 1993). Non-ideality in solute breakthrough curves are often modeled using kinetic terms. Sugita et al. (1995a) present an alternative explanation for solute breakthrough curves which display

non-ideal behavior such as solute spreading, early breakthrough, and tailing. They contend that, in some cases, non-ideality may be caused by pore scale variation in the retardation factor due to pore size distribution. A model which incorporates the pore scale variation in retardation factor produced symmetrical breakthrough curves for non-reactive solutes and non-ideal breakthrough curves for reactive solutes in the absence of any kinetic processes (Sugita et al., 1995b). These results provide support for the role particle scale heterogeneity may have on solute transport. Szecsody et al. (1998) investigated the effect of particle scale heterogeneity on $Co^{II/III}EDTA$ transport using batch and column experiments. Reaction parameters based on batch data did not reproduce column experiments in some cases. Simulations which incorporated particle scale heterogeneity were able to accurately describe the differences in the batch and column data.

1.10 Goals

The purpose of this work was (1) to examine the linearity, reversibility, and time effects on sorption processes and (2) to investigate the physical and chemical effects that changes in water content have on U(VI) leaching from U(VI)-contaminated sediment containing particles ranging from clay-size to gravel. Previous work has indicated that sorption processes in batch style experiments may display hysteresis (Guo and Wu, 2009) and that the time to reach sorption equilibrium may take minutes (Giammar and Hering, 2009) to months (Kaplan et al., 1996). It was hypothesized that U(VI) would reach sorption equilibrium within 96 hours of contact with Hanford sediments and that the sediments would display hysteresis during batch desorption experiments.

In regard to the effects changes in water content have on U(VI) leaching, previous work has indicated that the presence of immobile water and exposure to reactive surfaces may change as a

function of water content in heterogeneous sediment mixtures composed of < 2 mm material (Gamerdinger et al. 2001b; Wellman et al. 2008a, 2001b). The presence of gravel under saturated conditions has been shown to lead to two-region flow, contain reactive surfaces with varying release rates, and to dilute sorption sites (Liu et al., 2008). Therefore, the presence of gravels is likely to affect the geochemical and hydrologic controls on the fate and transport of U(VI) in the subsurface. I hypothesized that at high water contents, solution will fill all of the pores and that a majority of the solution will flow through the largest pores, which will be composed of the less chemically reactive coarse particles containing little to no contaminant U(VI). Much of this solution will bypass the sorbed U(VI), which is associated with the finer particle sizes. As water content decreases, solution will be restricted to increasingly smaller pores, which are composed of the smaller and more reactive particle sizes. As the solution is restricted to increasingly smaller pores, this will result in an increase in exposure to more of the highly reactive surfaces, which hold the majority of the sorbed U(VI), and overall will act to increase the transport and removal of U(VI) from the system. Methods of analysis included non-flowing batch adsorption experiments, non-flowing batch desorption experiments, and unsaturated leaching experiments on repacked pre-contaminated columns.

1.11 Objectives

The objectives of this research are to (1) determine the adsorption and desorption partitioning of U(VI) between the solid and solution phases on freshly contaminated and aged Hanford sediments, (2) determine distribution coefficients of U(V) in a column leaching experiment at two separate water contents, (3) compare changes in the distribution coefficients as a function of

water content, and (4) link any observed changes to changes in hydrodynamic and geochemical conditions as the sediment desaturates.

2. Materials and Methods

2.1 Characterization of Sediment

The sediment for the batch and leaching experiments was collected from the Hanford Formation in the Environmental Restoration Disposal Facility (ERDF) in the 200 West Area of the Hanford Reservation and is well described (Pace et al., 2003, 2007; Mayes et al., 2009). The mineralogy of the pre-treated < 2 mm sediment is listed in Table 1. The material collected from the 200 West Area was air dried and dry sieved into twelve size fractions ranging from 31.5 mm to less than 0.053 mm. Grain size statistics of two grab samples from core 2-26 in the 300 Area Hanford, Washington, were provided by Pacific Northwest National Laboratory (PNNL) (J.M. Zachara, personal communication, 2009). The two samples displayed a large amount of variability as the gravel percentage ranged from 83% to 54%. An average of the two grain size distributions was used to construct a grain size distribution curve (Figure 4). Interpolation of the mean grain size distribution was used to determine the mass percent makeup of each of the twelve size fractions (Table 2) for the repacked columns.

2.2 Sediment Contamination

A batch type methodology was used to contaminate the < 2 mm size sediments that were to be used in the leaching experiments. The term "sediment contamination" or "contamination event" will be used to refer to the sediments contaminated for the leaching experiments to distinguish them from the sediments contaminated in the batch experiment (discussed in the following section). Sediment contamination was performed in 250 ml centrifuge bottles at a 200 g/l solid-to-solution ratio (1:5 by mass). The mass of each of the six size fragments < 2 mm for each sample bottle was individually weighed and reconstituted in a sample bottle. In this way it was

assured that each sample bottle contained the same grain size distribution. A total of 46 bottles were used in the sediment contamination process.

Two solutions of a synthetic groundwater, which approximates the composition of the groundwater in the 300 Area of the Hanford Site, were made containing the electrolytes listed in Table 3. Previously performed thermodynamic analyses (Liu et al., 2008; Wellman et al., 2008b) on synthetic groundwater with similar ionic species and concentrations, pH, and U(VI) concentrations has shown that the system is below saturation with respect to any solid phase U(VI).

A salt of $UO_2(NO_3)_2$ x $6H_20$ was used to contaminate the synthetic groundwater solutions resulting in two solutions containing 56.6 and 62.5 ug/l of uranium, respectively. Previous studies (Kaplan et al., 1996; Um et al., 2005, 2007) have shown U(VI) sorption to conform to the linear sorption isotherm within these concentrations. Twenty-four samples were initially contaminated with the 56.6 ug/l uranium solution. The samples were placed on a platform shaker (Model # 6000, Eberbach Scientific Instruments and Apparatus, Ann Arbor, MI) for forty-eight hours. The samples were then centrifuged (Allegra 6KR, Beckman Coulter, Fullerton, CA) for twenty minutes at two thousand rpms. The supernatant was removed from the bottles using a large capacity syringe and stored for analysis. pH was measured on the supernatant from all samples. The sediments were then contaminated a second time following the same procedure and using the same solution concentration in order to ensure effective sorption of uranium. The supernatant of the two contamination events was combined for each sample and the concentration of the combined supernatants was later used to determine the mass of sorbed U(VI). The remaining twenty-two bottles of sediment were contaminated using the

solution containing 62.5 ug/l of uranium. The same procedure as described above was followed with these samples. Following contamination, the supernatant was analyzed for uranium using kinetic phosphorimetry (model KPA-11, Chemchek Instruments, Richland, WA).

"Point" estimate distribution coefficients were determined for each sediment sample based on the equilibrium between the sorbed and solution phases at a single solute concentration. Hereafter these values will be referred to as Kd_{Cont} to distinguish them from distribution coefficients obtained through other means. The Kd_{Cont} for each soil sample was determined using the following equation

$$Kd_{Cont} = \frac{(C_0 - C_{sup})}{C_{sup}} \times \frac{V_{added}}{M_{sed}} \quad (2)$$

where C_0 is the initial concentration of U(VI) in the contaminating solution, C_{sup} is the concentration of the supernatant, V_{added} is the volume of contaminating solution added to the sediment, and M_{sed} is the sediment mass.

Following the second contamination and subsequent decantation, 100 ml of uncontaminated synthetic groundwater was used to rinse the contaminated sediments. The rinse step was performed in order to remove any interstitial uranium-spiked groundwater solution from the sediments prior to column packing. Immediately following addition of the rinse solution, the sediments were centrifuged for twenty minutes at two thousand rpms. The bottles were decanted and the rinse water stored for analysis. The rinsing was repeated a second time again using 100 ml of synthetic groundwater. pH was measured on both rinses. In the current and following calculations, a distinction is made between U_{Mass}, which refers to the total mass of uranium in the

sample bottle (sorbed + interstitial), and $U_{Sorbed\ Mass}$, which refers only to the sorbed fraction of uranium. U_{Mass} was determined using the following equation

$$U_{Mass} = (C_0 \times V_{added}) - (C_{sup} \times V_{added}) - (C_{rinse\,1} \times (V_{rinse\,1} - V_{rinse\,1\ interstitial})) - (C_{rinse\,2} \times (V_{rinse\,2} + V_{rinse\,1\ interstitial} - V_{rinse\,2\ interstitial})) \quad (3)$$

where 1 and 2 refer to the first and second rinses and interstitial is the solution which remained in the pores following decanting.

2.3 Batch Adsorption Experiments

Batch adsorption experiments were performed on uncontaminated < 2 mm ERDF sediment over a range of concentrations to determine a distribution coefficient for the sediment based on the linear sorption isotherm. The linear sorption isotherm can be described by the equation

$$S_e = Kd\, C_e \quad (4)$$

where S_e is the sorbed concentration at equilibrium (mass of solute sorbed/mass of sediment) and C_e is the concentration of solute in solution at equilibrium (mass of solute in solution/volume of solution).

Sediment was individually weighed out according to the distribution in Table 2 and placed in 30 ml centrifuge bottles at a 200 g/l solid-to-solution ratio. The sediments were pre-equilibrated with synthetic groundwater to establish equilibrium between the sediment and synthetic groundwater. Pre-equilibration was performed by adding synthetic groundwater to the sediments, shaking for 24 hours, centrifuging, and decanting. The pH of the supernatant was measured. This process was repeated until the pH of the supernatant did not change significantly from its value prior to addition to the sediment. Five concentrations of U(VI)-spiked groundwater were added to the sediment. Three reps of each sample concentration were

contaminated for a total of fifteen samples. In addition, U(VI)-spiked groundwater was added to three control sample bottles containing no sediment to determine whether any sorption to the container walls occurred. The samples were placed on a platform shaker for a total of seven days. At 48 and 96 hours the samples were centrifuged, a solution pH measurement taken, and a supernatant sample obtained to examine the effect of contact time on uranium sorption. The volume of supernatant sampled was minimized. However, the solid-to-solution ratio was slightly altered following the removal of each sample. After 168 hours (7 days) the samples were centrifuged, decanted, pH measured, and the supernatant analyzed. $U_{Sorbed\ Mass}$ was determined using the following equations at 48, 96, and 168 hours, respectively

$$U_{Sorbed\ Mass\ 48} = (C_0 \times V_{added}) - (C_{Sup\ 48} \times (V_{added} + V_{interstitial})) \quad (5)$$

$$U_{Sorbed\ Mass\ 96} = (C_0 \times V_{added}) - (C_{sup\ 96} \times (V_{added} + V_{interstitial} - V_{rem\ 48})) - (C_{sup\ 48} \times V_{rem\ 48}) \quad (6)$$

$$U_{Sorbed\ Mass\ 168} = (C_0 \times V_{added}) - (C_{sup\ 168} \times (V_{added} + V_{interstitial} - V_{rem\ 48} - V_{rem\ 96})) - (C_{sup\ 48} \times V_{rem\ 48}) - (C_{sup\ 96} \times V_{rem\ 96}) \quad (7)$$

where $V_{interstitial}$ is the volume of interstitial solution from the equilibration step remaining in the bottles prior to addition of the U(VI)-spiked synthetic groundwater, V_{rem} is the volume of solution removed, and 48, 96, and 168 denote the hours since the experiment began.

The average sorbed concentration of the three reps was plotted as a function of the average supernatant concentration of the three reps for each of the five contaminating concentrations. A regression line was fit to the data and the slope of the line was taken as the distribution coefficient (Kd_{batch}). Note that this approach differs from the "point" Kd used in the contamination event. The Kd_{batch} is based on the slope of a line through several points.

Therefore, much more certainty may be attributed to the Kd_{batch} values than from the Kd_{Cont}. The latter is subject to a much greater level of variation because it is based on a single point.

2.4 Desorption Experiments

Desorption experiments were performed on two samples from the sediment contamination experiment and all 15 samples from the batch experiment; three reps at five concentrations. Uncontaminated synthetic groundwater was added to the contaminated sediment at a 200 g/l solid-to-solution ratio. The samples were placed on the platform shaker and given time to equilibrate. The two samples from the sediment contamination event were given 96 hours to equilibrate as this was the amount of time given for adsorption. The sediment from the batch experiment was given seven days to equilibrate in order to match the adsorption equilibration time. The sediment was centrifuged and decanted following the same procedures as the adsorption experiment and the supernatant was analyzed for U(VI). A desorption Kd for the material from the contamination event was determined using the following equation

$$Kd_{des\,Cont} = \frac{\dfrac{U_{Mass} - (C_{sup} \times (V_{added} + V_{rinse\ 2\ interstitial}))}{M_{sed}}}{C_{sup}} \qquad (8)$$

where $Kd_{des\,Cont}$ is the desorption distribution coefficient measured on the sediment from the contamination event, U_{Mass} was derived using equation 3, V_{added} is the volume of clean synthetic groundwater added, and $V_{rinse\ 2\ interstitial}$ is the volume of rinse 2 which remained in the sediment pores following decanting. Sediment desorption was repeated three times for each sample. The initial mass of U(VI) in the sample bottles (U_{Mass} in equation 8) for each subsequent desorption was taken as the top line of equation 8 (i.e. U_{Mass}-(C_{Sup} x (V_{added}+$V_{rinse\ 2\ interstitial}$))) from the

previous calculation plus the mass of U(VI) remaining in solution in the interstitial porewater determined by

$$U_{Mass\,interstitial} = (C_{sup} \times V_{interstitial}) \quad (9)$$

A desorption Kd from the batch experiment sediment ($Kd_{des\ batch}$) was determined based on the slope of the desorption isotherm. The initial mass of U(VI) in each sample bottle was determined by taking the result of equation 7 and adding the mass of U(VI) remaining in solution in the interstitial porewater or

$$U_{Mass} = U_{Sorbed\ Mass\ 168} + (C_{sup\ 168} \times V_{interstitial}) \quad (10)$$

The sorbed mass following desorption equilibration was determined by

$$U_{Sorbed\ Mass} = U_{Mass} - (C_{sup} \times (V_{added} + V_{interstitial})) \quad (11)$$

where U_{Mass} is determined from equation 10. The sorbed concentration and supernatant concentrations were then averaged for each of the three reps and the sorbed concentration was plotted as a function of supernatant concentration. A linear regression line was fitted to the data and the slope of the line was taken as the $Kd_{des\ batch}$. Desorption was repeated three times. The initial mass of U(VI) in each sample bottle (equation 10) for each subsequent desorption was determined using the results of equation 11 and adding the uranium remaining in the porewater determined using equation 9.

2.5 Column Leaching Experiments

Two columns (columns A and B) were packed in increments by dividing the columns (total length=30.5 cm and diameter=4.4 cm) into nine 3 cm and one 3.5 cm subsections. The mass of material > 2 mm needed for each column was determined by multiplying the volume of the

column by the goal bulk density by the percentage of material > 2 mm on the previously described grain size distribution curve. The six size fractions of material > 2 mm were individually weighed out and combined to form the gravel needed for each 3 or 3.5 cm layer. The columns were packed by combining the gravel material pre-weighed for each layer with the < 2 mm contaminated fraction. Rinse water remained in the pores of the contaminated material and resulted in a moist mixture of gravel and fine material. The columns were packed in 3 cm layers by adding the moist mixture to the column and gently tamping the material as it was being packed. Care was taken to avoid any type of layering of material during packing. Pre-saturated porous disks (60 cm bubbling pressure, Porosity C, Ace Glass, Vineland, NJ) were inserted into both endcaps of the columns as a means of distributing solution across the entire face of the top of the columns. In addition, a thin layer of clean quartz sand was placed at the top and bottom of the column to ensure a consistent hydraulic connection between the porous disks and the gravelly material. The physical properties of the columns were determined using the dry mass of material added to the columns, the volume of the columns, and assuming a particle density of 2.65 g/cm^3.

Mass corrected distribution coefficients ($Kd_{mass\ avg}$) were determined for each column using the average Kd_{Cont} of the < 2 mm fraction packed into each column and assuming the gravel fraction is inert (i.e. Kd=0). The following equation was used to obtain $Kd_{mass\ avg}$

$$Kd_{mass\ avg} = (1 - f)\, Kd_{Cont\ avg} \tag{12}$$

where f is the mass fraction of material > 2 mm in the column. Recent research (Um et al., 2009) has shown that Hanford formation gravels may possess some sorptive capacity and the most accurate method of estimating a total distribution coefficient on soil that contains material > 2 mm is to measure the Kd on both the < 2 mm and > 2 mm fraction and make a correction based

on the mass fraction of each portion. However, due to the difficulties in accommodating particles > 2 mm in a batch experiment, and the lack of ability to measure small changes in solution U(VI) concentration likely to occur as a result of the minimal sorption of gravels, the above equation was deemed the most appropriate. Implications of this assumption are discussed in the results section.

Four holes were drilled into the upper portion of the column to allow air to enter the column during the leaching portion of the experiments. Hardware was placed in the holes and secured using epoxy. Tubes were attached to the hardware and clamped in order to control exposure to the atmosphere. The columns were saturated by pumping the synthetic groundwater solution from the bottom of the column at a rate of 1 ml/h. The experiments were run from high water content to low water content in an effort to keep the $\theta(h_c)$ relationship on the main drying curve and to avoid hysteresis.

Each column was placed on an analytical balance (GP-12K, A&D, San Jose, CA) as a means of measuring the average water content throughout the duration of the experiments. The balances have a capacity of 12,000 grams and accuracy of 0.1 gram (±.005% water content). The balances were connected to a personal computer through a serial connection. WinCT software (A&D, San Jose, CA) was used to log the mass of the columns at prescribed intervals throughout the duration of the experiments. The initial stable mass reading following startup of the experiments was taken as the saturated column mass. This mass was converted to a water content equal to the estimated porosity. Estimated water contents through the duration of the experiments were calculated from the difference in the original stable mass reading. Abrupt shifts in column mass were periodically recorded by the software. These shifts were attributed to

maintenance of the column setup and removal of sample tubes from the fraction collector. When abrupt changes in mass correlated with column maintenance as recorded in maintenance logs, the changes in mass were corrected for by adding or subtracting the difference in mass before the maintenance to the mass after the maintenance.

The columns were leached with the uranium-free synthetic groundwater from the top using a medical infusion pump. The lower end of the column was connected to a vacuum chamber which allowed adjustment of the lower boundary tension. Tension was measured using a tensimeter (Soil Measurement Systems, Tucson, AZ). Effluent was collected in an automated fraction collector (Retriever II, Teledyne Isco, Inc., Lincoln, NE). The volume of each sample was determined by dividing the mass of the solution by the specific density of the solution assumed to be 1 g/cm^3. pH was measured periodically on freshly collected effluent samples and remained within ±0.35 pH units of the synthetic groundwater influent solution through the duration of experiments. Bromide (25 mg/l) and pentafluorobenzoic acid (PFBA) (25 mg/l) spiked synthetic groundwater solutions were used as non-reactive tracers to determine physical transport parameters. The Br^- was used at the higher pumping rate once the column was believed to have reached hydraulic steady-state (i.e. no change in water content as a function of time). PFBA was injected after the pumping rate was lowered. Br^- was analyzed using ion chromatography (ICS 1500, Dionex, Sunnyvale, CA) for column B and a specific ion probe for Br^- for column A. Concentrations of PFBA in column B were determined using a total organic carbon analyzer (TOC-VCSH, Shimadszu, Japan).

The leaching experiments were initiated with the columns fully saturated. The numerical modeling software HYDRUS 2D/3D (Šimůnek and Šejna, 2007) was used to determine the

optimal boundary conditions for the columns which would lead to a unit hydraulic gradient, steady-state conditions, and two separate water contents within the columns. Following initiation of the experiments, the upper and lower boundary conditions had to be adjusted from those determined using the numerical modeling software. The column mass and discharge were monitored at the beginning of each experiment as a means of determining when steady-state conditions were met. Steady-state conditions were assumed to have been reached when the column mass stabilized and the discharge of effluent was consistent over time. The concentration of U(VI) eluting from the columns was measured on effluent samples. When the breakthrough curve began to tail, indicating the U(VI) eluting from the column had reached a steady, consistent value, the upper boundary flux was lowered in order to reach a lower water content. The lower boundary tension was left unchanged. In the following sections, experiment 1 refers to the leaching experiment performed at the higher water content, and experiment 2 refers to the leaching experiment performed at the lower water content.

2.6 Column Hydrologic Properties

The saturated hydraulic conductivity of the columns was measured using a modified constant head method (Figure 5) following the conclusion of the leaching experiments. The columns were re-saturated by pumping the SGW solution from the bottom of the column at a constant rate of 1 ml/h. The pumps were then connected to the tops of the columns. A long piece of tubing was attached to one of the air holes on each column and extended vertically from near the top of the column as a method of measuring pressure head at the point of the air hole within the column. The other three air holes were sealed. The lower column boundary was left under atmospheric pressure. The SGW solution was pumped from the top of the column at a constant rate. Solution

was allowed to fill the air hole tubing and time was given to allow the height of rise to stabilize. Following stabilization of pressure head in the top of the column, effluent was collected at regular time intervals. The height of water rise in the air hole tube was measured and taken as the pressure head at the point of the air hole in the column. The lower boundary was set as the reference point for gravitational head (z=0) and pressure head was assumed to be zero at this point as it was exposed to the atmosphere. The total head at the air hole was taken as the height of the air hole above the bottom of the column (z) plus the height of rise of the solution in the air hole tubing (p). Effluent discharge was averaged over a two hour time period. K was then solved for using equation 1 where Q is the average discharge over the two hour time period, A is the column area, and the head gradient was the height of rise of the solution in the air hole tubing plus the elevation head $(p + z = \partial h)$ over the distance of the air hole from the bottom of the column (∂L).

Following saturated hydraulic conductivity measurements, estimates of the $\theta(h_c)$ relationship were derived for each column. The saturated columns were placed on the balances and the saturated column mass was noted. The effluent tube was re-attached to the vacuum chamber. The air holes on the top endcap were opened slightly to allow air to enter the column. A 10 cm lower boundary capillary pressure head was imposed on the columns. Solution draining from the column was collected in the vacuum chamber. The change in mass was logged through the duration of the experiments. When the mass of the column was no longer changing, equilibrium was assumed to have been reached between θ and h_c. The solution that drained from the column was collected and stored. The capillary pressure head was then increased to derive another pair of θ and h_c values. This process was repeated at 20, 40, 60, and 80 cm capillary pressure. The

change in mass from the original saturated mass and the estimated porosity of the column was used to estimate the volumetric water content at each tension. U(VI) concentration was measured on the solution collected at each capillary pressure head.

The TrueCell software package was used to determine the $\theta(h_c)$ relationship at the physical point in the column where the capillary pressure was imposed using average $\theta(h_c)$ relationship obtained for each column. In TrueCell the $\theta(h_c)$ relationship is expressed using the Brooks-Corey expression (1964) given as

$$\theta_w = \theta_{wr} + (\theta_{ws} - \theta_{wr})\left(\frac{h_d}{h_c}\right)^{\lambda} \qquad h_c > h_d \tag{13}$$

$$\theta_w = \theta_{ws} \qquad h_c < h_d \tag{14}$$

where θ_w is the volumetric water content, θ_{wr} is the irreducible volumetric water content, θ_{ws} is the saturated volumetric water content, h_d is the displacement capillary pressure head, and λ is the pore size distribution index. The average volumetric water content and capillary pressure head were measured values. The displacement capillary pressure head and pore size distribution index were fitted parameters. The saturated average volumetric water content was set equal to the estimated porosity. In order to minimize the number of fitted parameters the irreducible volumetric water content was set equal to zero. This effectively reduced the Brooks-Corey expression to the Campbell empirical model (1974) given as

$$\theta_w = \theta_{ws}\left(\frac{h_d}{h_c}\right)^{\frac{1}{b}} \tag{15}$$

where 1/b is the pore size distribution index.

2.7 Estimation and Solute Transport Parameters

2.7.1 Solute Transport Governing Equations

The most commonly used governing equation describing one-dimensional chemical transport in soil is the convection-dispersion equation (CDE) given by

$$R\frac{\partial C}{\partial t} = D\frac{\partial^2 C}{\partial x^2} - v\frac{\partial C}{\partial x} \tag{16}$$

where D is the dispersion coefficient, C is the concentration, v is the mean pore water velocity, x is the distance, t is time, and R is the retardation factor given as

$$R = \frac{v_w}{v_s} \tag{17}$$

where the subscripts w and s stand for water and solute, respectively. This equation effectively describes the solute velocity with respect to the mean pore water velocity. An R equal to 1 indicates that the contaminant did not react with the soil and traveled at the same velocity as the groundwater. An R > 1 indicates that the contaminant is retarded by interaction with the soil. In some cases R < 1; this generally indicates some type of anion exclusion or preferential flow. Retardation can also be expressed as

$$R = 1 + \frac{\rho_b Kd}{\theta} \tag{18}$$

where ρ_b is the soil's bulk density, Kd is a distribution coefficient, and θ is the volumetric water content. The mean pore water velocity, v, in equation 16 is expressed as

$$v = \frac{q}{\theta} \tag{19}$$

where q is the Darcy flux from equation 1. The dispersion coefficient, D, in equation 16, can be expressed as

$$D = \alpha v + D^* \tag{20}$$

where α is dispersivity and D* is the diffusion coefficient. Dispersivity describes the degree to which a solute spreads due to pore size velocity variations. The diffusion coefficient describes solute movement due to concentration gradients.

Equation 18 is based on an equilibrium linear sorption isotherm, meaning there is a linear relationship between the amount of solute sorbed to the solid particles and the amount of solute in solution. Equilibrium models assume that sorption is rapid when compared to the pore water velocity and that the solute will reach equilibrium with the sorbed phase. In some cases the Kd may decrease with increasing concentration of the contaminant. This may be due to saturation of the most favorable sorption sites and a subsequent decrease in available sorption sites. In this case sorption may be better modeled with the Freundlich isotherm given as

$$S_e = KC_e^{\,n} \tag{21}$$

where S_e is the sorbed concentration, K is the adsorption capacity parameter, C_e is the concentration of solution at equilibrium, and n is the adsorption intensity parameter.

Two region transport is described with the mobile-immobile equation (Coats and Smith, 1964). This model is a form of the convection-dispersion equation in which observed preferential flowpaths in heterogeneous media divide the soil water into regions of mobile and immobile water. This model relies on several assumptions regarding the transport of solutes within

heterogeneous media. Advection and dispersion take place only in the mobile soil water while diffusion occurs in both the mobile and immobile region and is solely responsible for the exchange between the two regions. Sorption processes occur in both the mobile and immobile regions. The dimensionless mobile-immobile equation is given as (Toride et al., 1995)

$$\beta R \frac{\partial C_m}{\partial T} = \frac{1}{P} \frac{\partial^2 C_m}{\partial X^2} - \frac{\partial C_m}{\partial X} - \omega(C_m - C_{im}) - \mu_m C_m \quad (22)$$

$$(1-\beta) R \frac{\partial C_{im}}{\partial T} = \omega(C_m - C_{im}) - \mu_{im} C_{im} \quad (23)$$

where the subscripts m and im signify the mobile and immobile regions, C represents the relative concentration, $\beta=\theta_m/\theta$, P is the Peclet number and is equal to v_mL/D, ω is the mass transfer coefficient, X is dimensionless distance, T is dimensionless time or pore volume, μ is a decay coefficient, and q is the Darcy flux.

P, the Peclet number, describes the degree to which advection dominates contaminant transport over dispersion, and under physical equilibrium conditions, can be expressed as

$$P = vL/\alpha v \quad (24)$$

which can then be reduced to length (L) over dispersivity(α).

The Br^- and PFBA tracer breakthrough data were fitted to both Equations 16 and 22 using CXTFIT (Tang et al., 2009). The goodness of fit of the model predictions with the experimental data was quantified using the root mean square error (RMSE) given as

$$RMSE = \sqrt{\frac{\sum_{i=1}^{n_d} (C_i(t) - {}^*C_i(t))^2}{n_d - n_p}} \quad (25)$$

where $C_i(t)$ is the experimental concentration at time (t), $^*C_i(t)$ is the model predicted concentration at time (t), n_d is the number of data points used in the model, and n_p is the number of adjustable parameters. The lower the RMSE the better the model was assumed to fit the experimental data. It is important to note that the method of calculating the RMSE considers the number of data points incorporated in the model and the number of adjustable parameters and adjusts the computed value accordingly. Therefore, if two models fit the experimental data equally well, but one has a greater number of adjustable parameters, it will be allocated a higher RMSE and the model with fewer adjustable parameters will be assumed to provide the best fit to the experimental data.

2.7.2 Leached Mass Ratio Approach

The leached mass ratio (LMR) approach (Shackelford and Glade, 1997) was used to analyze the U(VI) leaching curves of the repacked columns. This approach employs an analytical solution to the convection dispersion equation in terms of leached mass rather than instantaneous concentrations as is used in more traditional approaches. The approach is essentially a modification of the traditional method of analyzing breakthrough curves based on instantaneous concentrations. A summary of the method is described below. For a complete derivation see Shackelford and Glade (1997). A general solution to the convection dispersion equation was described by van Genuchten (1981) and van Genuchten and Alves (1982) subject to a pulse solute input concentration boundary condition from time t = 0 to time t= t_0 is given as

$$C_r(x,t) = C_i + (C_0 - C_i)f(x,t); \qquad 0 < t \leqslant t_0 \tag{26}$$

$$C_r(x,t) = C_i + (C_0 - C_i)f(x,t) - C_o f(x,t - t_0); \qquad t > t_0 \tag{27}$$

where C_r is resident concentration, C_i is the initial solute concentration in the soil, C_0 is the solute concentration of an influent solution, and x is distance. An analytical solution to the above equations in terms of instantaneous concentrations is presented by Lindstrom et al. (1967) and is given as

$$f(x,t) = \frac{1}{2}\left(\operatorname{erfc}\left(\frac{Rx - vt}{2(DRt)^{1/2}}\right) + 2\left(\frac{v^2 t}{\pi DR}\right)^{1/2} \exp\left(-\left(\frac{Rx - vt}{2(DRt)^{1/2}}\right)^2\right) - \left(1 + \frac{vx}{D} + \frac{v^2 t}{DR}\right)\exp\left(\frac{vx}{D}\right)\right.$$
$$\left.\operatorname{erfc}\left(\frac{Rx + vt}{2(DRt)^{1/2}}\right)\right) \tag{28}$$

The function f(x,t) describes the effluent concentration with respect to the influent concentration and varies from 0 to 1. A schematic illustration of the use of this equation can be found in Figure 6. Figure 6a represents the column setup before solute is added. Figure 6b represents some time $t < t_0$ where the influent solution at concentration C_0 is being pumped into the column and the ratio of the effluent concentration to the influent concentration (C_e/C_0) can be determined by equation 28. If t_0 is long enough, f(x,t) equals 1 (i.e. Figure 6c where $C_0=C_e$). At this point the solute is evenly distributed throughout the soil and is assumed to be in equilibrium with the soil. For $t > t_0$ the soil is flushed with a solution containing no solute.

The leached mass ratio approach for advective leaching described by Shakelford and Glade (1997) employs an analytical solution to equation 27 which describes the mass of contaminant leached with respect to the total mass of contaminant (M_0) in the column at $t > t_0$ (Figure 7a).

The solution is derived by first spatially differentiating equation 28 (i.e. $\frac{\partial C_r(x,t)}{\partial x}$) to determine the local concentration gradient. Equation 28 is presented in terms of resident concentrations. Concentrations of effluent in finite columns are more appropriately modeled using flux-averaged concentrations (van Genuchten and Parker, 1984) given as

$$J(L,t) = \theta[v C_r(L,t) - D\frac{\partial C_r(L,t)}{\partial x}] \tag{29}$$

where J is the solute mass flux. The results of the first step and equation 28 (i.e. $C_r(x,t)$) are plugged in to equation 29 to convert to flux-averaged concentrations. The resulting equation is integrated with respect to time to determine the cumulative mass leached which is normalized to the total mass of contaminant in the column at a given pore volume. The final solution is given as

$$LMR_M = \Sigma\frac{(\Delta m)}{M_0} = \frac{T}{R} - \frac{1}{2}\{(\frac{T}{R} - 1)\text{erfc}(\frac{R - T}{2(TR/P)^{1/2}}) + (\frac{T}{R} + 1)\exp(P)\text{erfc}(\frac{R + T}{2(TR/P)^{1/2}})\} \tag{30}$$

where LMR_M is the leached mass ratio with respect to M_0, which is the total contaminant mass in both the sorbed and solution phases, and Δm is the increment of contaminant mass in a given volume of column effluent.

The use of this method is depicted in Figure 7. In Figure 7a the column contains a total amount of contaminant equal to M_0. This is essentially an equivalent situation as the traditional approach to modeling a pulse of contaminant when f(x,t) in equation 28 is equal to 1 (Figure 6c). In figure 7b the soil is flushed with a solution containing no contaminant (i.e. $t > t_0$) and the mass of contaminant leached (Δm) with respect to the total mass of contaminant (M_0) is equal to the

solution presented in equation 30 and varies from 0-1. In Figure 7c, all of the contaminant has been flushed from the soil and pore water and the LMR_M=1.

Column effluent was collected in approximately 2-6 ml increments throughout the duration of the experiments. The increment of solute mass (Δm) was determined for each sample that was chemically analyzed by numerically integrating the leaching curve from the cumulative volume eluted at that sample to the cumulative volume eluted of the previously analyzed sample using the trapezoid rule for integration. The increment of solute mass was then normalized with respect to the total solute mass (M_o). M_o was the total U(VI) in the column as determined from Equation 3 for each sample packed into the column. The normalized values were incrementally summed for each sample to give the cumulative leached mass ratio ($\Sigma(\Delta m)/(M_o)$). Pore volumes were determined by multiplying the column length, area, and estimated water content to establish the volume of one pore volume. The cumulative volume eluted was divided by the estimated pore volume to determine the total number of pore volumes eluted at each sample.

At a given pore volume the cumulative leached mass ratio ($\Sigma(\Delta m)/(M_o)$) should equal the analytical solution to the CDE for a given Peclet number and retardation factor. The Peclet number for each experiment was calculated using the dispersivity derived from non-reactive curve fitting and solving equation 24. The leached mass ratio was determined at each pore volume for which a sample was analyzed by summing the normalized leached mass as well as solving the analytical solution to the CDE (Equation 30). The differences between the predicted and observed data (residuals) were summed and squared (SSQ). Solver was used in Excel to minimize the sum of squares of the residuals by optimizing the retardation factor. When the

residuals had been minimized, the optimized value of the retardation factor was used to solve for the distribution coefficient by rearranging equation (18) resulting in

$$K_d = \frac{\theta(R - 1)}{\rho_b} \tag{31}$$

The convection-dispersion equation and the leached mass ratio approach assume steady-state flow within the column. Transient upper boundary conditions were imposed on the column at the beginning of the experiment in an effort to reach a steady-state condition. In addition, the upper boundary condition was again changed in order to reach a second water content. This resulted is transient conditions within the column which could affect sorption processes. The use of steady-state models to describe transient processes has been shown, in some cases, to yield similar results as those predicted by transient models (Wierenga, 1977; Beese and Wierenga, 1980). However, the use of a steady-state model to describe transient conditions should be considered in interpreting the results.

3. Results and Discussion

3.1 Distribution Coefficient Values Determined from Sediment Contamination

The calculated Kd_{Cont} for each sample from the sediment contamination are presented in Table 4. Kd_{Cont} values ranged from 1.78-4.84 ml/g. An analysis of variance (ANOVA) was performed on the Kd_{Cont} values to determine whether there was a significant difference between the group of sediment contaminated with the 56.6 ug/l uranium solution and the group contaminated with the 62.5 ug/l uranium solution. The results (Table 5) show that there was a significant difference between the two groups at the 95% confidence level ($p < 0.05$). If the linear sorption model holds true for these sediments, then one would expect no significant difference between the two groups contaminated with different solution concentrations. Due to the fact that the sediment was not pre-equilibrated with synthetic groundwater prior to addition of the U(VI)-spiked solution, an ANOVA was performed on the pH of the supernatant in order to determine whether the difference in Kd_{Cont} values could be attributed to other chemical reactions which may have occurred as the sediment and U(VI) spiked solution were equilibrating. The results (Table 6) indicate that there was not a significant difference between the pH of the supernatant of the groups of sediment contaminated with two different solution concentrations at the 95% confidence level ($p < 0.05$). Sorption site limitation was not a contributing factor to the variation in Kd_{Cont} values as the mean Kd_{Cont} increases with increasing solution concentration. It is not clear what caused the discrepancy between the Kd_{Cont} values of the two sediment groups. Variations in the mineralogy and surface reactivity may have played a role. Every attempt was made to obtain replicate sediment samples in each sample bottle as each of the six size fractions < 2 mm was weighed out and reconstituted. In the absence of any other explanation, variations in mineralogy and reactivity within one or more size fraction probably caused the observed variations in the Kd_{Cont} values of the sediment.

3.2 Batch Adsorption Experiments

Results of the U(VI) batch adsorption experiments at 48, 96, and 168 hours are presented in Figures 8, 9, and 10, respectively. The resulting data was modeled with both the linear sorption isotherm and the Freundlich isotherm. The results of the modeling can be found in Table 7. Both models provided good fits with the Freundlich isotherm displaying slightly higher R^2 values. As can be seen in Table 7, the n values in the Freundlich isotherm are all close to 1, indicating that the Freundlich fit approaches that of the linear isotherm. Because the linear isotherm provided a good fit and is much less complicated to incorporate into analytical solute transport models, it was used in the analysis of the leaching experiments.

In examining the Kd_{batch} values obtained at 48, 96, and 168 hours, the results show a peak in adsorption at 96 hours. However, as the 95% confidence intervals overlap, any time effects on U(VI) adsorption are inconclusive. These results indicate that 48 hours was an adequate amount of time to reach equilibrium.

The mean Kd_{Cont} values of the sediment contaminated with 56.6 and 62.5 ug/l U(VI) were 2.78 and 3.85 ml/g, respectively. The Kd_{batch} value at 48 hours was 4.70 ml/g ± 0.882. The difference in the values may be attributed to the uncertainty associated with the "point" method of determining Kd_{Cont}. The Kd_{batch} values are based on 15 samples over a range of five contaminating concentrations. The Kd_{Cont} values are based on one sample at one contaminating concentration. Therefore, the Kd_{Cont} is subject to more error than the Kd_{batch} value.

The Kd_{Cont} and Kd_{batch} values reported here are similar to values reported for other Hanford Area sediments (Um et al., 2005; Gamerdinger et al., 2001a). Um et al. (2005) found "point" Kd

values of 0.46 ml/g ± 0.05, 1.8 ml/g ± 0.07, and 5.23 ml/g ± 1.33 for various sediment samples from the 200 Area. Those researchers then performed a batch experiment on the same samples with U(VI) concentration ranging from 12-1190 ug/l U(VI). They found sorption to be linear within this range with Kd values of 1.3, 4.9, and 7.3 ml/g for each of the same samples used in the "point" analysis. The values in Um et al. (2005) show similar trends as in this experiment in that Kd values based on the linear sorption isotherm were higher than those based on a single point estimate. The differences between the values in the Um et al. (2005) study were attributed to differences in the final pH of the solutions. Differences in pH values cannot explain the variation in Kd_{Cont} and Kd_{batch} values in this study. The average pH of the supernatant in the sediment contamination and in the batch experiments were 7.83 and 7.82, respectively. The pre-equilibration step was not performed with the sediment used in the contamination event. Therefore, it is possible that other chemical reactions in the contamination event may have occurred as the sediment and solution were equilibrating which were not reflected in a difference in pH but which resulted in a difference in uptake of U(VI).

3.3 Desorption Experiments

The results of the desorption experiments on the sediment contaminated in the batch experiment following the first, second, and third desorption equilibrations are presented in Figures 11, 12, and 13, respectively. The method of calculating the sorbed concentration involved determining the mass of U(VI) sorbed to the sediment, subtracting the amount released by examining the volume and concentration of the desorption wash, and mathematically accounting for the volume and concentration of the interstitial U(VI) solution remaining in the pore water following decanting the sediments. Following these steps resulted in a calculated negative sorbed

concentration for the sediment contaminated with the lowest U(VI) concentration solution following the second and third desorption equilibration. This mass balance error is most likely due to a small error in either a volume measurement and/or greater analytical uncertainties in measuring lower U(VI) concentrations.

The fitted $Kd_{des\ batch}$ values and coefficients of determination can be found in Table 8. The 95% confidence intervals of all $Kd_{des\ batch}$ values overlap indicating no statistically significant difference between the values. The $Kd_{des\ batch}$ values are all higher than the Kd_{batch} values indicating U(VI) desorption hysteresis. However, as the 95% confidence intervals of the $Kd_{des\ batch}$ values overlap those of the Kd_{batch} values, the presence of desorption hysteresis is inconclusive. Um et al. (2005) present desorption Kd measurements on 200 Area sediments. The values for sediment < 2 mm ranged from 3.32-10.8 ml/g and were approximately one order of magnitude greater than those determined in adsorption batch experiments.

The results of desorption on the sediment samples from the contamination event (samples Y1 and Y2) are presented in Figures 14 and 15. Table 9 lists the mass percent of the total adsorbed U(VI) released from the sediment following each desorption and the mass percent of U(VI) released that was held by the sediment prior to each desorption. In both samples Y1 and Y2 the percentage of adsorbed U(VI) prior to washing which desorbs decreases with each subsequent desorption. For example, following the first desorption wash, sample Y1 releases 43.2% of the adsorbed mass. Following the second and third wash, sample Y1 releases 26.9% and then 12.1% of the adsorbed mass. This trend indicates that as less U(VI) is available for desorption, a smaller percentage will desorb. This could be attributed to the presence of a suite of sorption sites which hold the U(VI) with varying degrees of strength. If this is the case, then the initial

desorption wash removes U(VI) from the weaker sites and the mass of U(VI) remaining is held by increasingly stronger sorption sites. The result is that less and less U(VI) is released to solution with each subsequent wash. Another potential explanation is that a portion of the sorbed U(VI) is non-labile and will not be removed from the sediment. In this case the percentage of U(VI) released decreases due to the fact that a portion of the sorbed U(VI) is not available for desorption.

A regression line was fitted to the adsorption and desorption equilibrated states of samples Y1 and Y2. Both fitted regression lines resulted in slopes of 3.02 and positive y-intercepts with coefficients of determination of 0.999. The fitted regression line provided y-intercepts of 4.23E-8 and 3.03E-8 for sediment samples Y1 and Y2, respectively. Assuming these values are equal to the non-labile U(VI) sorbed concentrations, the non-labile U(VI) mass was determined for each sediment sample. This calculation resulted in non-labile U(VI) masses of 1.69 and 1.21 ug for sediment samples Y1 and Y2, respectively, or 24% and 18% of sorbed U(VI) mass, respectively.

Similar figures as those plotted for samples Y1 and Y2 were made for the sediments used in the batch experiment. Figures 16, 17, 18, and 19 are the mean adsorbed and desorbed equilibrated states of the three reps of sediment contaminated with 15.1, 31.0, 71.8, and 80.1 ug/l of U(VI), respectively. It is important to note that Figures 11-13 show the results of desorption washes on the sediment from the batch experiment over a range of contaminant concentrations. Figures 16-19 show the results of desorption washes on the average of three reps of sediment contaminated with one concentration. Tables 10 and 11 list the mass percent of the total adsorbed U(VI) released from the sediment following each desorption and the mass percent of U(VI) released

that was held by the sediment prior to each desorption. Tables 10 and 11 also contain point estimates of the Kd determined by dividing the sorbed concentration by the equilibrated aqueous concentration following adsorption and three desorption washes. The sediments used in the batch experiment display a different trend than the Y1 and Y2 sediment. The $Kd_{des\ Cont}$ increased with each subsequent wash, whereas the point estimate desorption Kd values from the batch sediments generally decreased with each subsequent wash with synthetic groundwater. In looking at the mass percent of U(VI) released following each wash, the sediment from the batch experiment released an increasing percentage of U(VI) mass with each subsequent wash. For example, the sediment from the batch experiment equilibrated with 31.5 ug/l of U(VI) released 33.2%, 38.2%, and 48.8% of the adsorbed mass following each wash. This was the opposite trend noted in sediment samples Y1 and Y2 and indicates that as less U(VI) is available for desorption, a larger percentage will desorb. In essence, nearly the same mass of U(VI) is desorbing with each wash even though there is less and less available.

The difference in U(VI) released following the washes between sediment samples Y1 and Y2 and the sediment used in the batch experiment is most likely attributable to an aging difference. Sediment samples Y1 and Y2 sat undisturbed for seven months following the adsorption portion of the experiment. This time may have allowed the U(VI) to move into a more favorable arrangement on the sediment. The desorption equilibration on the sediment from the batch experiment began immediately following the adsorption portion of the experiments. Therefore, the U(VI) did not have time to reach the most favorable adsorbed arrangement and was easily desorbed. These results indicate that aging increases U(VI) affinity for the solid phase and that

the U(VI) will be increasingly more difficult to remove with both age and as less U(VI) is available for desorption.

Kaplan et al. (1996) saw a similar trend in a U(VI) batch experiment on 200 Area sediments from the Hanford Site; their distribution coefficients consistently increased over a 13 month period. Several explanations were given: (1) the crystallization of calcite buried sorbed U(VI), (2) sorption is diffusion limited and time increases contact with more sorption sites, (3) the shaking process broke sediments providing additional sorption sites, and (4) the growth of microbial populations increased sorption sites. The sediments described in the current study sat undisturbed and motionless for seven months, so explanation (3) cannot explain the trends seem in this study. Recent research, performed since the publication of the Kaplan et al. (1996) study, provides evidence that explanations (1) and/or (2) may be responsible for the aging effect.

Reeder et al. (2000, 2001) found that U(VI) could be incorporated into calcite during laboratory precipitation experiments. Multiple types of binding surfaces are available for adsorption on calcite. These researchers found that U(VI) is incorporated into calcite differently during different growth steps on the calcite face which was attributed to the multiple binding sites on the calcite terraces to which U(VI) may adsorb. Elzinga et al. (2004) investigated the interaction of U(VI) species in the presence of calcite. Their results indicated the presence of two adsorption complexes that change with adsorbate surface coverage. At low surface coverage U(VI) may exist as an adsorbed calcium triscarbonate ($Ca_2UO_2(CO_3)_3$) complex as described by Reeder et al. (2001). As surface loading increases a second species is found with luminescence that is intermediate between the calcium triscarbonate and that of uranyl incorporated into polycrystalline calcite. With the sediment that aged, there is a possibility that some of the U(VI)

adsorbed onto one of the calcite binding surfaces. As additional crystals of calcium carbonate formed during aging, the U(VI) may have been incorporated into the crystalline structure of the calcite. The result is that the aged sediment contained U(VI) incorporated into the crystalline calcite structure, which would exhibit different retention characteristics than other adsorbed U(VI) complexes.

Recently, Stubbs et al. (2009) identified several classes of hosts for uranium in Hanford sediment. One of the identified hosts was voids within basaltic lithic fragments. These voids formed interconnected paths through the clasts. Access to reactive sites within these clasts would be through diffusion and therefore time dependent. If some of these clasts were present in the sediment used in this experiment, then this could also explain the aging effects on U(VI) desorption. As sediment samples Y1 and Y2 sat for seven months, some of the U(VI) may have diffused into these voids and adsorbed on the surface of the voids. During the desorption experiments, the clean synthetic groundwater may not have time to reach these less accessible sites, resulting in a large sorbed concentration following desorption. The U(VI) contaminating solution in the batch experiments may not have had time to reach the inner voids during the batch adsorption experiment. Therefore, the U(VI) that adsorbed during the batch experiments was completely accessible during the desorption wash and was removed, whereas the fraction of sorbed U(VI) associated with these sites in the contamination event remained sorbed following desorption due to the inability of the solution to reach these sites.

The mineralogy of the sediment used in these experiments is listed in Table 1 (from Pace et al., 2003). These researchers found significant amounts of plagioclase, a major constituent of basalt, in the ERDF sediments. Calcite is mentioned as one of the major sand size constituents.

Therefore, to accurately discern the effects of aging on the sediment, solid phase speciation performed by spectroscopy is needed to accurately characterize the speciation of U(VI) in the aged samples from the sediment contamination event. This is beyond the scope of the present study, but it is recommended for future research.

3.4 Column Physical and Hydrologic Properties

The physical properties of the two columns used in the leaching experiments are listed in Table 12. The goal bulk density of the columns prior to packing was 2.00 g/cm^3. However, space remained at the top of the columns once all of the pre-weighed material had been packed. Additional material was weighed and packed to fill in the remaining space resulting in a higher bulk density than originally planned. The saturated hydraulic conductivities of the two columns were quite similar and ranged from 2.04 x 10^{-6} cm/s to 2.06 x 10^{-6} cm/s.

The point estimate of the Brooks and Corey function for the $\theta(h_c)$ relationship for column B determined using the column lower boundary in TrueCell is presented in Figure 20, along with the measured average SWRC values. The results for column A are not available due to the excessive amount of time required for the capillary pressure head and water content to equilibrate in that column; column A was still equilibrating at 40 cm capillary pressure head at the end of four months. Point estimates of the SWRC for column B were achieved up to 80 cm capillary pressure head over the course of four months. The fitted capillary displacement pressure (air entry value) for column B was 8.239 cm. The fitted pore size distribution was 0.183. The sum of squares of the residuals between the experimental water content data and the fitted data was 5.5 x 10^{-5}.

Kozak and Ahuja (2005) report pore size distribution indexes based on 1323 soils from 5350 horizons and 11 textural classes from Rawls et al. (1982). The pore size distribution index determined for the columns in this study, 0.183, fell between that of a clay loam, 0.194, and a sandy clay loam, 0.168 as reported by Kozak and Ahuja (2005). The highest pore size distribution index reported was sand at 0.591 and clay was the lowest with a pore size distribution index of 0.131.

The U(VI) concentration of pore water collected at various capillary pressure heads during measurement of the average $\theta(h_c)$ relationship for columns A and B can be found in Figure 21. As can be seen from the figure, the U(VI) concentration of the pore water increases as capillary pressure increases for both columns A and B. This may be attributable to the fact that the solution is being pulled from increasingly smaller pores as capillary pressure head is increased. These smaller diameter pores are composed of the finer particles, which are believed to contain the greatest mass of sorbed U(VI) per unit of surface area. Therefore, the solution in the finest pores have the greatest exposure to reactive surfaces resulting in the highest U(VI) concentration in solution.

3.5 Non-Reactive Tracer Modeling

Results of the non-reactive tracer modeling can be found in Figures 22, 23, and 24. Complete tracer breakthrough was only achieved with Br^- in column B. The boundary conditions for column A were adjusted to reach a lower water content before the Br^- concentration reached the influent concentration. This was done because an analysis of the U(VI) breakthrough curve performed during leaching at the high water content indicated that nearly 50% of the U(VI) mass had been leached from the column. There was a concern that if the column was left at the high

water content for a period of time long enough to reach full Br^- breakthrough, all of the U(VI) would leach from the column. Because the goal of the experiments was to examine the effect of changes in water content on U(VI) leaching, the decision was made to lower the water content. Shortly after adjusting boundary conditions on column A to reach the lower water content, the effluent tube was left clamped after collecting sample tubes. This resulted in the conclusion of experiment 2 in column A, the failure to get full Br^- breakthrough, and the failure to obtain a non-reactive tracer breakthrough curve in column A at the low water content.

The Br^- experimental data and model fit for column A at the high water content can be found in Figure 22. The results of the non-reactive tracer modeling can be found in Table 13. The known parameters were the column length, pulse duration, and water content. The fitted parameters in the CDE were dispersivity and flux. The fitted parameters in the mobile-immobile model were dispersivity, the mobile water fraction, the mass transfer coefficient, and the flux. The data were better fit with the CDE with RMSEs of 0.0302 and 0.0528 for the CDE and MIM fits, respectively. The experimental data and model predicted data for column B at the high water content can be seen in Figure 23. The CDE provided a better fit than the MIM with RMSEs of 0.0537 and 0.0552, respectively. The PFBA breakthrough curve for column B at the low water content can be found in Figure 24. Full breakthrough was not reached with PFBA due to equipment malfunction. The experimental data was better fit with the CDE than the MIM with RMSEs of 0.0121 and 0.0201 for the CDE and MIM, respectively.

The results of the non-reactive tracer at the high water content show good agreement between the two columns. Even with the minimal data from column A, the fitted parameters resulted in similar values for dispersivity and flux. The fitted fluxes for columns A and B were slightly

lower than the 0.066 cm/h predicted by the pumping rate and column dimensions. The fitted flux for column B at the low water content was also slightly lower that the 0.016 cm/h as predicted by the pumping rate. The dispersivity increased moving from high water content to low water content. This effect was expected and likely due to the increase in the tortuosity of the flowpaths as water content decreased.

The presence of immobile water has been observed by several researchers studying the transport of U(VI) in heterogeneous sediment mixtures and is often attributed to the continuity of the fine material (Kaplan et al., 1996; Wellman et al, 2008a). In sediment mixtures dominated by fine material, there is a continuity of fine pores and solution is restricted to these pores under increasingly unsaturated conditions. In these cases immobile water is minimized. In sediment mixtures dominated by coarser material, the fine material is generally located in isolated zones and there is not a continuity of fine material. In these sediment mixtures the isolation of the flow into regions results in the formation of immobile water. In light of these findings, the columns in this study were packed in such a way as to attempt to ensure continuity of fine material. This was not done in an effort to eliminate immobile water. It was done in an effort to minimize film flow and maintain matrix flow within the column. Based on non-reactive tracer fitting, it appears that immobile water was minimized in these columns. It is important to note that the better fit with the CDE than the MIM may be due to the limited number of data points available for fitting and the larger number of fitted parameters in the MIM model. As was mentioned in section 2.7, the RMSE provides a penalty as more parameters are used for fitting. This penalty decreases in significance as the number of experimental data points increases. Therefore, the limited number of data points and the larger number of fitted parameters may have been

responsible for the better fit provided by the CDE. To accurately determine the presence of immobile water, multiple tracers and stop flow interruption techniques must be used, which were deemed infeasible in these experiments.

3.6 Distribution Coefficient Values Determined from Leaching Experiments

The leaching curves and estimated water contents for columns A and B can be seen in Figures 25 and 26, respectively. Peak concentrations in the two curves were quite similar given that the initial U(VI) sorbed mass in column A (0.046 mg) was 50% less than in column B (0.069 mg).

The distribution coefficient values determined using the mass average method ($Kd_{mass\ avg}$) and the leached mass ratio method ($Kd_{effective}$) are presented in Table 14. The $Kd_{mass\ avg}$ values are greater than the $Kd_{effective}$ values determined at both high and low water contents. The general trend of all of the data show the $Kd_{effective}$ increased as the water content was lowered.

There was some unexpected variation in $Kd_{effective}$ between the two columns for both experiments 1 and 2. Column B had a higher $Kd_{effective}$ than column A for both methods. This is most likely related to the variation in Kd_{Cont} values discussed in section 3.1. A majority of the sediment contaminated with 56.6 ug/l of U(VI), which had a statistically significant lower mean Kd_{Cont}, was packed into column A. A majority of the sediment packed into column B was composed of the sediment with the higher mean Kd_{Cont}. The reason for the discrepancy between mean Kd_{Cont} values of the sediment contaminated with two different solution concentrations was attributed to variations in mineralogy. It seems that the effect is evident in the optimized $Kd_{effective}$, in that the Kd_{Cont} and the $Kd_{effective}$ are both higher for column B.

The calculated $Kd_{effective}$ values are all less than the $Kd_{mass\ avg}$ values determined from the average Kd_{Cont} of each column and assuming the gravel portion is inert. One would expect that the $Kd_{effective}$ values measured at the higher water content would be closest to the $Kd_{mass\ avg}$ values. However, the results in Table 14 show that as water content is lowered, the $Kd_{effective}$ values approach that of the $Kd_{mass\ avg}$ values. The residence time for the sediment contamination was 96 hours. The residence times in the leaching experiments were determined by dividing the column length by the average linear velocity of the solution which was determined by fitting the CDE to the non-reactive tracer data. The residence time at the high water content was 82.9 and 87.5 hours for columns A and B, respectively. If there was a kinetic effect, then we would expect to see higher $Kd_{effective}$ values than $Kd_{mass\ avg}$ values due to the fact that the $Kd_{effective}$ values were desorption Kds (i.e. the inability to reach equilibrium would result in low concentrations eluting from the column and a high Kd). In addition, results from the batch experiment suggest a hysteretic effect in desorption. Based on such results, one would expect to see higher $Kd_{effective}$ values than $Kd_{mass\ avg}$ values.

The solid-to-solution ratio cannot explain the difference in the $Kd_{effective}$ values and $Kd_{mass\ avg}$ values. In the contamination event the solid-to-solution ratio was 200 g/l. This provided adequate sediment exposure to the contaminant solution. The solid-to-solution ratio of the leaching experiments was calculated by dividing the bulk density by the estimated water content. The solid-to-solution ratio of the leaching experiments at the high water content was approximately 15,000 g/l in columns A and B during experiment 1. If solute exposure to reactive surfaces were a contributing factor to $Kd_{effective}$ values then it would be expected that less U(VI) would be released to solution due to less exposure to reactive surfaces which would

act to increase the $Kd_{effective}$ relative to the $Kd_{mass\ avg}$. In fact, the opposite trend was observed in the leaching experiments, indicating that the solid-to-solution ratio was not likely a factor in the variability between the $Kd_{effective}$ values and the $Kd_{mass\ avg}$ values.

The modified version of Equation 12, in which the mass fraction of material < 2 mm is multiplied by 0.77 (Cantrell et al. 2007) resulted in $Kd_{mass\ avg}$ values of 0.536 and 0.644 ml/g for columns A and B, respectively. This method results in values closer to $Kd_{effective}$ for columns A and B, but the values determined using the modified version of Equation 12 are still greater than those determined from the leaching experiments.

Previous research has shown that some of the gravel fraction may contain reactive sites (Um et al., 2009). However, this cannot explain the difference between the $Kd_{effective}$ values and $Kd_{mass\ avg}$ values. If a portion of the gravel were reactive, but not incorporated into the Kd_{Cont} or the calculation of $Kd_{mass\ avg}$, then it would be expected that the $Kd_{effective}$ would be higher than the $Kd_{mass\ avg}$ due to the presence of more sorption sites in the sediment than would be accounted for in the $Kd_{mass\ avg}$. A more likely explanation for the difference in the values is that a portion of the < 2 mm fraction is non-reactive in addition to the > 2 mm fraction. The Kd_{Cont} values were derived for the < 2 mm portion of sediment. If a portion of this sediment were non-reactive, but incorporated into the Kd calculation, then this would decrease the overall Kd_{Cont} but increase the reactive fraction in the $Kd_{mass\ avg}$ calculation. If we assume that the fraction of material > 1 mm is all inert, then we can remove the 1-2 mm mass from the calculation of Kd_{Cont} for all samples packed into the column. This calculation was performed on the sediment packed into column A and the result was an average Kd_{Cont} of 3.62 ml/g, which, as expected, is slightly higher than the 2.89 ml/g for the < 2 mm fraction. The fraction of material considered inert now increases from

76% to 86%. The $Kd_{mass\ avg}$ making the assumption that the > 1 mm sediment is inert is 0.504 ml/g. This value is much closer to the column A $Kd_{effective}$ determined at the high water content. This calculation therefore supports the possibility that not only is the gravel fraction is inert, but a portion of the < 2 mm fraction is as well.

The leached mass ratio experimental data and the model predicted fit to the data can be seen in Figures 27-30. The model fits were much better at the low water content than the high water content. This can be seen visually upon inspection of Figures 27-30. In column A at the high water content approximately 44% of the U(VI) mass is leached from the columns. In column A at the low water content approximately 6% of the U(VI) mass is leached. In column B at the high water content approximately 24% of the U(VI) is leached. In column B at the low water content 16% of the U(VI) mass is leached. As more mass of U(VI) is leached, there is greater opportunity for the experimental data to vary around the idealized model.

The model fit was strongly affected by the large pulse of U(VI) that elutes from the column at the beginning of the experiments. In looking at the leached mass ratio model fits in Figures 27 and 29, the experimental data are near, and slightly below, the model fit during the rising limb of the U(VI) breakthrough curves for each figure. At some point near the peak U(VI) concentration, the experimental data rise above the model fit line in both columns. As the breakthrough curve begins to level off, the experimental data cross the model fit line and decrease in slope. The slope of the leached mass ratio model line is predominately a function of the retardation factor. The change in slope of the experimental data indicates that the distribution coefficient is decreasing during this initial portion of the experiment at the high water content. After the large pulse of U(VI) is eluted from the columns, the slope of the leached mass ratio

experimental data decreases, indicating an increase in the retardation factor. The low $Kd_{effective}$ values at the high water content may be attributable to the large pulse of U(VI) that elutes from the column initially. It appears that once the pulse elutes from the columns, the slope of the leached mass ratio experimental data decreases, indicating an increase in retardation and therefore the distribution coefficients.

Residence times can be used to determine whether a kinetic effect could explain the differences in distribution coefficients. The average residence times for column A and column B experiment 1 were 82.5 hours and 87.9 hours, respectively. The average residence times for columns A and B experiment 2 were 291.9 and 276.7 hours, respectively. Differences in measured distribution coefficients attributed to residence time variations are generally explained by an inability for a sediment/solution mixture to reach equilibrium. In regards to experiment 1, the residence time was shorter and the U(VI) released to solution was greater relative to the sorbed concentration than in experiment 2. This indicates that the sediment/solution mixture had time to reach equilibrium and that residence time was not likely a factor in explaining the differences in $Kd_{effective}$ values at the different water contents.

The solid-to-solution ratio was calculated for the leaching experiments to determine if the difference in $Kd_{effective}$ values at the different water contents may be explained by exposure to reactive surfaces and greater mixing with the aqueous phase. If there is less solution per unit mass of sediment in the second experiment, the higher $Kd_{effective}$ at the low water content may be attributed to less solution exposure to the contaminated sediment. For instance, Zheng and Wan (2005) found that increases in the volume:mass ratio, or the inverse of the solid-to-solution ratio, resulted in increased U(VI) released to solution. The solid-to-solution ratios were approximately

15,000 g/l in columns A and B during experiment 1 and approximately 17,000 g/l in columns A and B during experiment 2. The variation in solid-to-solution ratio was not distinctly different at the two water contents, so it is not believed that the solid-to-solution ratio played a role in causing the difference in $Kd_{effective}$ values at the two water contents.

The trend in increased $Kd_{effective}$ with decreasing water contents may be attributable to the pore regime through which the solution was traveling. A physicochemical interpretation of the effect of changes in water content on U(VI) leaching can be found in Figures 31 and 32. This conceptual model was developed in light of the non-reactive tracer breakthrough which indicated minimal immobile water within the columns. At the high water content, nearly all of the pores are filled with solution. This includes a large exposure to the less reactive gravel portion, which is considered to have little effect on sorption processes. During advective transport, as some of the U(VI) desorbs, it moves into pores composed of the less-reactive gravel through advection, dispersion, or diffusion where it is able to move at or near the average linear solution velocity with little interaction with the sediment. As the water content is lowered, the solution is restricted to finer and finer pores, because the largest diameter pores are the first to drain during desaturation. An illustration of this phenomenon is depicted in Figures 31. The small diameter pores are composed of the finest material, which possess the greatest surface area per unit mass and are the most reactive. As the solution is restricted to the finer pores, any U(VI) that desorbs is likely to be quickly adsorbed due to exposure to the highly reactive surfaces, resulting in retardation of the advancing solute front. Figure 32 provides a closer look at the conceptual pore regime and geochemical reactions occurring as water content is lowered. The overall effect is that at high water content less sorption occurs and $Kd_{effective}$ is lower. As the water content is

lowered, more adsorption is occurring per unit volume of solution, the $Kd_{effective}$ increases, and the solute front is increasingly retarded relative to the average solution velocity. It is important to note that the changes in water content were relatively small between the two experiments. The average water contents of experiment 1 were 0.146 and 0.147 for columns A and B, respectively. The average water contents of experiment 2 were 0.134 and 0.127 for columns A and B, respectively. It is not clear whether these changes in water content were great enough to substantially change the solute's exposure to reactive surfaces in the columns.

Two potential explanations for the large pulse may be inferred from the results of the batch desorption experiments. The first is the slow release of U(VI) from sorption sites in the voids of basalt lithic fragments. The large initial pulse may be due to the desorption of easily accessed sorbed U(VI). Following the release of the easily accessed U(VI), the U(VI) associated with the voids in the basalt lithic fragments would be released slowly by diffusion resulting in the near steady release of U(VI) following the initial pulse. Therefore, the low $Kd_{effective}$ at the high water content would be the result of the easily accessed U(VI) desorbing. The high $Kd_{effective}$ at the lower water content would be due to the slow release of U(VI) from the sorption sites associated with the voids within the basalt lithic fragments. The results of the non-reactive tracer modeling do not indicate the presence of immobile water in the columns as might be expected if the basalt lithic fragments contained voids accessed by diffusion only. However, the presence of these types of sorption sites cannot be completely ruled out based on the non-reactive tracer curve fitting performed in these experiments. If these voids do exist within the sediments used in the columns, their overall porosity, and in effect the immobile water fraction, would be quite low

relative to the volume of the entire column or of the overall porosity of the system, and in turn, not likely detected with a single non-reactive tracer.

The second explanation for the large pulse may be explained by the presence of multiple binding sites within the sediment that hold the U(VI) with varying degrees of strength. As was discussed by Sugita et al. (1995a) non-ideality in contaminant transport may be caused by pore scale variation in the retardation factor. This pore scale variation may be caused by adsorbents that hold U(VI) with various degrees of strength. The use of multi-site models in which a portion of the reactive sites are equilibrium sites and a portion of the sites are kinetically controlled have been used successfully to describe U(VI) transport (Barnett et al., 2000) and desorption (Liu et al., 2008). The presence of heterogeneous sorption sites in these sediments may also be partly responsible for the variations in $Kd_{effective}$ values determined at the different water contents. There is evidence for this in the results of the desorption experiments on freshly contaminated sediments and the results of desorption on the aged contaminated sediment samples. In examining the results of the desorption experiments on the freshly contaminated sediments at one contaminant concentration over three desorption washes (Figures 16-19), it was noted that the point estimated Kd values generally decreased with each wash. However, if a Kd is determined by calculating the slope of the line between two points, then there is an increase in Kd with each wash. For instance, in performing these calculations on the sediment contaminated with 71.8 ug/l of U(VI) (Figure 18), the slope of the line between the adsorbed equilibrated state and that following the first wash is 4.03 ml/g. The slope of the line between the first and second desorption wash is 8.44 ml/g. The slope of the line between the second and third desorption wash is 12.3 ml/g. This phenomenon may be due to heterogeneity of sorption sites. It is

possible that some of the intitially sorbed U(VI) was associated with both strong and weak sites. The U(VI) removed at the high water content would be the U(VI) associated with the weaker sites. As more of the U(VI) associated with the weaker sites is removed, the U(VI) associated with increasingly stronger sites remains. As the water content was lowered, the remaining U(VI) would be associated with stronger sorption sites resulting in higher $Kd_{effective}$ values at the lower water content.

The results of the desorption experiments on sediment samples Y1 and Y2 indicate that some of the U(VI) may be bound within the crystal structure of calcite given adequate time for the calcite to crystallize. Following contamination, the sediments that were packed in the column sat undisturbed for forty days prior to being saturated. This potentially could have been enough time for U(VI) adsorbed on to calcite to be incorporated into the crystal structure as additional calcite crystallized. If this were the case, then potentially some of the adorbed U(VI) may have desorbed during the initial portion of the leaching experiment at the high water content, resulting in a lower $Kd_{effective}$. This would be the fraction of U(VI) released during the large pulse at the high water content. As this fraction desorbed, the U(VI) incorporated into the calcite would remain. As the water content lowered, the U(VI) associated with the calcite would be removed much more slowly, resulting in a higher $Kd_{effective}$, which was observed during experiment 2. The presence of U(VI) incorporated into the crystal structure of calcite could potentially explain the trends seen the in the leached mass ratio model fits if the forty days the sediments sat prior to column leaching were enough time for the U(VI) to crystallize within the calcite.

The two potential explanations for the aging effect in the desorption experiments are not mutually exclusive. Both mechanisms could potentially be playing a role in the aging effect seen

in the desorption experiments as well as the trends in the leaching experiment in which $Kd_{effective}$ increased with decreasing water content. As was mentioned previously, U(VI) speciation analysis using absorption spectroscopy is needed to accurately characterize the bound U(VI) on the aged sediments from the contamination event and the sediment in the leaching experiment to identify the exact mechanism responsible for the trends seen in the desorption experiments as well as to aid in interpretation of the leaching experiments

4. Conclusions and Suggestions for Future Research

Results of the batch adsorption experiment on sediment collected from the Environmental Restoration Disposal Facility in the 200 Area of Hanford, Washington, indicated that 48 hours was an adequate amount of time for U(VI) to reach steady-state sorption. Distribution coefficients determined from batch desorption ($Kd_{des\ batch}$) data were all greater than distribution coefficients determined during adsorption (Kd_{batch}) suggesting U(VI) desorption hysteresis in the ERDF sediments. However, the results were not statistically significant at $p < .05$. Results of three desorption washes on contaminated sediment that sat undisturbed for seven months show a decrease in the percentage of U(VI) mass released to solution as the sorbed U(VI) concentration decreased. The opposite trend was observed for freshly contaminated sediments; the percentage of U(VI) released to solution increased with each wash. The variations in the trends were attributed to either calcite crystallization in the aged sediment, which may have incorporated a portion of the adsorbed U(VI) into its crystal structure, or the presence of voids within basalt lithic fragments accessed only by diffusion.

Non-reactive tracer experimental data collected at both high and low water contents of leaching experiments on contaminated ERDF sediment were modeled with the convection dispersion equation and the mobile-immobile model. The convection dispersion equation provided a better fit to the data at both the high and low water content as quantified using the root mean square error. The model fit dispersivities increased moving from high water content to low water content which was attributed to an increase in the tortuosity of the flowpaths as water content decreased.

Results of analytical modeling of the leaching experiments show an increase in the distribution coefficient ($Kd_{effective}$) as water content is lowered. Several potential explanations were proposed

to describe the observed behavior. First, a physicochemical interpretation which relates the solution pathway to exposure to reactive surfaces as water content is lowered was presented. At the high water content, a majority of the pores were filled with solution including pores composed of the less reactive gravel fraction. During leaching, U(VI) released from the contaminated sediments could move into these pores through advection, dispersion, and diffusion. Once the U(VI) in solution moved into these pores, it would move at or near the average solution velocity as it would have little interaction with the less reactive coarse fraction of sediment, resulting in low retardation and a low distribution coefficient. As the sediment desaturated, the largest particles would drain first and solution would be restricted to increasingly smaller diameter pores composed of the more reactive sediment. The U(VI) in solution in the finer pores would have greater interaction with the sediment due to the higher reactivity of the sediment relative to the coarse sediment of the larger diameter pores. This would overall act to increase the distribution coefficient and in turn the retardation factor and U(VI) transport would be increasingly retarded relative to the average solution velocity.

Two additional explanations for the increase in distribution coefficients with decreasing water content were proposed in light of the results of the desorption experiments on both the aged and the freshly contaminated sediments. The first explanation involves sorption sites within the voids of basalt lithic fragments. These sorption sites would be accessed only by diffusion. The large pulse of U(VI) removed at the higher water content, which resulted in a low $Kd_{effective}$, could potentially be the result of weakly held sorbed U(VI), which was easily removed from the sediment. Following removal of the portion of U(VI), the U(VI) associated with the sorption sites of the basalt lithic fragments would slowly release U(VI) to solution, which happened to

occur as the water content was lowered, resulting in a higher $Kd_{effective}$. The second explanation involves heterogeneity of sorption sites. Evidence for heterogeneity of sorption sites was presented based on the results of desorption experiments on freshly contaminated sediments; the Kd calculated based on the slope of the line between equilibrated states following each of three desorption washes increased with each wash indicating that a range of sorption sites that hold U(VI) with varying strength may be present in the sediment. The incorporation of adsorbed U(VI) as calcite crystallized in the aged sediments was also proposed as being responsible for variations in release rates. Evidence for the incorporation of U(VI) into the crystal structure of calcite was presented by Elzinga et al. (2004) and Reeder et al. (2001). The sediments used in the leaching experiments sat for forty days after being contaminated, but prior to leaching. If this was enough time for calcite crystallization, then there is the potential that some of the U(VI) was incorporated into the crystal structure of calcite. As leaching began, the adsorbed U(VI) may have been released to solution, resulting in the large pulse of U(VI) that eluted from the columns at the beginning of the experiments. The U(VI) incorporated into the calcite would be removed much more slowly. The result is that as the experiments were initiated, at the high water content, the adsorbed U(VI) was removed, resulting in a lower overall $Kd_{effective.}$ As the water content was lowered a large portion of the U(VI) remaining in the columns was associated with the calcite and not easily removed, resulting in a higher $Kd_{effective..}$ This would account for the trends seen in the leached mass ratio model fits, in which at the higher water content, the experimental data vary around the model indicating a change in retardation before water content was changed.

Additional leaching experiments are needed to determine whether the increases in $Kd_{effective}$ with decreases in water content were due to physical effects and solute exposure to reactive surfaces

or some type of chemical heterogeneity in which variations in sorption site strength or access to sorption sites caused the variation in $Kd_{effective}$ at the different water contents. These experiments were potentially biased towards a low $Kd_{effective}$ at the high water content simply due to the order in which they were run (i.e. high water content to low water content). U(VI) associated with weaker sites may have leached at the high water content resulting in a low $Kd_{effective}$, while U(VI) associated with the stronger sites was leached at the lower water content resulting in a high $Kd_{effective}$. Leaching experiments run simultaneously on several replicate columns at several different water contents would help in distinguishing the water content effect from a chemical heterogeneity effect.

This work indicates that aging may increase U(VI) affinity for the solid phase and that speciation of U(VI) may change in time as well. This has important implications for the Hanford Site, where there is ongoing research regarding the persistence of a U(VI) plume in the vadose zone and underlying aquifer. Predictions of release rates may be underestimated if changes in U(VI) speciation with time are not accounted for in modeling studies. Additional spectroscopic and luminescence work is need to accurately identify the U(VI) phase in the aged sediment and the columns from the leaching experiments in order to identify the mechanisms behind the aged sediment's increased affinity for the solid phase.

References

Barnett, M.O., P.M. Jardine, S.C. Brooks, and H.M. Selim. 2000. Adsorption and transport of uranium(VI) in subsurface media. Soil Science Society of America Journal. 64:908-917.

Beese, F. and P.J. Wierenga. 1980. Solute transport through soil with adsorption and root water uptake computed with a transient and a constant-flux model. Soil Science. 129:245-252.

Bellin, A., A. Rinaldo, W.J.P. Bosma, S.E.A.T.M. van der Zee, and Y. Rubin. 1993. Linear equilibrium adsorbing solute transport in physically and chemically heterogeneous porous formations 1. Analytical solutions. Water Resources Research. 29:4019-4030.

Bjornstad, B. 2002. Standardized stratigraphic nomenclature for post-Ringold-Formation sediments within the Central Pasco Basin. DOE/RL-2002-39. Rev-0.

Bosma, W.J.P., A. Bellin, S.E.A.T.M. van der Zee, and A. Rinaldo. 1993. Linear equilibrium adsorbing solute transport in physically and chemically heterogeneous porous formations 2. Numerical results. Water Resources Research. 29:4031-4043.

Bouwer, H. and R.C. Rice. 1984. Hydraulic properties of stony vadose zones. Ground Water. 22:696-705.

Brakensiek, D.L. and W.J. Rawls. 1994. Soil containing rock fragments: Effects on infiltration. Catena. 23:99-110.

Brooks, R.H. and A.T. Corey. 1964. Hydraulic properties of porous media. Hydrol. pap.3. Colorado State University, Fort Collins, CO.

Brooks, R.H. and A.T. Corey. 1966. Properties of porous media affecting fluid flow. Proceedings, American Society of Civil Engineers, Irrigation and Drainage Division. 92. IR2:61-87.

Butcher, R., C. Hinz, M. Flury, and H. Fluhler. 1995. Heterogeneous flow and transport in an unsaturated stony soil monolith. Soil Science Society of America Journal. 59:14-21.

Campbell, G.S. 1974. A simple method for determining unsaturated conductivity from moisture retention data. Soil Science. 117:311-314.

Cantrell, K.J., J.M. Zachara, P.E. Dresel, K.M. Krupka, and R.J. Serne. 2007. Geochemical processes data package for the vadose zone in the single-shell tank waste management area at the Hanford Site. PNNL-16663. Pacific Northwest National Laboratory. Richland, WA.

Coats, K.H. and B.D. Smith. 1964. Dead-end pore volume and dispersion in porous media. Society of Petroleum Engineers Journal. 25:793-803.

Cousin, I., B. Nicoullaud, and C. Coutadeur. 2003. Influence of rock fragments on the water retention and water percolation in a calcareous soil. Catena. 53:97-114.

Dane, J.H., M. Oostrom, and B.C. Missildine. 1992. An improved method for the determination of capillary pressure-saturation curves involving TCE, water and air. Journal of Contaminant Hydrology. 11:69-81.

Dong, W.M. and S.C. Brooks. 2006. Determination of the formation constants of ternary complexes of urnayl and carbonate with alkaline earth metals (Mg2+, Ca2+, Sr2+, and Ba2+) using anion exchange method. Environmental Science and Technology. 40:4689-4695.

Dunn, A.J. and G.R. Mehuys. 1984. Relationship between gravel content of soils and saturated hydraulic conductivity in laboratory tests. In: Erosion and Productivity of Soils Containing Rock Fragments. Soil Science Society of America, Madison, WI, Ch. 10, pp. 91-101.

Elzinga, E.J, C.D. Tait, R.J. Reeder, K.D. Rector, R.J. Donohoe, and D.E. Morris. 2004. Spectroscopic investigation of U(VI) sorption at the calcite-water interface. Geochimica et Cosmochimica Acta. 68:2437-2448.

Fuhrmann, M., H. Zhou, J. Neiheisel, M.A.A. Schoonen, and R. Dyer. 1997. Sorption/desorption of radioactive contaminants by sediment from the Kara Sea. The Science of the Total Environment. 202:5-24.

Gamerdinger, A.P. and D.I. Kaplan. 2000. Application of a continuous-flow centrifugation method for solute transport in disturbed, unsaturated sediments and illustration of mobile-immobile water. Water Resources Research. 36:1747-1755.

Gamerdinger, A.P., D.I. Kaplan, D.M. Wellman, and R.J. Serne. 2001a. Two-region flow and rate limited sorption of uranium(VI) during transport in an unsaturated silt loam. Water Resources Research. 37:3147-3153.

Gamerdinger, A.P., D.I. Kaplan, D.M. Wellman, and R.J. Serne. 2001b. Two-region flow and decreased sorption of uranium(VI) during transport in Hanford groundwater and unsaturated sands. Water Resources Research. 37:3155-3162.

Giammar, D.E. and J.G Hering. 2001. Time scales for sorption-desorption and surface precipitation of uranyl on goethite. Environmental Science and Technology. 35:3332-3337.

Grenth, I, J. Fuger, R.J.M. Konings, R.J. Lemire, A.B. Muller, C. Nguyen-Trung Cregu, and H. Wanner. 1992. Chemical thermodynamics of uranium. Elsevier Science, Amsterdam, the Netherlands.

Grenth, I., M.C.A. Sandino, I. Puidomenech and M.H. Rand. 1995. “Corrections to the NEA-TDB review.” In: Chemical thermodynamics of Americium (R.A. Silva, G. Bidoglio, M. Rand, P.B. Robouch, H. Wanner and I. Puigdomenech, eds.), pp. 347-374. Elsevier Science. Amsterdam, the Netherlands.

Guillaumont, R., T. Fanghanel, V. Neck, J. Fuger, D.A. Palmer, I. Grenthe and M.H. Rand. 2003. Update on the chemical thermodynamics of uranium, neptunium, plutonium, americium, and technetium. Elsevier B.V., Amsterdam, the Netherlands.

Guo, Z.J. and W.S. Wu. 2009. Sorption and desorption of uranium(VI) on silica: Experimental and modeling studies. Radiochimica Acta. 97:133-140.

Hillel, D. 1980. Fundamentals of Soil Physics. New York: Academic Press.

Jalbert, M., J.H. Dane, and H.H. Liu. 1999. TrueCell: Physical point Brooks-Corey parameters using pressure cell data, User's guide for version 1.2. Department of Agronomy and Soils, Special Rep. Alabama Agricultural Experiment Station, Auburn University, Auburn, AL.

Kaplan, D.I. and R.J. Serne. 1995. Distribution coefficient values describing iodine, neptunium, selenium, technetium, and uranium sorption to Hanford sediments. PNNL-10379. Pacific Northwest National Laboratory. Richland, WA.

Kaplan, D.I., R.J. Serne, A.T. Owen, J. Conca, T.W. Wietsma, and T.L. Gervais. 1996. Radionuclide adsorption distribution coefficients measured in Hanford sediments for the low level waste performance assessment project. PNNL-11485. Pacific Northwest National Laboratory. Richland, WA.

Kaplan, D.I., T.L. Gervais, and K.M. Krupka. 1997. Uranium(VI) sorption to sediments under high pH and ionic strength conditions. Radiochimica Acta. 80:201-211.

Kaplan, D.I., I.G. Kutnyakov, A.P. Gamerdinger, R.J. Serne, and K.E. Parker. 2000. Gravel-corrected Kd values. Ground Water. 38:851-857.

Kozak, J.A. and L.R. Ahuja. 2005. Scaling of infiltration and redistribution of water across soil textural classes. Soil Science Society of America Journal. 69:816-827.

Lindenmeier, C.W., R.J. Serne, J.L. Conca, A.T. Owen, and M.I. Wood. 1995. Solid waste leach characteristics and contaminant-sediment interactions volume 2: Contaminant transport under unsaturated moisture contents. PNNL-10722. Pacific Northwest National Laboratory. Richland, WA

Lindstrom, F.T., R. Haque, V.H. Freed, and L. Boersma. 1967. Theory of the movement of some herbicides in soils: Linear diffusion and convection of chemicals in soils. Environmental Science and Technology. 1:561-565.

Liu, C., J.M. Zachara, N.P. Qafoku, and Z. Wang. 2008. Scale dependent desorption of uranium from contaminated subsurface sediments. Water Resources Research.44:W08413.

Liu, H.H. and J.H. Dane. 1995. Improved computational procedure for retention relations of immiscible fluids using pressure cells. Soil Science Society of America Journal. 59:1520-1524.

Mayes, M.A., G. Tang, P.M. Jardine, L.D. McKay, X.L. Yin, M.N. Pace, J.C. Parker, F. Zhang, T.L. Mehlhorn, and R.N. Dansby-Sparks. 2009. Influence of sedimentary bedding on reactive transport parameters under unsaturated conditions. Soil Science Society of America Journal. 73:1938-1946.

McKinley, J.P., J.M. Zachara, J. Wan, D.M. McCread, and S.M. Heald. 2007. Geochemical controls on contaminant uranium in vadose Hanford Formation sediments at the 200 Area and 300 Area, Hanford Site, Washington. Vadose Zone Journal. 6:1004-1017.

Mehuys, G.R., L.H. Stolzy, J. Letey, and L.V. Weeks. 1975. Effect of stones on the hydraulic conductivity of relatively dry desert soils. Soil Science Society of America Proc. 39:37-42.

Moyes, L.N., R.H. Parkman, J.M. Charnock, D.J. Vaughan, F.R. Livens, C.R. Hughes, and A. Braithwaite. 2000. Uranium uptake from aqueous solution by interaction with goethite, lepidocrocite, muscovite, and mackinawite: An x-ray absorption spectroscopy study. Environmental Science and Technology. 34:1062-1068.

Pace, M.N., M.A. Mayes, P.M. Jardine, T.L Mehlhorn, J.M. Zachara, and B.N. Bjornstad. 2003. Quantifying the effects of small-scale heterogeneities on flow and transport in undisturbed cores from the Hanford formation. Vadose Zone Journal. 2:664-676.

Pace, M.N., M.A. Mayes, P.M. Jardine, L.D. McKay, X.L. Yin, T.L. Mehlhorn, Q. Liu, and H. Gurleyuk. 2007. Transport of Sr^{2+} and $SrEDTA^{2-}$ in partially–saturated and heterogenous sediments. Journal of Contaminant Hydrology. 91:267-287.

Peck, A.J. and J.D. Watson. 1979. Hydraulic conductivity and flow in non-uniform soil. In Workshop on Soil Physics and Heterogeneity. CSIRO Division of Environmental Mechanics, Canberra, Australia, February 12-14, 1979.

Peterson, R.E. (Editor). 2008. Uranium contamination in the subsurface beneath the 300 Area Hanford Site, Washington. PNNL-17034. Pacific Northwest National Laboratroy, Richland, Washington. (Contributors: Peterson, R.E., M.L. Rockhold, R.J. Serne, P.D. Thorne, and M.D. Williams)

Poesen, J. and H. Lavee. 1994. Rock fragment in top soils: Significance and processes. Catena. 23:1-28.

Ravina, I. and J. Magier. 1984. Hydraulic conductivity and water retention of clay soils containing coarse fragments. Soil Science Society of America Journal. 48:736-740.

Rawls, W.J., D.L. Brakensiek, and K.E. Saxton. 1982. Estimation of soil water properties. Trans. ASAE. 25:1315-1320.

Reeder, R.J., M. Nugent, G.M. Lamble, C.D. Tait, and D.E. Morris. 2000. Uranyl incorporation into calcite and aragonite; XAFS and luminescence studies. Environmental Science and Technology. 34:638-644.

Reeder, R.J., M. Nugent, C.D. Tait, D.E. Morris, S.M. Heald, K.M. Beck, W.P. Hess, and A. Lanzirotti. 2001. Coprecipitation of uranium(VI) with calcite: XAFS, micr-XAS, nd luminescence characterization. Geochemica et Cosmochimica Acta. 65:3491-3503.

Riley, R.G., and J.M. Zachara. 1992. Chemical contaminant on DOE lands and selection of contaminant mixtures for subsurface science research. US-DOE, Office of Energy Resources. Washington, D.C.

Russo, D. 1983. Leaching characteristics of a stony desert soil. Soil Science Society of America Journal. 47:431-438.

Serne, R.J., C.F. Brown, H.T. Schaef, E.M. Pierce, M.J. Lindberg, Z. Wang, P.L. Gassman, and J.G. Catalano. 2002. 300 Area uranium leach and adsorption project. PNNL-14022. Pacific Northwest National Laboratory. Richland, WA.

Shackelford, C.D. and M.J. Glade. 1997. Analytical mass leaching model for contaminated soil and soil stabilized waste. Ground Water. 35:233-242.

Šimůnek, J. and M. Šejna. 2007. HYDRUS (2D/3D) software package for simulating the two- and three-dimensional movement of water, heat, and multiple solutes in variably-saturated media. Version 1.02. PC-Progress. Prague, Czech Republic.

Stewart, B.D., M.A. Mayes, and S. Fendorf. 2010. Impact of uranyl-calcium-carbanato complexes on uranium(VI) adsorption to synthetic and natural sediments. Environmental Science and Technology. 44:928-934.

Stubbs, J.E., L.A. Veblen, D.C. Elbert, J.M. Zachara, J.A. Davis, and D.R. Veblen. 2009. Newly recognized hosts for uranium in the Hanford Site vadose zone. Geochimica et Cosmochimica Acta. 73:1563-1576.

Sugita, F. and R.W. Gillham. 1995a. Pore scale variation in retardation factor as a cause of nonideal reactive breakthrough curves 1. Conceptual model and its evaluation. Water Resources Research. 31:103-112.

Sugita, F., R.W. Gillham, and C. Mase. 1995b. Pore scale variation in retardation factor as a cause of nonideal reactive breakthrough curves 2. Pore network analysis. Water Resources Research. 31:113-119.

Szecsody, J.E., J.M. Zachara, A. Chilakapati, P.M. Jardine, and A.S. Ferrency. 1998. Importance of flow and particle-scale heterogeneity on $Co^{II/III}$EDTA reactive transport. Journal of Hydrology. 209:112-136.

Tang, G., M.A. Mayes, J.C. Parker, and P.M. Jardine. 2010. CXTFIT/Excel-A modular adaptable approach for parameter estimation, sensitivity analysis and uncertainty analysis. Computer and Geosciences. doi:10.1016/j.cageo.2010.01.013

Toride, N., F.J. Leij, and m. Th. van Genuchten. 1995. The CXTFIT code for determining transport parameters from laboratory or field tracer experiments. Version 2.0. U.S. Salinity Laboratory, Agricultural Research Services, USDA, Riverside, CA.

Um, W., R.J. Serne, B.N. Bjornstad, H.T. Schaef, C.F. Brown, V.L. LeGore, K.N. Geiszler, S.R. Baum, M.M. Valenta, I.V. Kutnyakov, T.S. Vickerman, and M.J. Lindberg. 2005. Characterization of 200-UP-1 aquifer sediments and results of sorption-desorption tests using spiked uncontaminated groundwater. PNNL-15502. Pacific Northwest National Laboratory. Richland, WA.

Um, W., R.J. Serne, C.F. Brown, and G.V. Last. 2007. U(VI) adsorption on aquifer sediments at the Hanford Site. Journal of Contaminant Hydrology.93:255-269.

Um, W., R.J. Serne, C.F. Brown, and K.A. Rod. 2008. Uranium(VI) sorption on iron oxides in Hanford Site sediment: Application of a surface complexation model. Applied Geochemistry. 23:2649-2657.

Um, W., R.J. Serne, G.V. Last, R.E. Clayton, and E.T. Glossbrenner. 2009. The effect of gravel size fraction on the distribution coefficients of selected radionuclides. Journal of Contaminant Hydrology. 107:82-90.

van Genuchten, M. Th. and P.J. Wierenga. 1976. Mass transfer studies in sorbing porous media 1. analytical solutions. Soil Science Society of America Journal. 40:473-480.

van Genuchten, M. Th. 1980. A closed-form equation for predicting the hydraulic conductivity of unsaturated soils. Soil Science Society of America Journal. 48:50-55.

van Genuchten, M. Th. 1981. Analytical solutions for chemical transport with simultaneous adsorption, zero-order production, and firt-order decay. Journal of Hydrology. 49:213-233.

van Genuchten, M. Th. and W.J. Alves. 1982. Analytical solutions for the one-dimensional convetive-dispersive solute transport equation. U.S. Department of Agriculture. Technical Bulletin 1661.

van Genuchten, M. Th. and J.C. Parker. 1984. Boundary conditions for displacement experiments through short laboratory columns. Journal of the Soil Science Society of America. 48:703-708.

Verbist, K., J. Baetens, W.M. Cornelis, D. Gabriels, C. Torres, and G. Soto. 2009. Hydraulic conductivity as influenced by the stoniness in degraded drylands of Chile. Soil Science Society of America Journal. 73:471-484.

Waite, T.D., J.A. Davis, T.E. Payne, G.A. Waychunas, and N. Xu. 1994. Uranium(VI) adsorption to ferrihydrite: Application of a surface complexation model. Geochimica et Cosmochimica Acta. 58:5465-5478.

Wellman, D.M., A.P. Gamerdinger, D.I. Kaplan, and R.J. Serne. 2008a. Effect of particle-scale heterogeneity on uranium (VI) transport in unsaturated porous media. Vadose Zone Journal. 7:67-78.

Wellman, D.M., J.M. Zachara, C. Liu, N.P. Qafoku, S.C. Smith, and S.W. Forrester. 2008b. Advective desorption of uranium(VI) from contaminated Hanford vadose zone sediments under saturated and unsaturated conditions. Vadose Zone Journal. 7:1144-1159.

Wierenga, P.J. 1977. Solute distribution profiles computed with steady-state and transient water movement models. Soil Science Society of America Journal. 41:1050-1055.

Wierenga, P.J. and M.T. van Genuchten. 1989. Solute transport through small and large unsaturated soil columns. Ground Water. 27:35-42.

Zheng, Z., T.K. Tokunaga, and J. Wan. 2003. Influence of calcium carbonate on U(VI) sorption to soils. Environmental Science and Technology. 37: 5603-5608.

Zheng, Z. and Wan, J. 2005. Release of contaminant U(VI) from soils. Radiochim Acta. 93:211-217.

Appendix

Table 1. Mineralogy of 200W Area Hanford Formation sediment (from Pace et al., 2003).

Size Fraction	Mineralogy
Sand	Quartz>Plagioclase>Mica>Kaolinite>Chlorite>Calcite
Silt	Quartz>Mica>Plagioclase>Kaolinite>Chlorite>Smectite
Clay	Illite>Kaolinite>Chlorite/HIV*>Smectite>Quartz>Plagioclase

*Hydroxy-Interlayered Vermiculite

Table 2. Grain size distribution of repacked columns.

Grain Size (mm)	Mass % Makeup
>31.5	13.9
16-31.5	19.9
12.5-16	6.0
8-12.5	15.4
6.7-8	9.4
4.75-6.7	7.7
2-4.75	9.0
1-2	3.8
.5-1	3.1
.25-.5	3.0
.106-.25	3.4
.053-.106	1.6
<.053	3.8

Table 3. Chemical composition of synthetic groundwater (SGW).

Constituents	Concentration (mg/l)
Na^+	33.1
K^+	6.2
Ca^{2+}	40.1
Mg^{2+}	12.3
HCO_3^-	97.6
Cl^-	46.1
SO_4^-	60.6
NO_3^-	28.5
pH	7.85

Table 4. Measured distribution coefficients from contamination event.

Column A		Column B		Extra	
Sample	Kd_{Cont} (ml/g)	Sample	Kd_{Cont} (ml/g)	Sample	Kd_{Cont} (ml/g)
A1	3.50	J1	2.27	S2	3.94
A2	2.88	J2	3.63	T2	3.88
B1	2.06	K1	3.43	Y1	3.97
B2	3.12	K2	3.31	Y2	3.69
C1	2.21	L1	2.32		
C2	2.82	L2	2.43		
D1	3.53	M1	3.70		
D2	2.57	M2	3.73		
E1	3.24	N1	3.29		
E2	3.09	N2	3.61		
F1	2.08	O1	2.93		
F2	3.09	O2	4.63		
G1	3.28	P1	4.23		
G2	2.68	P2	3.04		
H1	3.28	Q1	4.20		
H2	1.78	Q2	3.76		
I1	2.29	R1	3.58		
I2	1.83	R2	4.84		
S1	3.18	T1	3.61		
X1	4.16	Z1	4.13		
X2	4.00	Z2	4.52		

Table 5. Results of ANOVA examining the difference in distribution coefficients between sediment contaminated with two different U(VI) solution concentrations.

Source of Variation	Sum of Squares	Degrees of Freedom	Mean Square	F Value	Probability
Solution Concentration	13.1	1.00	13.1	45.2	2.93E-08
Error	12.7	44.0	0.289		
Total Variation	25.8	45.0			

Table 6. Results of ANOVA examining the difference between the pH of the supernatant of the two groups of sediment contaminated with different U(VI) solution concentrations.

Source of Variation	Sum of Squares	Degrees of Freedom	Mean Square	F Value	Probability
Solution Concentration	0.0288	1.00	0.0288	3.75	0.0593
Error	0.338	44.0	0.00768		
Total Variation	0.367	45.0			

Table 7. Linear sorption and Freundlich isotherm fits to the batch adsorption experiments. The contaminating solution concentrations ranged from 5.55-80.1 ug/l.

Time	Linear Sorption Isotherm Fit		Freundlich Isotherm Fit		
	Kd_{batch} (ml/g)	R^2	K	n	R^2
48 hours	4.70 ± 0.882	0.989	0.891 ± 3.63	0.902 ± 0.236	0.996
96 hours	5.78 ± 1.08	0.990	2.34 ± 11.0	0.947 ± 0.267	0.995
168 hours	5.43 ± 1.24	0.985	1.03 ± 5.21	0.903 ± .291	0.993

± 95% Confidence Intervals

Table 8. Distribution coefficients determined on sediment from the batch desorption experiments.

	$Kd_{des\ batch}$ (ml/g)	R^2
Desorption #1	7.91 ± 2.33	0.975
Desorption #2	8.89 ±4.19	0.940
Desorption #3	8.44 ± 5.31	0.897

± 95% Confidence Intervals

Table 9. Mass percent of U(VI) desorbed from sediment samples Y1 and Y2 after each of three desorption equilibrations. The contaminated sediments sat undisturbed for seven months prior to desorption experiments.

Sediment Sample	Y1			Y2		
	$Kd_{des\ Cont}$ (ml/g)	Percent of Total Initially Sorbed U(VI) Mass Desorbed (%)	Percent of Previously Sorbed U(VI) Mass Desorbed (%)	$Kd_{des\ Cont}$ (ml/g)	Percent of Total Initially Sorbed U(VI) Mass Desorbed (%)	Percent of Previously Sorbed U(VI) Mass Desorbed (%)
Adsorption	3.97			3.69		
Desorption #1	6.97	43.2	43.2	5.76	47.0	47.0
Desorption #2	12.0	58.5	26.9	10.4	62.4	29.1
Desorption #3	31.4	63.5	12.1	22.1	68.7	16.9

Table 10. Mass percent of U(VI) desorbed from sediment samples contaminated with 15.1 and 31.5 ug/l U(VI) after each of three desorption equilibrations. The desorption experiments began immediately following the batch adsorption experiments.

Sediment Sample	15.1 ug/l			31.5 ug/l		
	Point Estimate Kd (ml/g)	Percent of Total Initially Sorbed U(VI) Mass Desorbed (%)	Percent of Previously Sorbed U(VI) Mass Desorbed (%)	Point Estimate Kd (ml/g)	Percent of Total Initially Sorbed U(VI) Mass Desorbed (%)	Percent of Previously Sorbed U(VI) Mass Desorbed (%)
Adsorption	6.28			6.87		
Desorption #1	8.50	34.7	34.7	9.21	33.2	33.2
Desorption #2	5.33	65.8	47.6	7.74	58.7	38.2
Desorption #3	1.12	93.2	80.2	5.07	78.9	48.8

Table 11. Mass percent of U(VI) desorbed from sediment samples contaminated with 71.8 and 80.1 ug/l U(VI) after each of three desorption equilibrations. The desorption experiments began immediately following the batch adsorption experiments.

Sediment Sample	71.8 ug/l			80.1 ug/l		
	Point Estimate Kd (ml/g)	Percent of Total Initially Sorbed U(VI) Mass Desorbed (%)	Percent of Previously Sorbed U(VI) Mass Desorbed (%)	Point Estimate Kd (ml/g)	Percent of Total Initially Sorbed U(VI) Mass Desorbed (%)	Percent of Previously Sorbed U(VI) Mass Desorbed (%)
Adsorption	5.52			5.42		
Desorption #1	7.21	38.6	38.6	8.22	35.2	35.2
Desorption #2	6.52	64.3	41.9	8.69	58.1	35.4
Desorption #3	4.28	83.2	52.8	6.30	76.3	43.3

Table 12. Columns A and B physical properties.

	Column A	Column B
Length (cm)	30.5	30.5
Diameter (cm)	8.8	8.8
Bulk Density (g/cm^3)	2.25	2.25
Porosity	.152	.152
Saturated Hydraulic Conductivity (cm/s)	2.04×10^{-6}	2.06×10^{-6}

Table13. Transport parameters determined from non-reactive tracer breakthrough.

	Residence Time (hours)	θ	Dispersivity† (cm)	Flux† (cm/h)	Peclet	RMSE
Column A Experiment 1 (High Water Content)	82.5	0.146	1.51 ± 0.438	0 .054 ±0 .002	20.2	0.0302
Column B Experiment 1 (High Water Content)	87.9	0.147	1.40 ± 0.154	0 .053 ± .0007	21.8	0.0537
Column A Experiment 2 (Low Water Content)	291.9*	0.134	NA	NA	NA	NA
Column B Experiment 2 (Low Water Content)	276.7	0.127	3.11 ± 0.311	0 .014 ± 0.0001	9.88	0.0121

NA-Not Available
†Fit to bromide data
*Calculated using Column B velocity
± Standard Error

Table 14. Relative saturation at high and low water contents and distribution coefficients determined for each experiment using the leached mass ratio approach.

Experiment	Column A Relative Saturation	Column B Relative Saturation	Method of determining Kd	Column A Kd (ml/g)	Column B Kd (ml/g)
Batch Experiment	1.00	1.00	Average (<2 mm)	2.89	3.58
			Mass Average ($Kd_{mass\ avg}$)	0.696	0.862
Experiment 1 (High Water Content)	.96	.97	Leaching Mass Ratio ($Kd_{effective}$)	0.329	0.453
			SSQ	2.7×10^{-2}	2.9×10^{-3}
Experiment 2 (Low Water Content)	.88	.84	Leaching Mass Ratio ($Kd_{effective}$)	0.431	0.741
			SSQ	6.7×10^{-6}	2.0×10^{-4}

Table 15. Cation concentrations for select effluent samples from columns A and B.

	Al (mg/l)	Ca (mg/l)	Fe (mg/l)	K (mg/l)	Mg (mg/l)	Mn (mg/l)	Na (mg/l)	Sr (mg/l)
Sample	Column A High Water Content							
A46	ND	172	0.252	15.3	46.2	0.082	42.4	0.927
A65	ND	220	0.335	15.7	61.6	0.061	49.7	1.21
A83	ND	153	0.217	13.2	42.8	0.043	41.8	0.842
A102	ND	119	0.130	100	28.4	0.027	35.1	0.547
A123	0.003	66.7	0.073	8.55	19.8	0.018	29.7	0.374
A141	ND	55.3	0.053	8.41	16.5	0.015	27.2	0.311
A164	ND	49.3	0.028	6.95	14.7	0.013	25.9	0.280
A182	0.005	46.9	0.026	6.77	13.8	0.012	24.9	0.268

	Al (mg/l)	Ca (mg/l)	Fe (mg/l)	K (mg/l)	Mg (mg/l)	Mn (mg/l)	Na (mg/l)	Sr (mg/l)
	Column A Low Water Content							
A209	ND	47.0	0.027	7.10	13.8	0.012	25.4	0.270
A212	0.001	44.9	0.027	6.64	13.2	0.011	24.4	0.262
A217	0.002	44.8	0.021	6.77	13.2	0.011	24.6	0.258
A233	0.002	44.2	0.028	6.32	13.1	0.008	24.4	0.257
	Column B High Water Content							
B10	ND	156	0.275	11.9	43.7	0.112	41.3	0.880
B31	0.005	231	0.403	13.7	65.1	0.116	51.7	1.51
B54	ND	166	0.280	12.3	46.4	0.078	44.8	0.926
B78	ND	116	0.135	9.21	27.6	0.041	35.1	0.530
B103	ND	56.8	0.061	7.04	16.7	0.022	28.1	0.320
B128	0.006	52.1	0.053	6.86	15.2	0.021	26.7	0.292
B132	ND	49.7	0.049	103	14.9	0.020	27.3	0.287
	Column B Low Water Content							
B135	0.005	53.1	0.114	7.21	15.7	0.023	27.8	0.301
B140	ND	52.6	0.055	7.35	15.4	0.021	27.4	0.301
B152	0.014	50.8	0.046	6.95	14.9	0.020	26.9	0.293
B187	0.026	51.2	0.046	7.03	15.1	0.020	27.0	0.291
B221	ND	50.9	0.045	6.76	14.9	0.018	26.6	0.290
B236	0.002	51.6	0.042	7.06	15.3	0.016	27.3	0.295
B256	ND	49.4	0.045	6.78	14.7	0.013	26.3	0.292

ND-Not Detectable

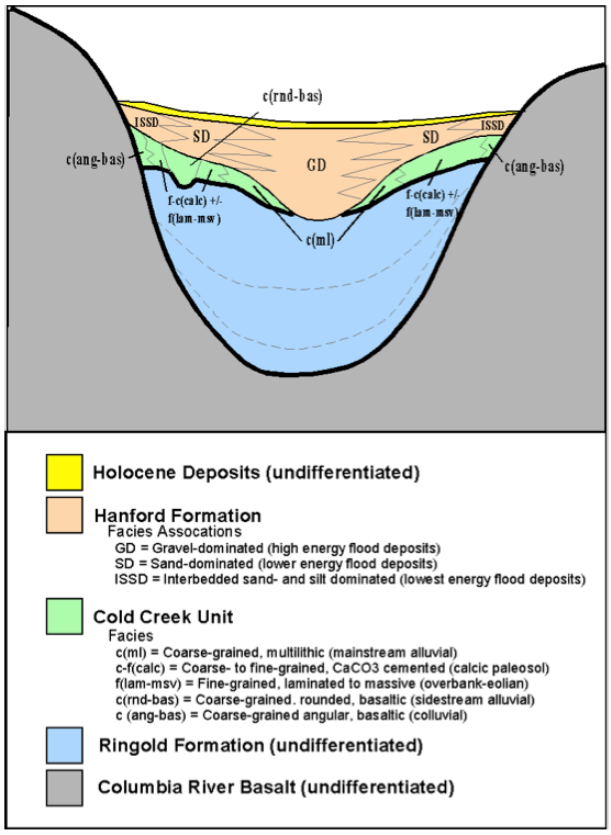


Figure 1. General representation of stratigraphic units within the Central Pasco Basin (from Bjornstad, 2002).

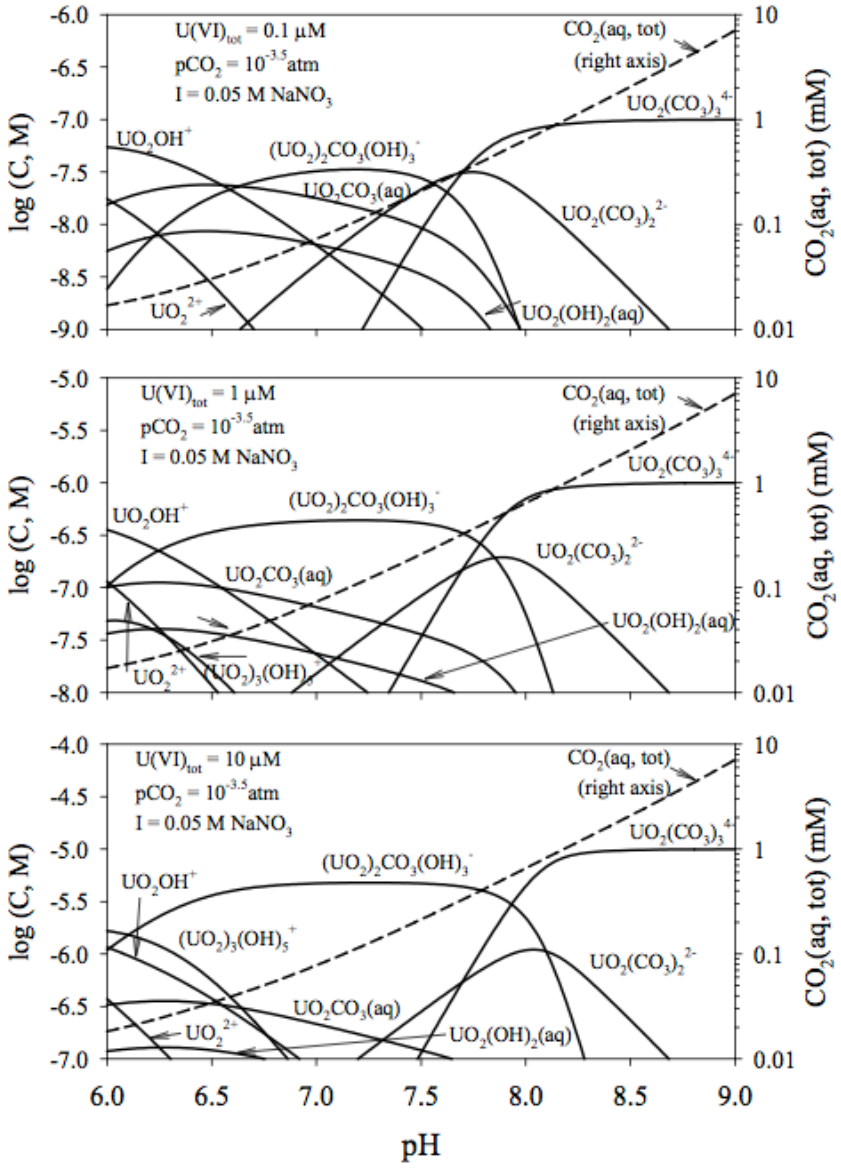


Figure 2. U(VI) speciation as a function of pH and carbonate concentration (from Peterson, 2008).

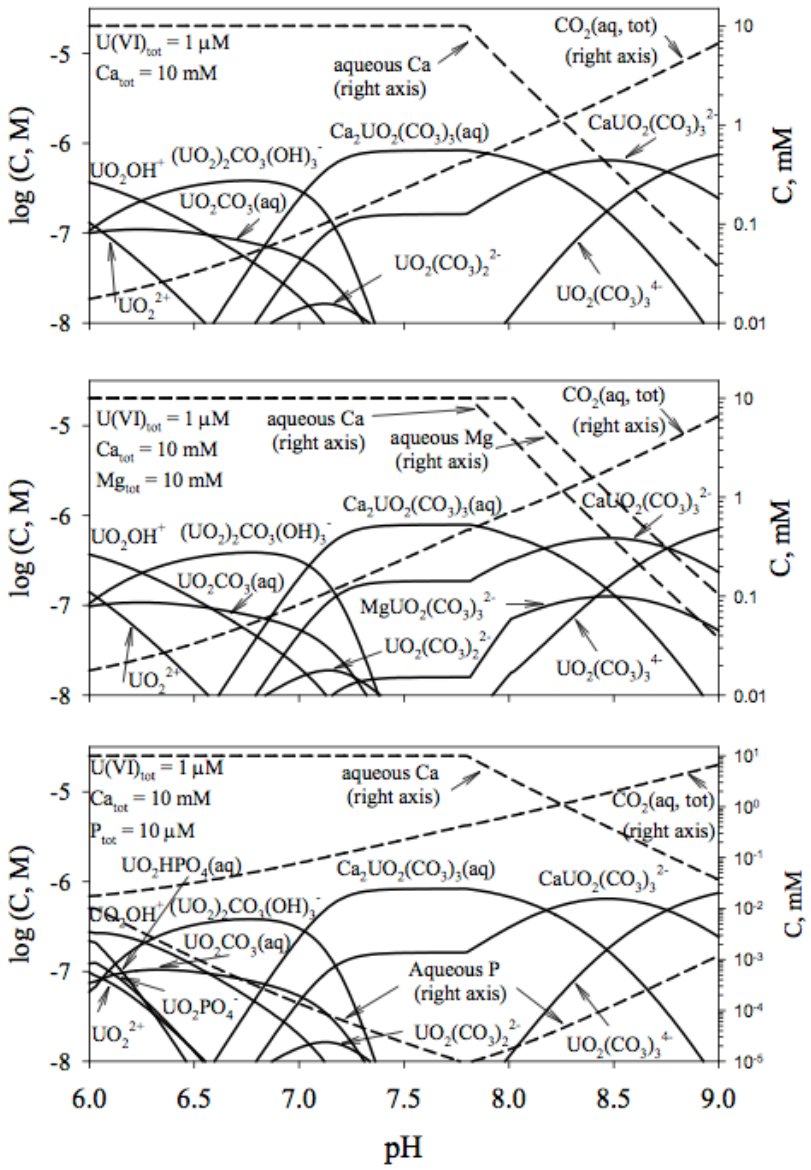


Figure 3. U(VI) speciation as a function of calcium, calcium and magnesium, and calcium and phosphate concentrations in the top, middle, and lower panels, respectively (from Peterson, 2008). The total concentrations of both calcium and magnesium were 10mM.

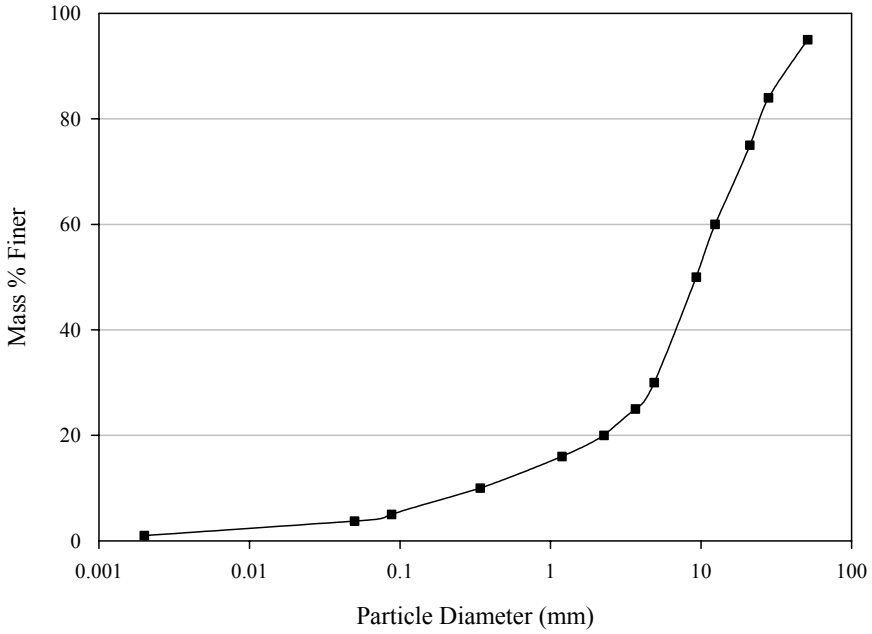


Figure 4. Average grain size distribution curve of two grab samples from Core 2-26, 300 Area, Hanford, WA.

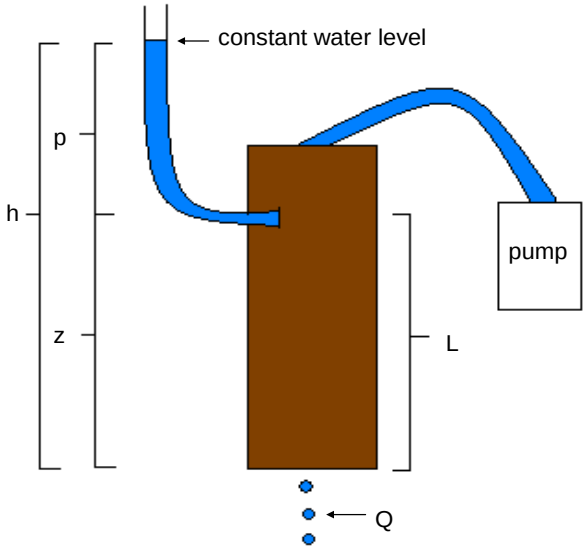


Figure 5. Modified constant head setup for measuring saturated hydraulic conductivity on repacked sediment cores.

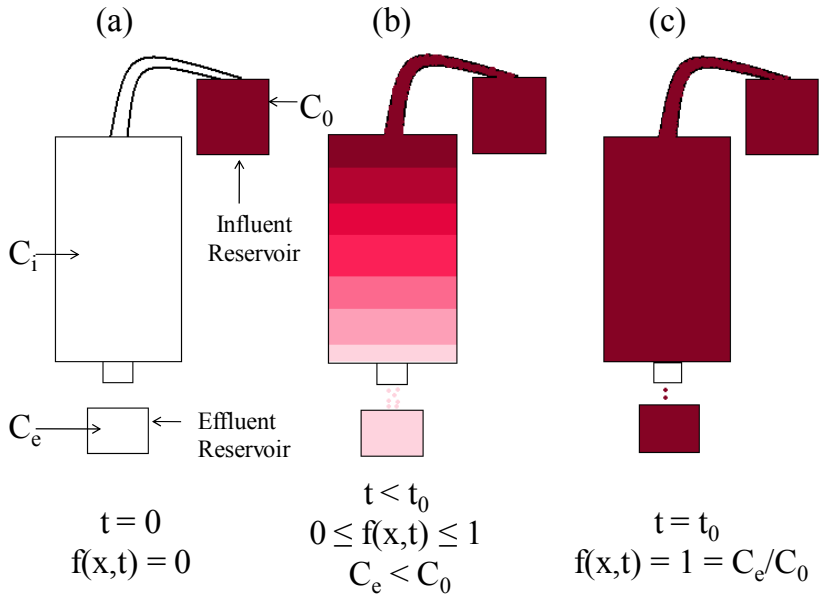


Figure 6. A schematic illustration of the traditional approach to modeling contaminant breakthrough in column experiments subject to a plug input concentration.

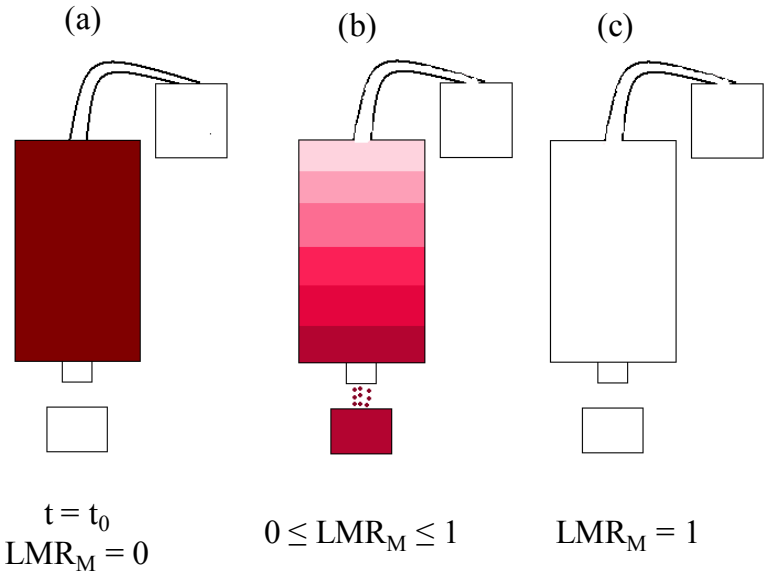


Figure 7. A schematic illustration of the leached mass ratio approach to modeling U(VI) breakthrough.

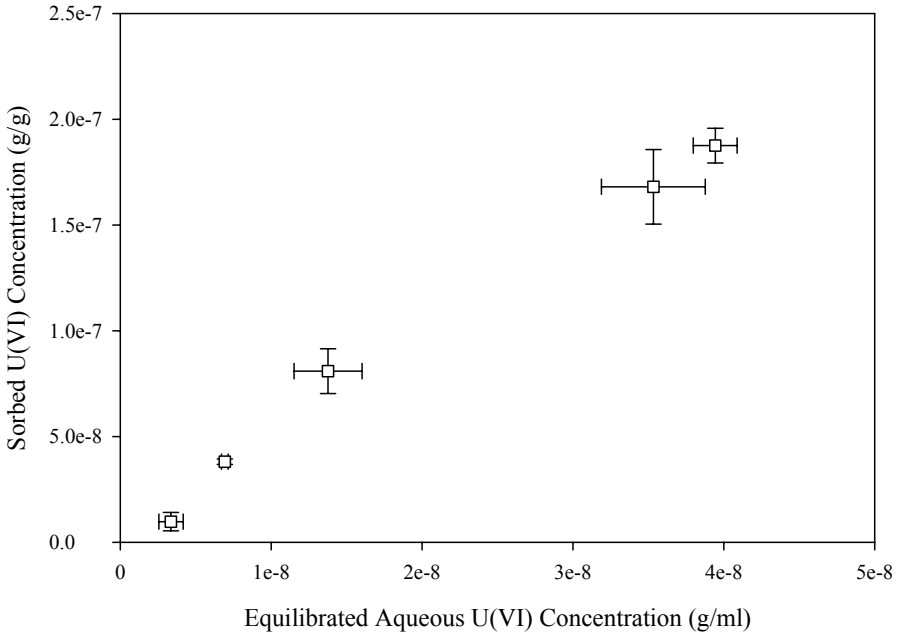


Figure 8. Results of batch adsorption experiment at 48 hours. Error bars represent 95% confidence intervals based on student t distribution.

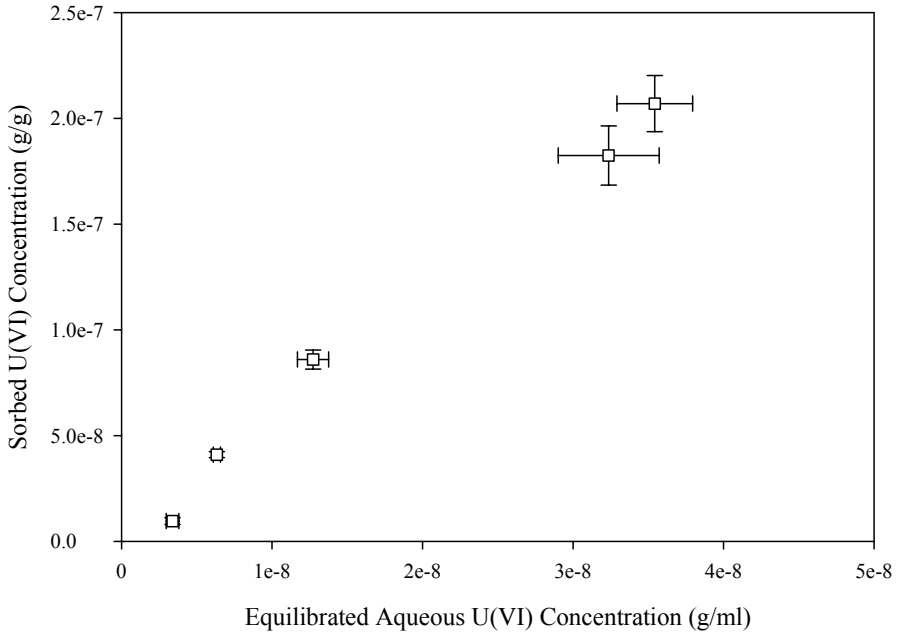


Figure 9. Results of batch adsorption experiment at 96 hours.

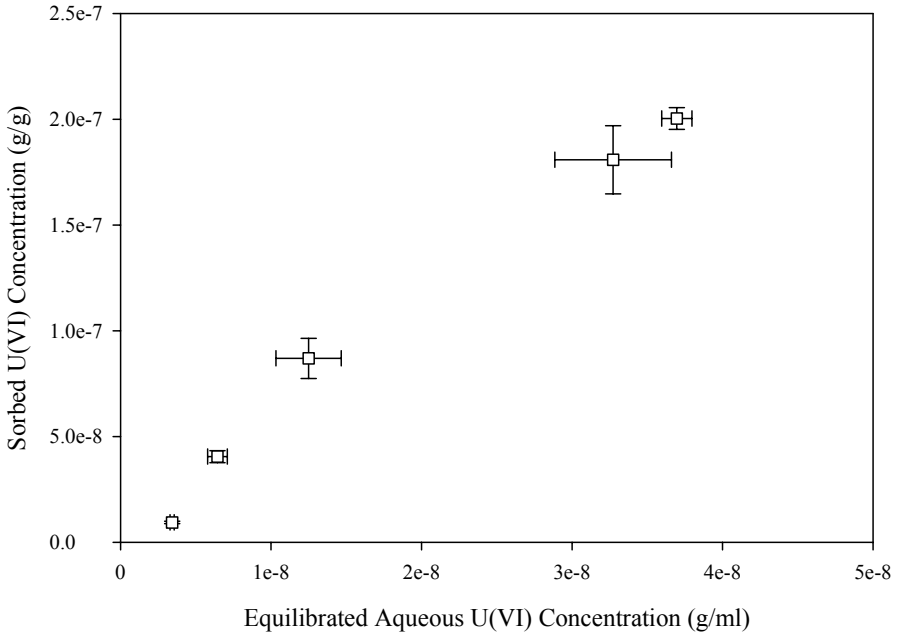


Figure 10. Results of batch adsorption experiment at 168 hours.

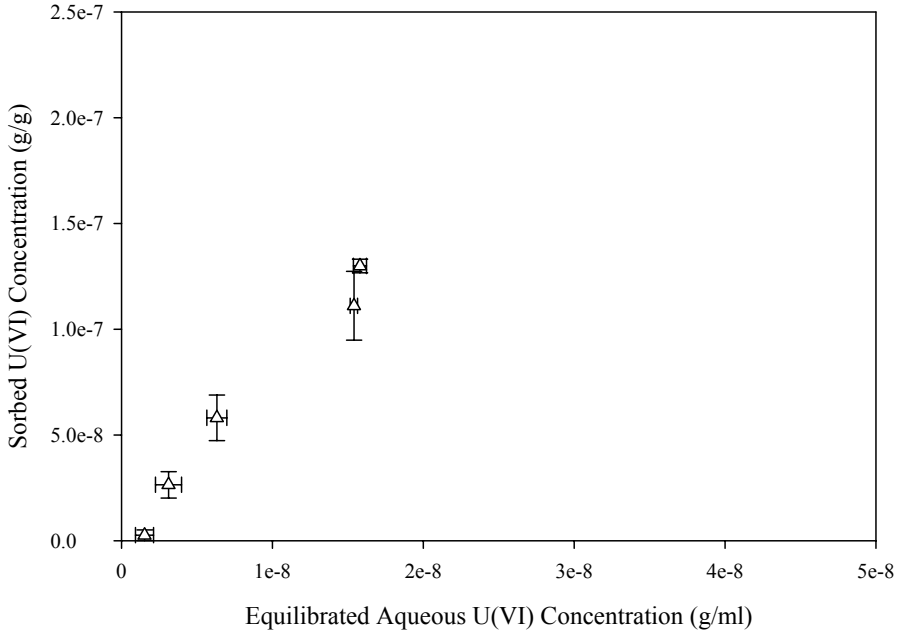


Figure 11. Results of the batch desorption experiment following the first desorption equilibration.

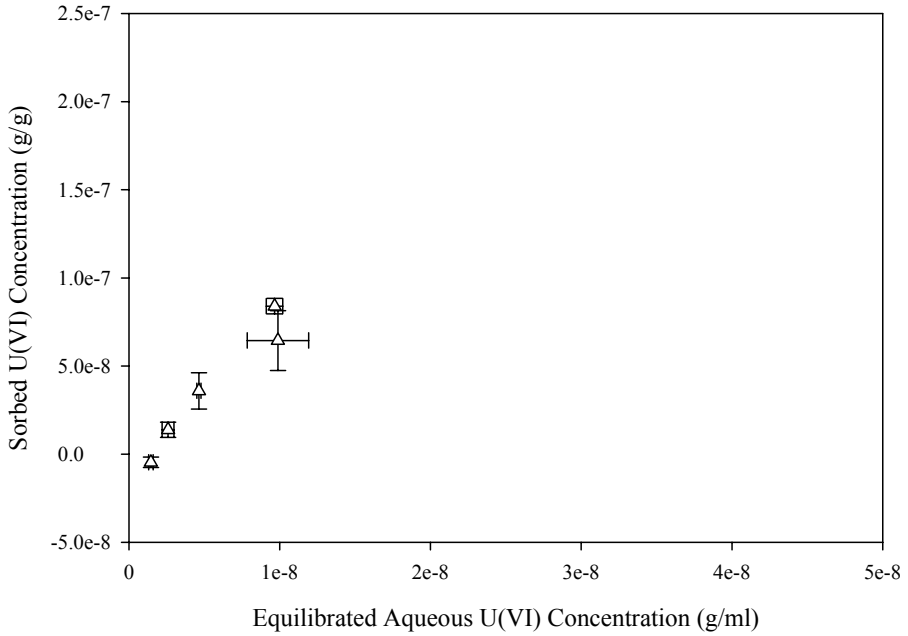


Figure 12. Results of the batch desorption experiment following the second desorption equilibration.

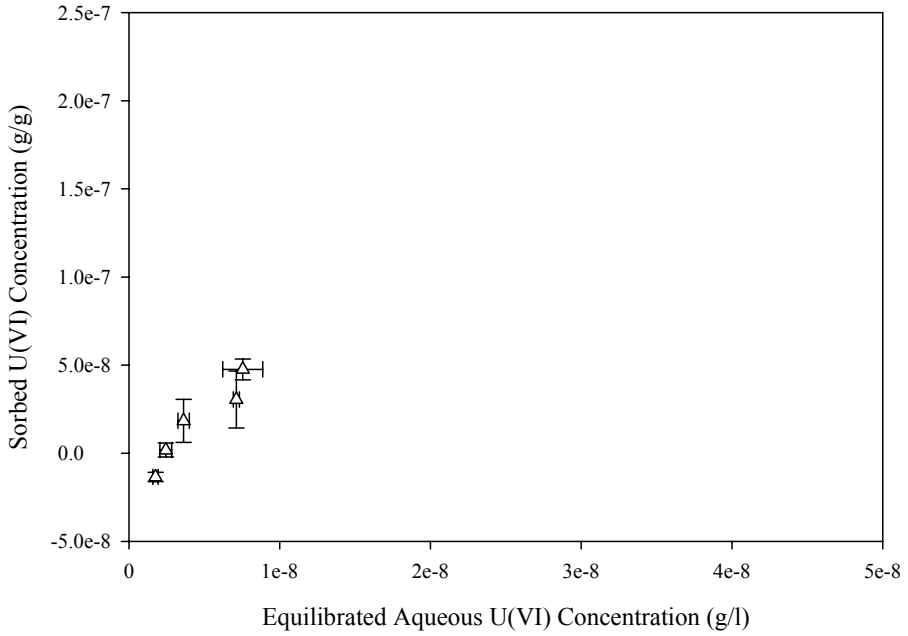


Figure 13. Results of the batch desorption experiment following the third desorption equilibration.

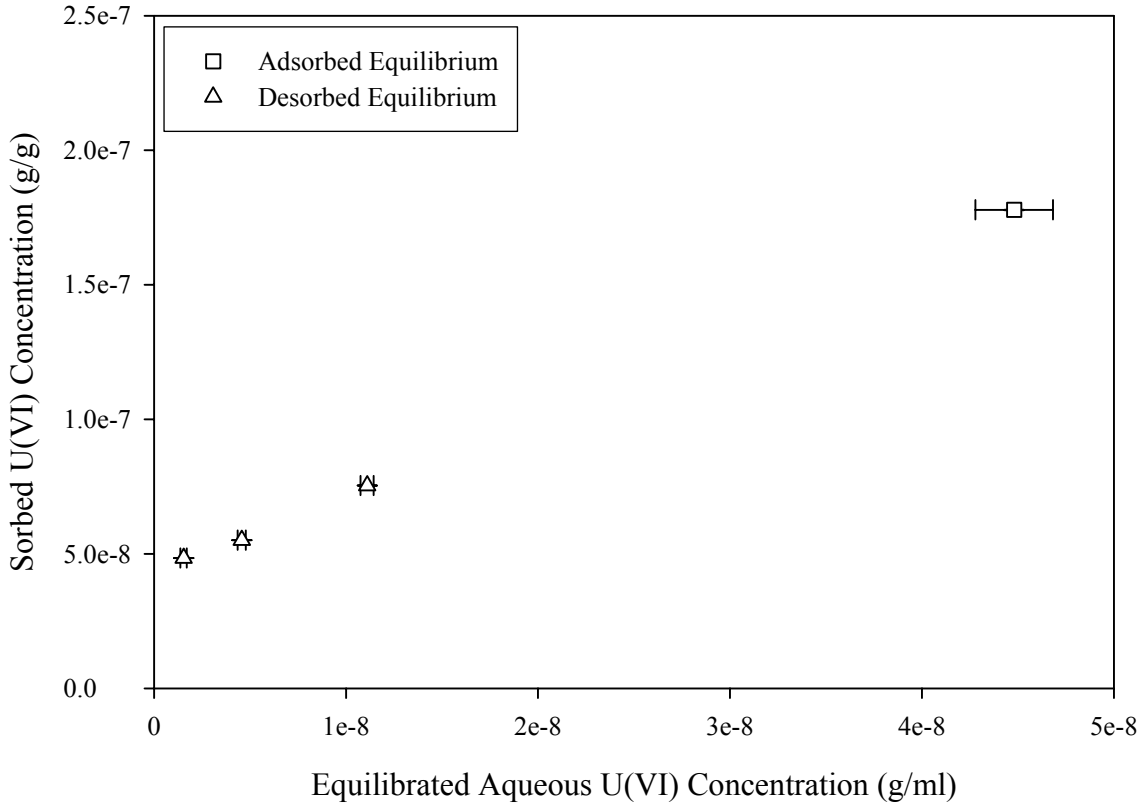


Figure 14. Sediment sample Y1 sediment/solution equilibrated state following adsorption and three desorption washes. The square symbolizes the adsorbed equilibration between the solid and solution phases. The three triangles represent the equilibrated state between solid and solution following each of three washes with the synthetic groundwater.

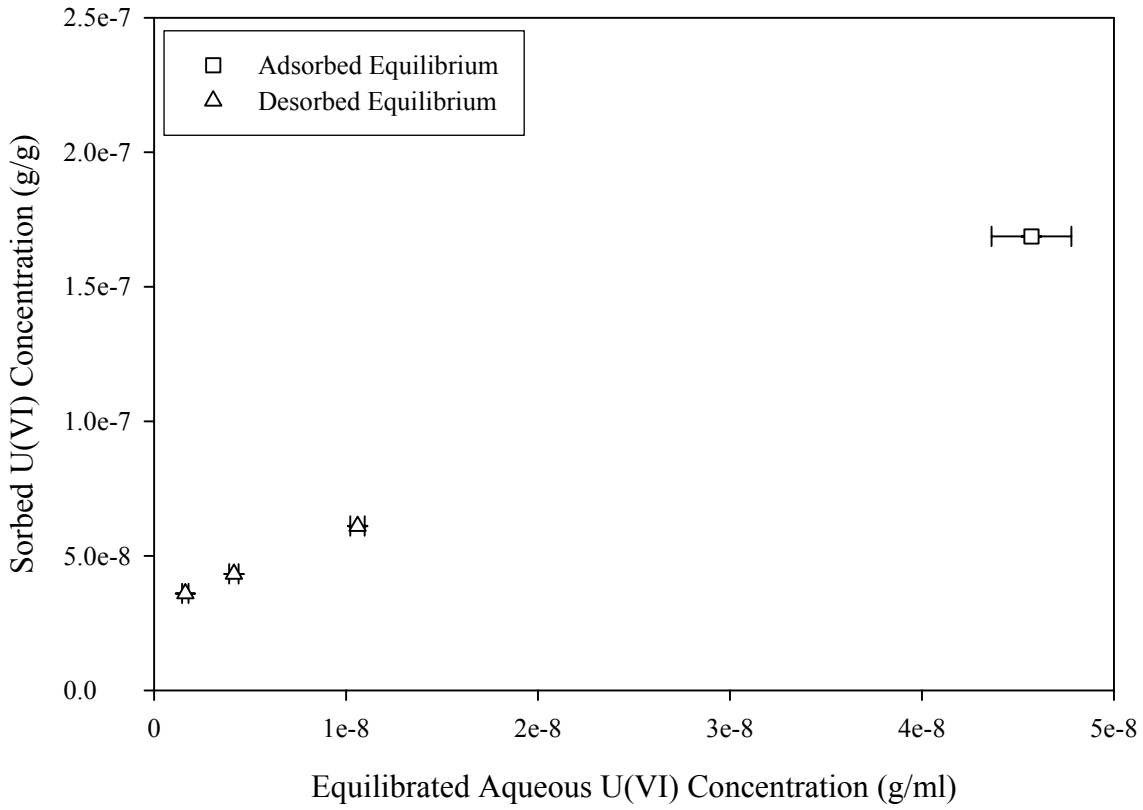


Figure15. Sediment sample Y2 sediment/solution equilibrated state following adsorption and three desorption washes.

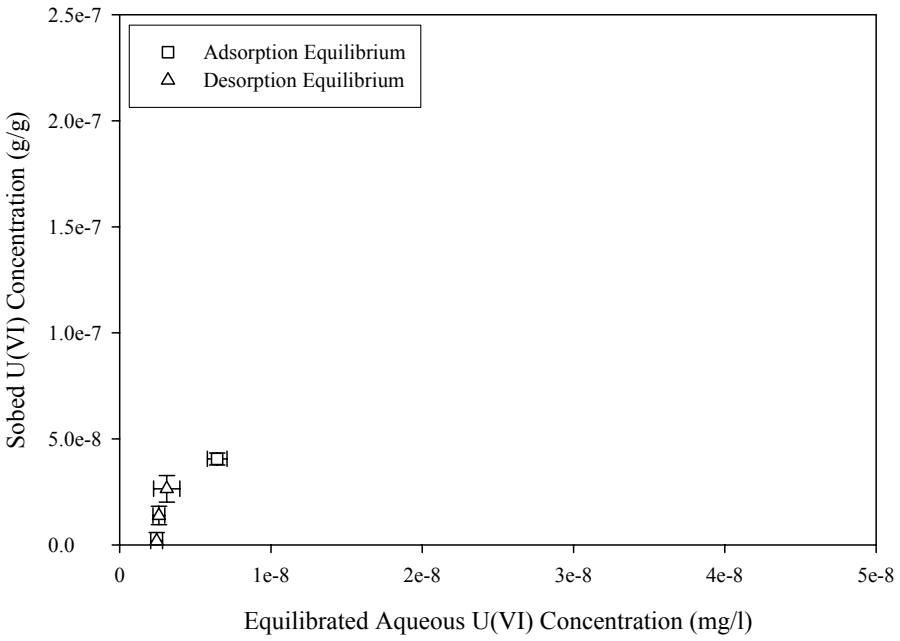


Figure 16. The mean sediment/solution equilibrated state of three sediment samples contaminated with 15.1 ug/l U(VI) following adsorption and three desorption washes.

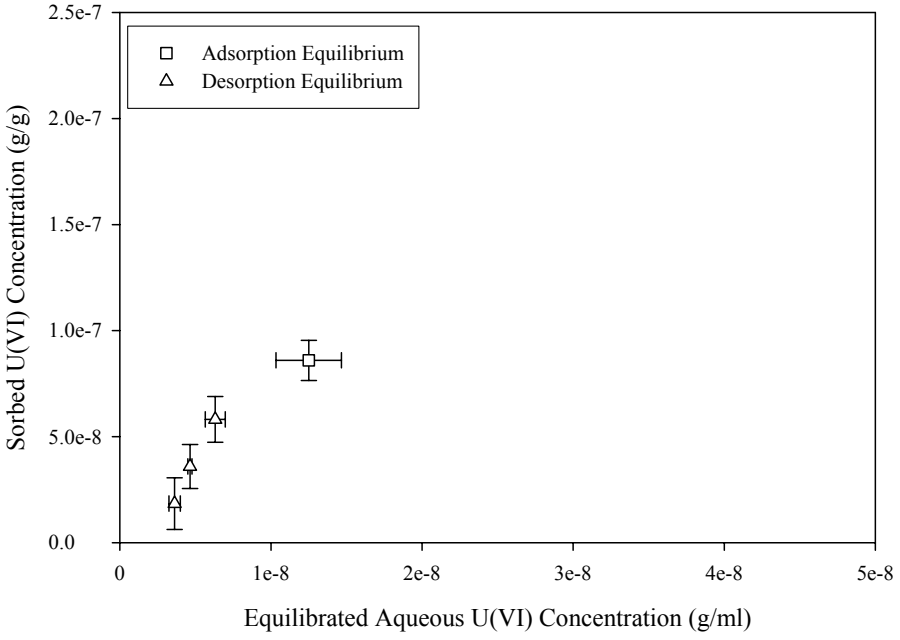


Figure 17. The mean sediment/solution equilibrated state of three sediment samples contaminated with 31.0 ug/l U(VI) following adsorption and three desorption washes.

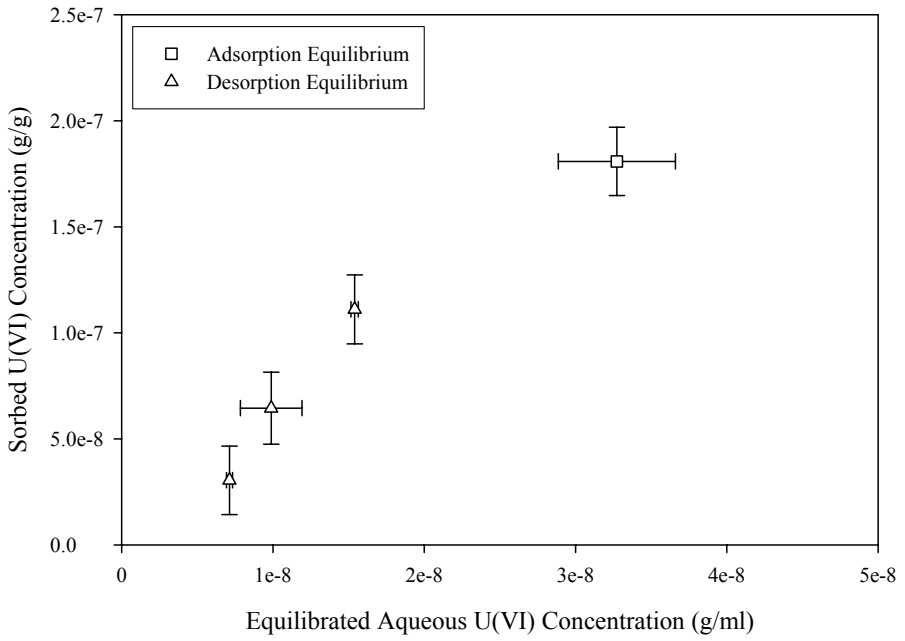


Figure 18. The mean sediment/solution equilibrated state of three sediment samples contaminated with 71.8 ug/l U(VI) following adsorption and three desorption washes.

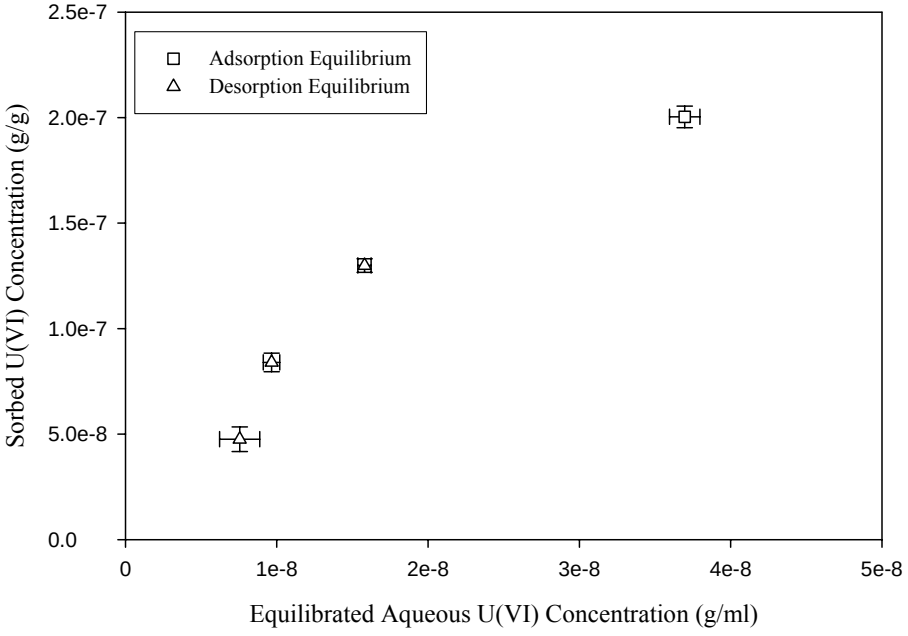


Figure 19. The mean sediment/solution equilibrated state of three sediment samples contaminated with 80.1 ug/l U(VI) following adsorption and three desorption washes.

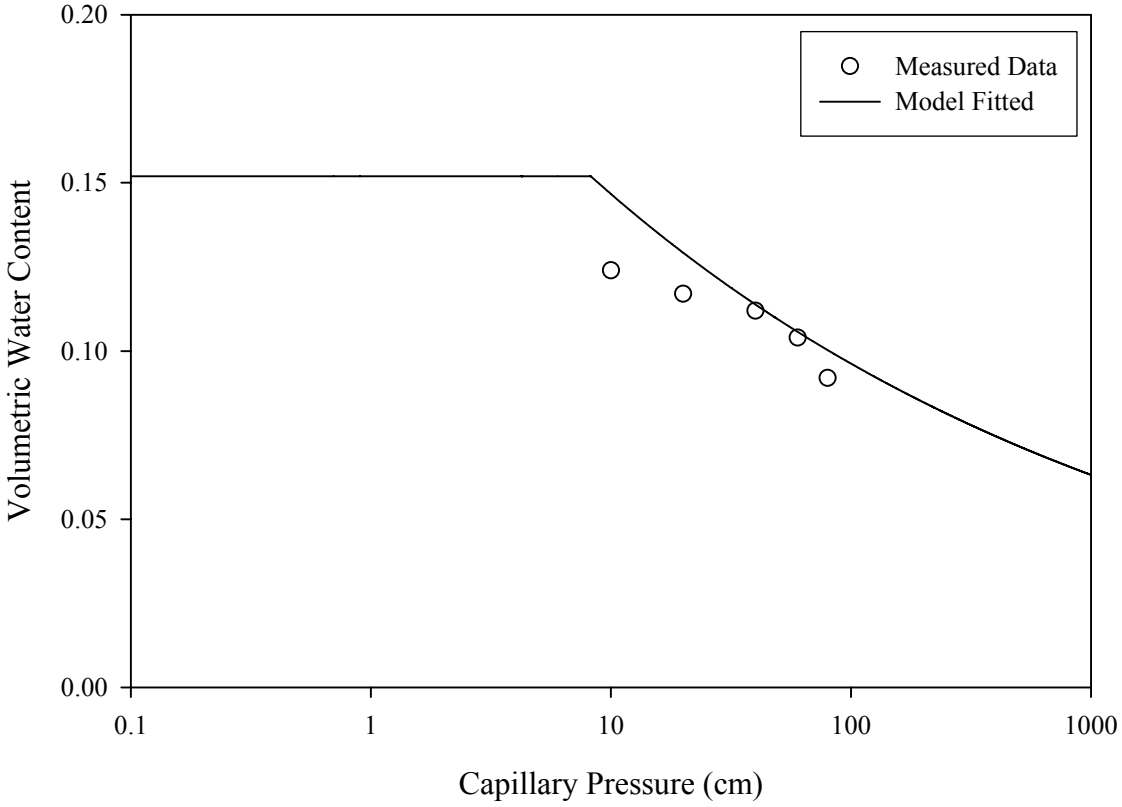
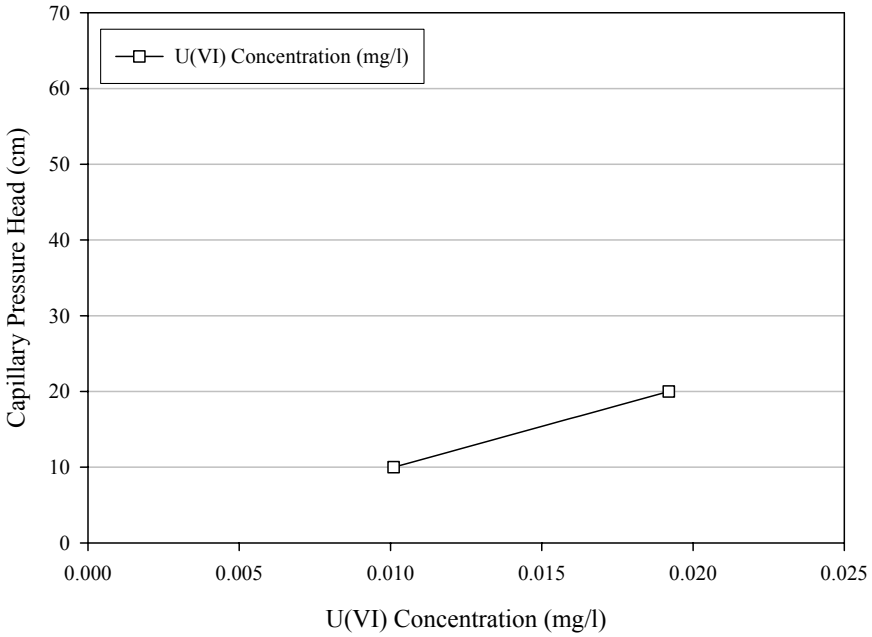


Figure 20. Average $\theta(h_c)$ relationship for column B and model fitted relationship using TrueCell software.



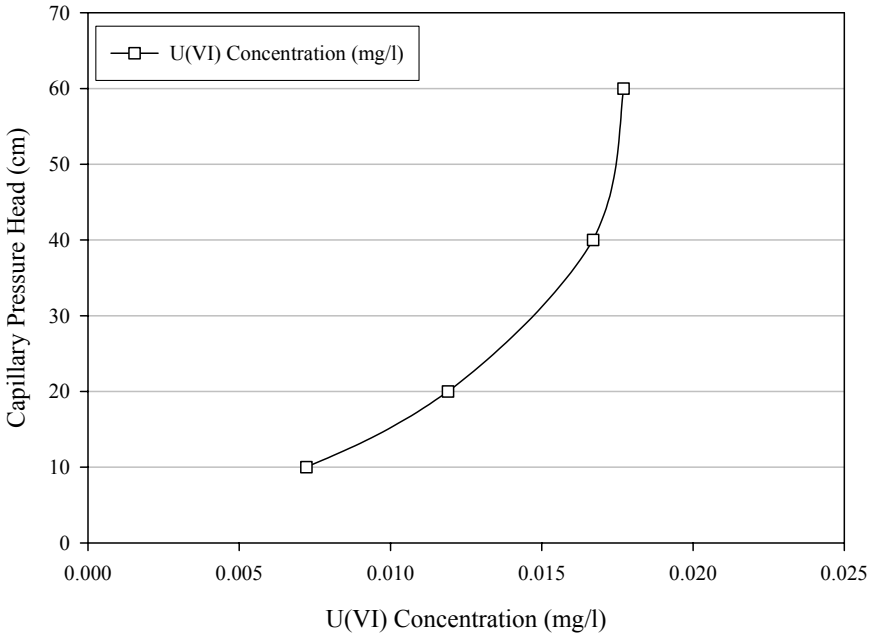


Figure 21. U(VI) concentrations of solution collected from column A (top) and B (bottom) while measuring the average $\theta(h_c)$ relationship of each column. The average $\theta(h_c)$ relationship was determined for each column following the leaching portion of the experiments

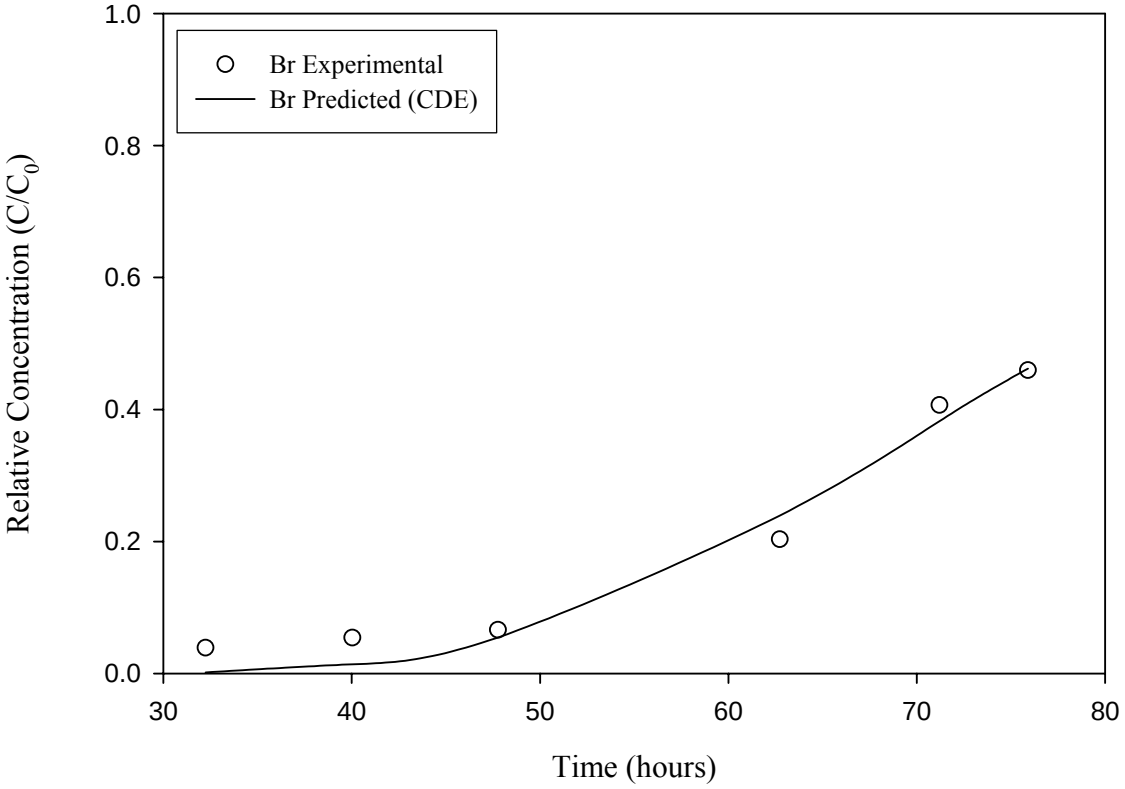


Figure 22. Column A bromide curve and model fit using the CDE.

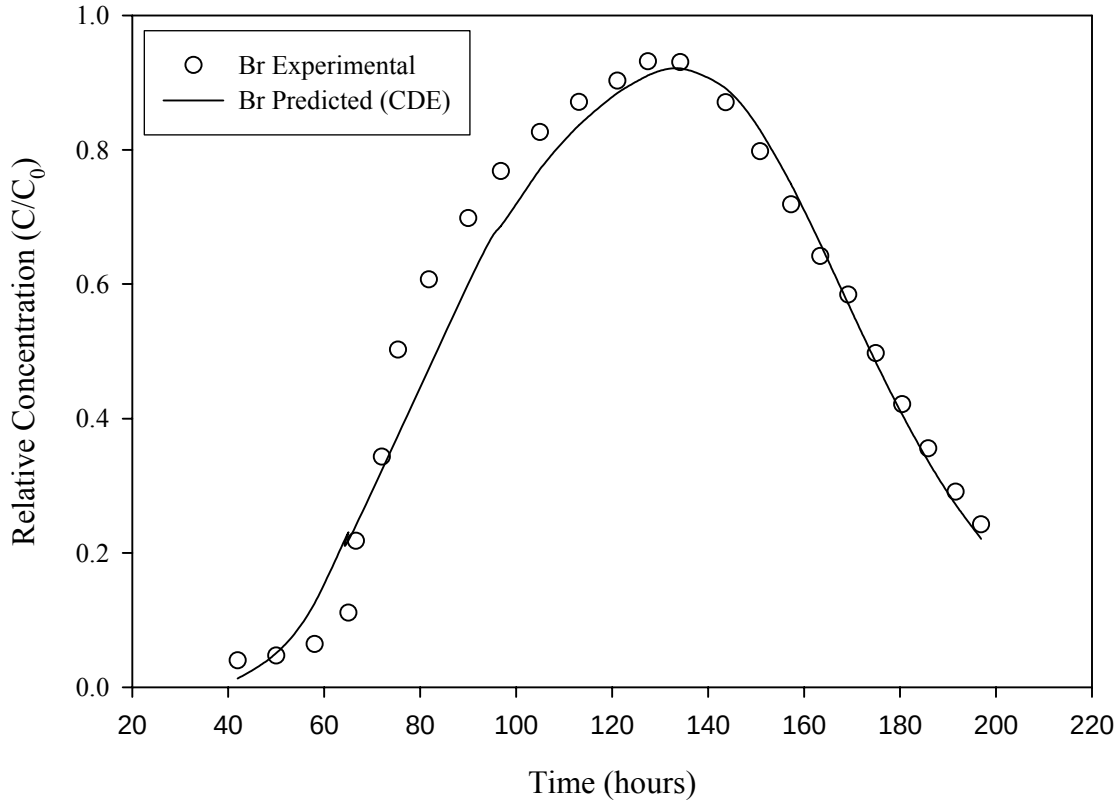


Figure 23. Column B bromide curve and model fit using the CDE.

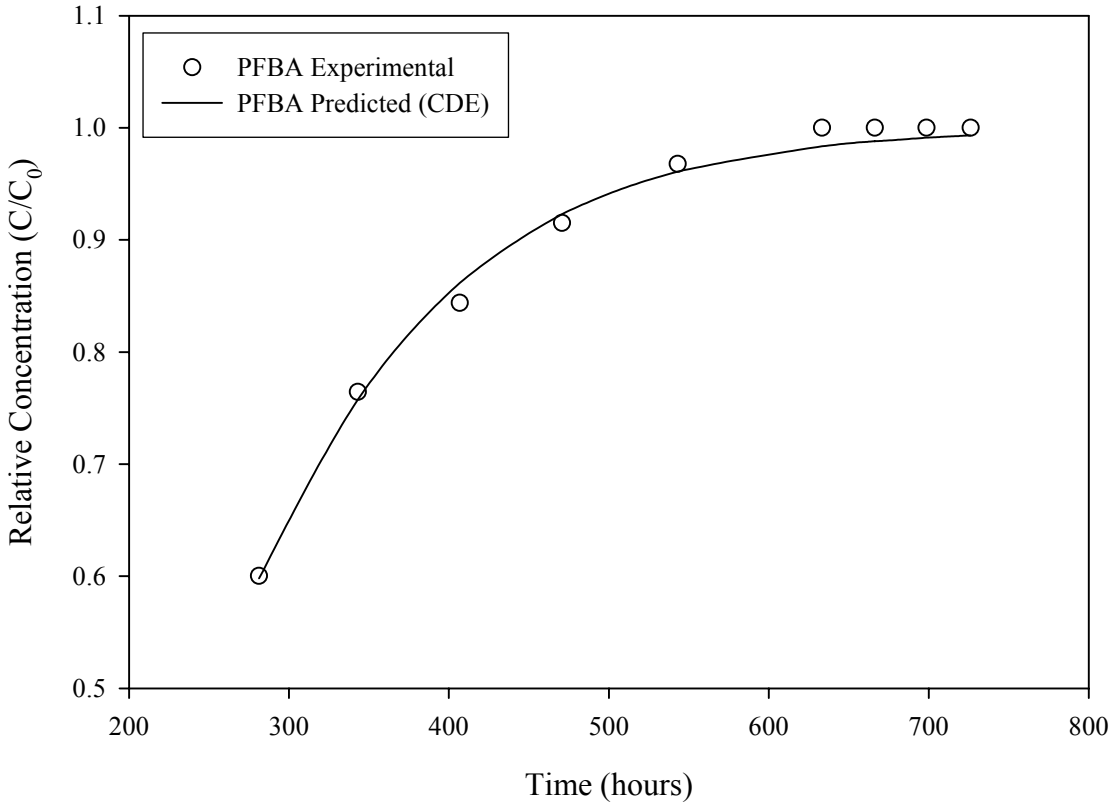


Figure 24. Column B PFBA curve and model fit using the CDE.

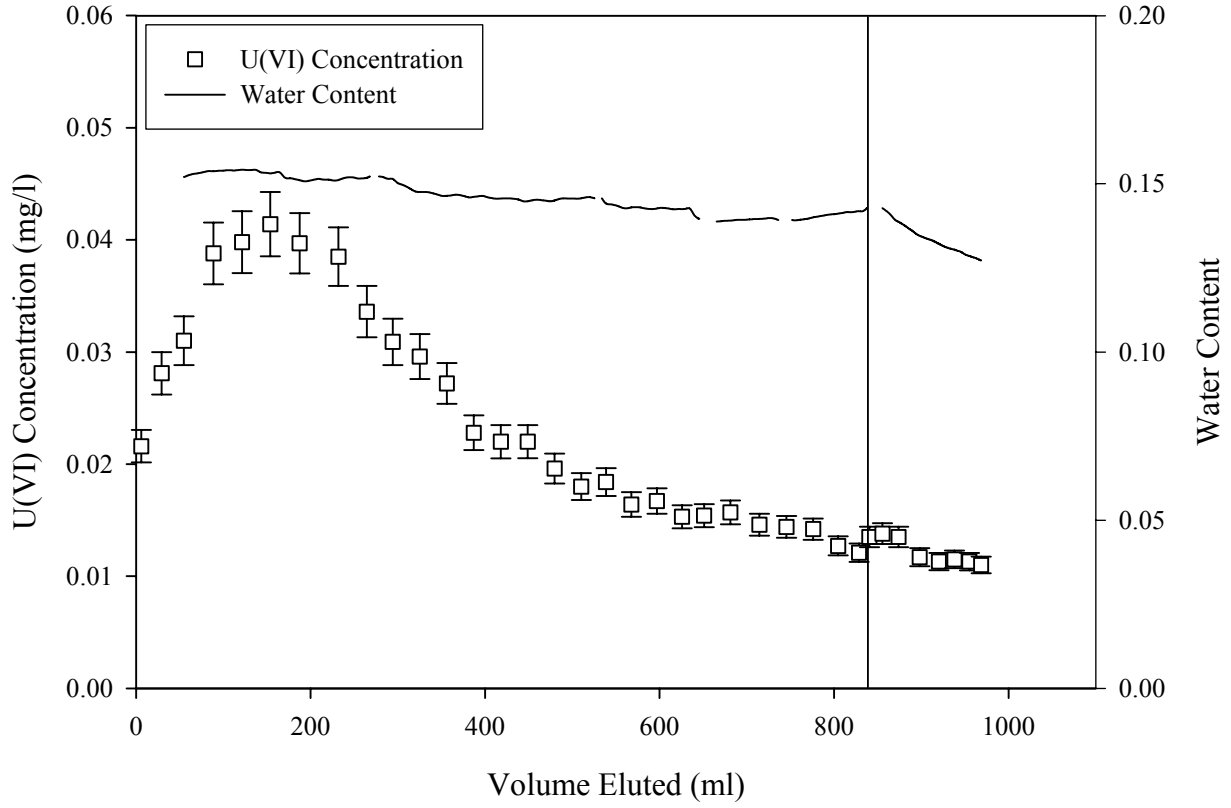


Figure 25. Column A leaching curve and estimated water content. The second experiment (low water content) begins after 838 ml has been eluted and is indicated by the solid vertical line. Error bars represent analytical error associated with uranium analysis.

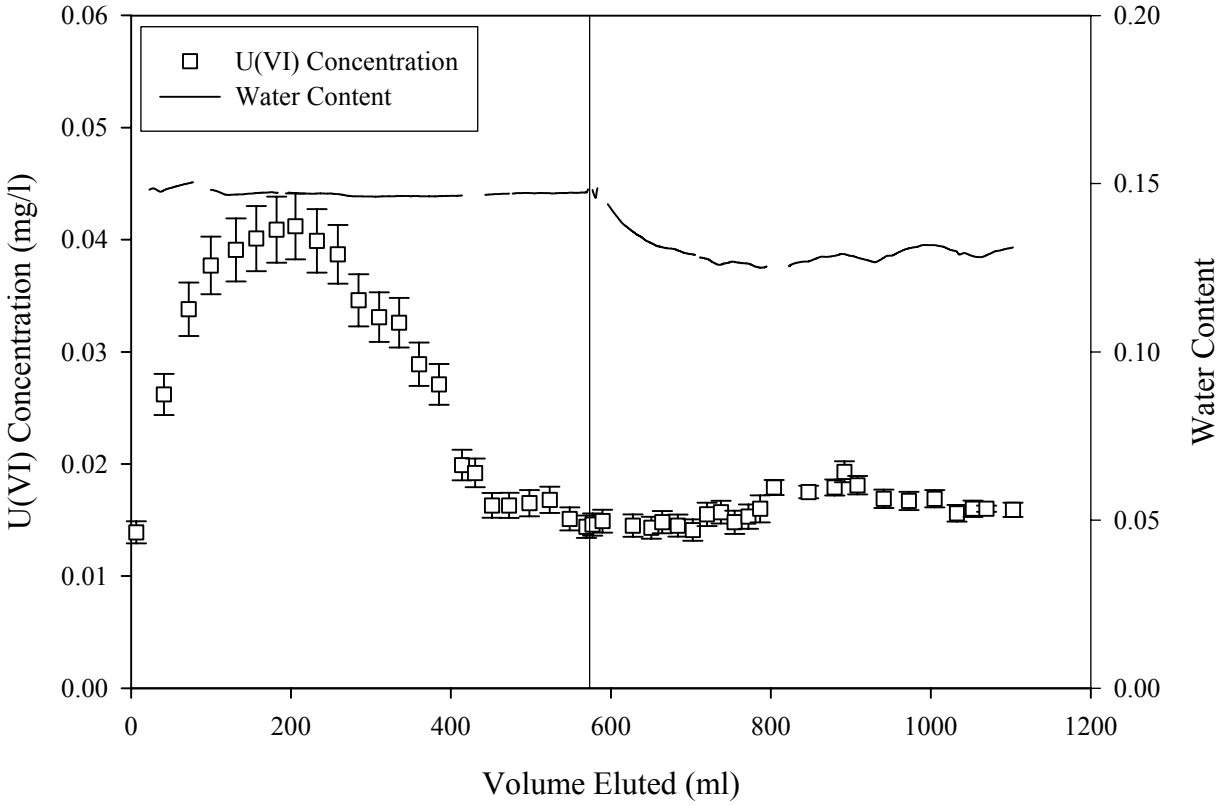


Figure 26. Column B leaching curve and estimated water content. The second experiment (low water content) begins after 573 ml has been eluted and is indicated by the solid vertical line. Error bars represent the analytical error associated with uranium analysis.

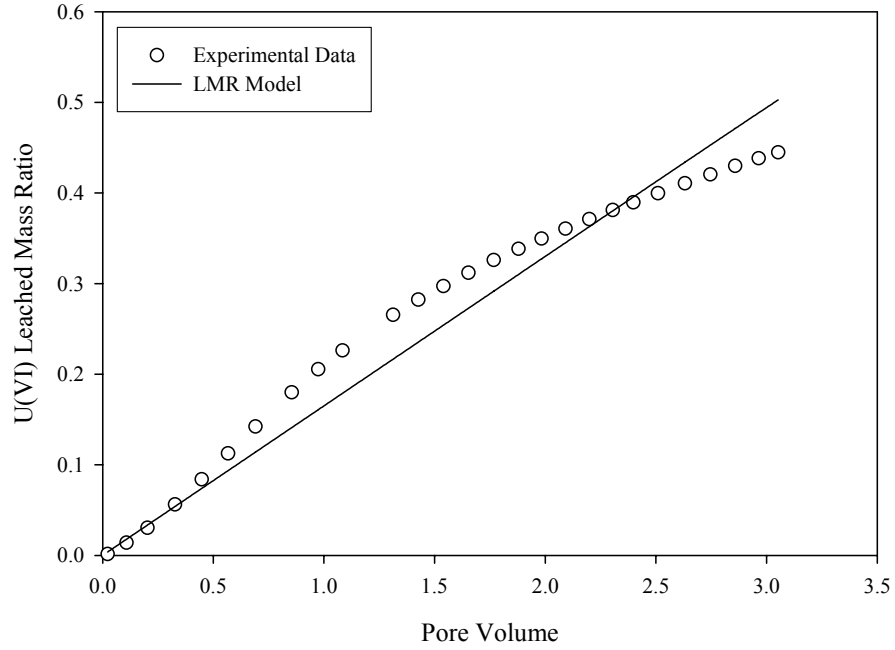


Figure 27. Column A experimental leached mass ratio and model fit at high water content.

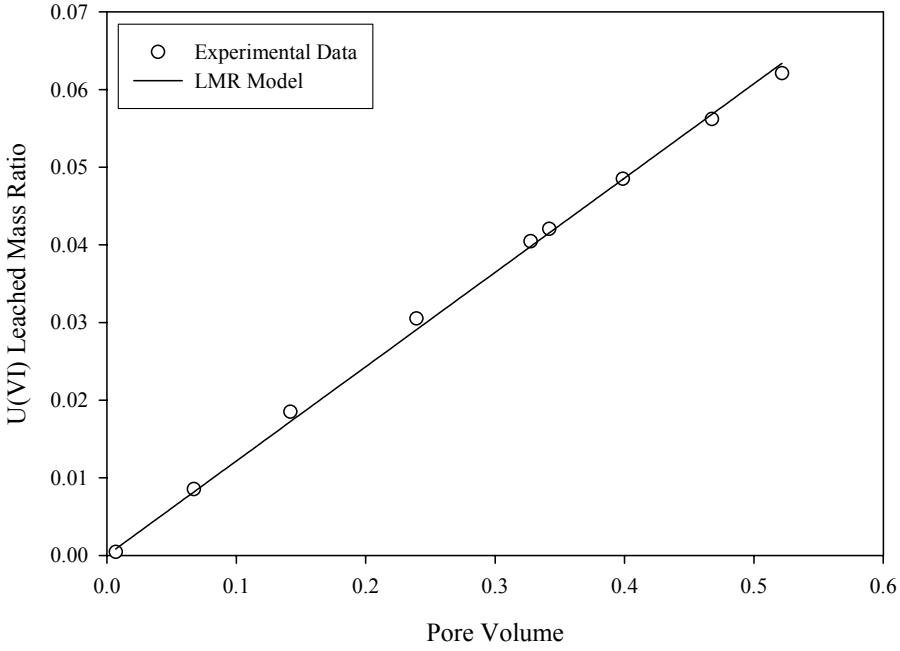


Figure 28. Column A experimental leached mass ratio and model fit at low water content.

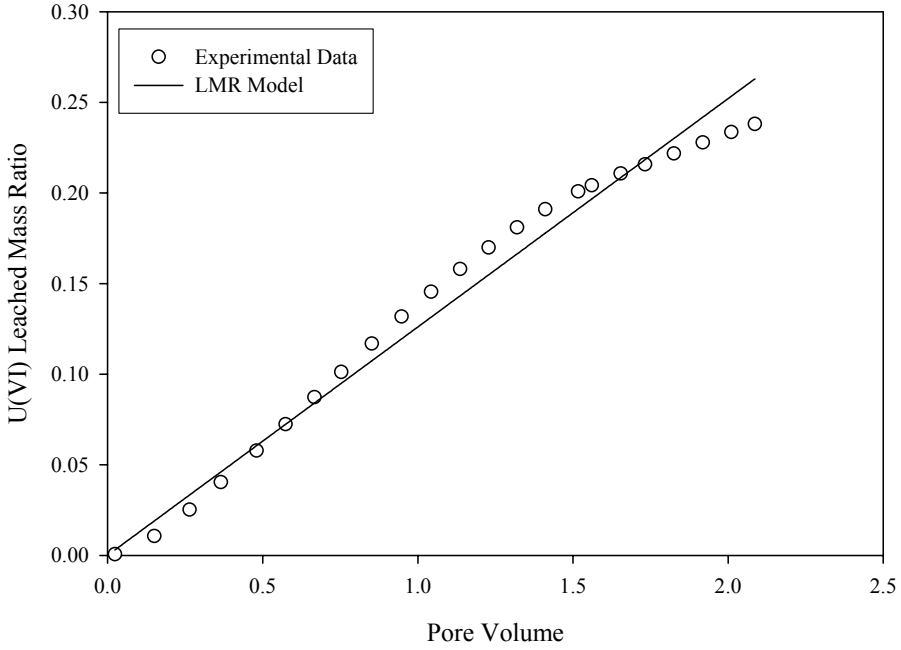


Figure 29. Column B experimental leached mass ratio and model fit at high water content.

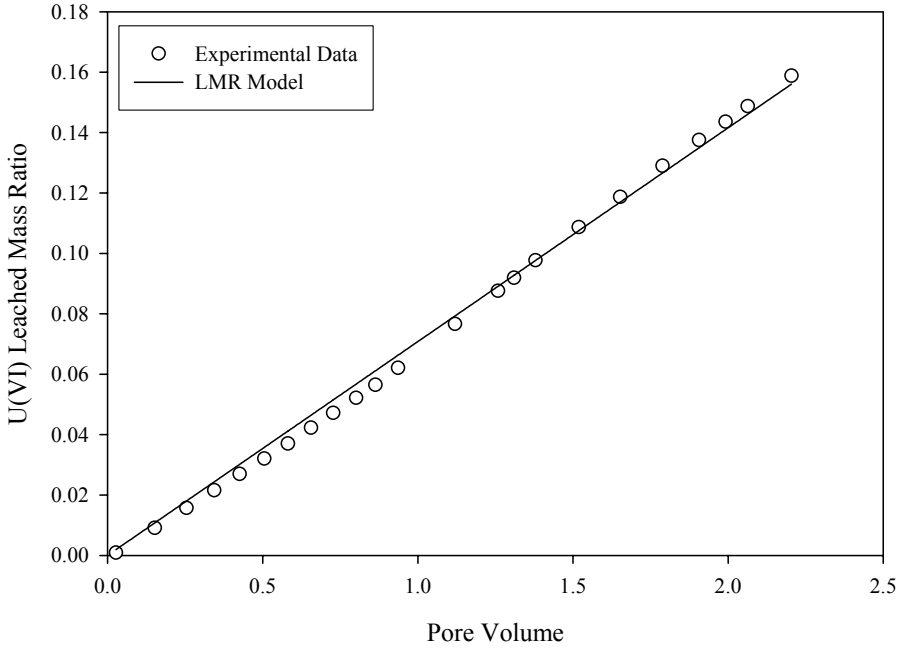


Figure 30. Column B experimental leached mass ratio and model fit at low water content.

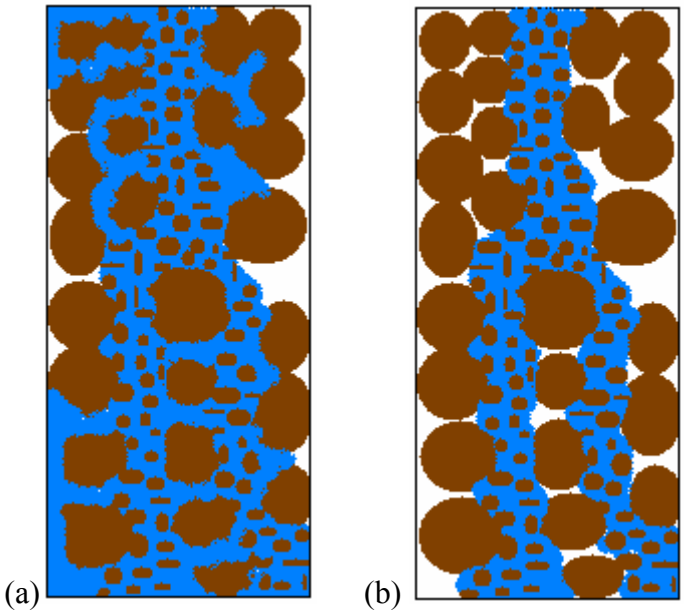


Figure 31. Depiction of solute pore regime under high water content (a) and low water content (b). At high water content the solute is in contact with more of the less reactive surfaces and Kd is lower. At low water contents, the solute is restricted to the finer pores and is in contact with much more reactive surfaces, thereby increasing Kd.

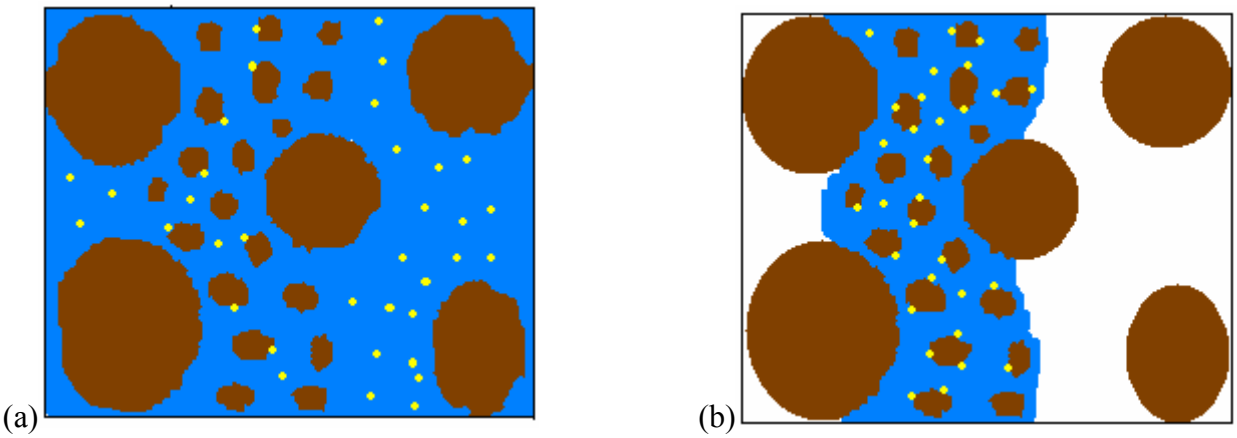


Figure 32. Smaller scale conceptual depiction of the effect of water content on solute transport. At high water content (a) much of the U(VI) (depicted in yellow) is in solution adjacent to non-reactive gravels, and therefore, much more mobile. At lower water contents (b), the U(VI) is more exposed to the reactive fraction and will be increasingly retarded relative to the higher water content.

Vita

Andrew Moore was born on January 12, 1979 in Memphis, Tennessee. Following graduation from White Station High School, he attended Appalachian State University where he received a Bachelor of Arts degree in Interdisciplinary Studies with a concentration in Environmental Policy and Planning. His degree from Appalachian State University included a minor in geology. During his last semester he took a course in hydrogeology, in which he excelled and enjoyed tremendously. He spent several year enjoying outdoor pursuits including a through-hike of the Appalachian Trail and a winter spent skiing in Alta, UT. In 2006, he entered Western Carolina University where he was involved in a number of water-related projects. He received his Bachelor of Science degree in Geology from Western Carolina University in May 2008. Andrew accepted a graduate teaching assistantship in the Department of Earth and Planetary Sciences at The University of Tennessee, Knoxville under Dr. Edmund Perfect for the fall of 2008. In the spring of 2009, he accepted a graduate research position at Oak Ridge National Laboratory under Dr. Melanie A. Mayes. He graduated with a Master of Science degree in Geology in August of 2010. Andrew hopes to work on environmental site investigation and remediation of contaminated groundwater in Asheville, NC.